



Rolle von Chronophin für die Cofilin-vermittelte Aktin-Dynamik in astrozytären Tumorzellen

(Role of Chronophin for cofilin-mediated actin dynamics in astrocytic tumour cells)

Inaugural-Dissertation

zur Erlangung des Doktorgrades
der Mathematisch-Naturwissenschaftlichen Fakultät
der Heinrich-Heine-Universität Düsseldorf

vorgelegt von

Oleg Fedorchenko
aus Kimovsk (Russland)

Düsseldorf, Juni 2009

Aus dem Institut für Biochemie und Molekularbiologie II
der Heinrich-Heine Universität Düsseldorf

Gedruckt mit der Genehmigung der
Mathematisch-Naturwissenschaftlichen Fakultät der
Heinrich-Heine-Universität Düsseldorf

Referent: Prof. Dr. Antje Gohla

Koreferent: Prof. Dr. Lutz Schmitt

Tag der mündlichen Prüfung: 22.06.2009

Contents

1	INTRODUCTION	10
1.1	The eukaryotic cytoskeleton	10
1.2	The regulation of actin cytoskeletal dynamics	10
1.3	The cofilin family of actin regulatory proteins	13
1.4	Characterisation of CIN	15
1.5	Role of the cofilin pathway in tumours	18
1.6	Characterisation of glial tumours	22
2	AIMS OF THE STUDY	25
3	MATERIALS	26
3.1	List of manufacturers and distributors	26
3.2	Chemicals	27
3.3	Reagents for immunoblotting	29
3.4	Reagents for immunohistochemistry	29
3.5	Cell culture, cell culture media and supplements	29
3.6	Cell lines	30
3.7	Protein and DNA standards	30
3.8	Kits	30
3.9	Enzymes	30
3.10	Reagents for microscopy	31
3.11	Solutions and buffers	32
3.12	RNA interference tools	35
3.13	List of primary antibodies	36
4	EXPERIMENTAL PROCEDURES	37
4.1	Transformation of bacteria	37
4.2	Plasmid isolation from E. coli	37
4.3	DNA gel electrophoresis and DNA preparation from gels	38

4.4	Isolation of total RNA	38
4.5	DNA constructs and cloning procedures	39
4.6	Cell culture	40
4.7	Transient transfection of cells	40
4.8	RNA interference as a tool for gene silencing	41
4.9	Production of shRNA-containing lentivirus and viral transduction	43
4.10	Validation of shRNA/siRNA-mediated protein knockdown	45
4.11	Acetone precipitation of proteins	46
4.12	Determination of protein concentration	46
4.13	SDS-polyacrylamide gel electrophoresis	47
4.14	Immunoblotting	47
4.15	Reprobing of Western blot membranes	48
4.16	Immunohistochemistry	48
4.17	Immunofluorescence microscopy	49
4.18	Proliferation assay	49
4.19	In vitro invasion assay	50
4.20	In vitro cell transformation assay	51
4.21	Sensitised emission FRET	51
4.22	In vitro phosphatase activity assays	53
5	RESULTS	55
5.1	CIN expression in mouse tissues	55
5.2	CIN expression in human brain and astrocytic gliomas	58
5.3	Deregulation of the Cofilin pathway in glial tumour samples	59
5.4	CIN knock-down	63
5.4.1	Choosing of appropriate cell line	63
5.4.2	CIN downregulation using siRNA	63
5.4.3	CIN downregulation by shRNA	65
5.5	Dysregulation of the cofilin pathway in CIN depleted GBM6840	65

5.6	Effect of CIN depletion on nuclear morphology	67
5.7	Subcellular CIN localisation during mitosis and cytokinesis	69
5.8	Effect of CIN depletion on the actin cytoskeleton	69
5.9	Effect of CIN depletion on anchorage-independent growth	72
5.10	Increased EGF signalling and invasion of CIN depleted cells	72
5.11	CIN regulation	74
5.11.1	CIN – CIB1 colocalisation in Hela cells	76
5.11.2	CIN – CIB1 interaction analysis by FRET	77
5.11.3	Effect of CIB1 on the CIN phosphatase activity	79
5.11.4	Effect of CIN phosphatase activity on CIB1 protein expression	80
6	DISCUSSION	83
6.1	CIN expression and cellular localisation analysis	83
6.2	Cofilin pathway in glioblastomas	85
6.3	Consequences of CIN depletion in GBM6840	85
6.4	CIN regulation	87
7	SUMMARY	90
8	ZUSAMMENFASSUNG	92
9	REFERENCES	94
10	<i>CURRICULUM VITAE</i>	104
11	ACKNOWLEDGEMENTS	106

Figure index

Figure 1: Actin-based structures in cells	11
Figure 2: Interplay between Arp2/3-complex and cofilin functions	12
Figure 3: Regulation of cofilin activity	14
Figure 4: Alignment of the conserved HAD motifs in putative CIN orthologs	16
Figure 5: A model for gene inactivation by RNA interference	42
Figure 6: pLKO.1-Puro vector map	43
Figure 7: Localisation of the used siRNA/shRNA in open reading frame of human CIN	45
Figure 8: Principle and requirements for FRET	52
Figure 9. Principle of the <i>in vitro</i> phosphatase activity assay	54
Figure 10: Characterisation of CIN antibody and analysis of CIN expression	55
Figure 11: Immunohistological analysis of CIN expression in murine embryos	56
Figure 12: CIN expression in the adult mouse brain	57
Figure 13: Histological analysis of CIN expression in human brain samples	58
Figure 14: Expression analysis of the cofilin pathway by real-time PCR	60
Figure 15: Dysregulation of the cofilin pathway in human brain tumour samples	62
Figure 16: CIN expression in different glioma model cell lines	64
Figure 17: CIN knockdown in glioma cell line GBM6840 with siRNA	64
Figure 18: CIN knock-down in GBM6840 using MISSION shRNA constructs	66
Figure 19: Analysis of nuclear morphologies in CIN-deficient glioblastoma cells	68
Figure 20: Endogenous CIN localisation in cells during mitotic cell division	70
Figure 21: Effect of CIN depletion on cell morphology	71
Figure 22: Effect of CIN depletion on cell growth	73
Figure 23: Effect of HGF and EGF on p-cofilin levels and invasive behaviour of CIN depleted and control GBM6840 cells	75
Figure 24: Colocalisation analysis of CIB1-GFP with endogenous CIN protein	76
Figure 25: FRET analysis of the CIN – CIB1 interaction	78
Figure 26: Effect of CIB1 and Ca ²⁺ on the CIN phosphatase activity	80
Figure 27: Effect of CIN phosphatase activity on CIB1 expression levels	81
Figure 28: Observed dysregulation of the cofilin pathway with cellular consequences	87

Abbreviations

ABC	avidin biotin complex
amp ^R	ampicillin resistance gene for the selection of bacteria
APS	ammonium persulfate
ATP	adenosine-5'-triphosphate
BCA	bicinchoninic acid
BES	N,N-bis[2-hydroxyethyl]-2- aminoethanesulfonic acid
BSA	bovine serum albumin
CFP	cyan fluorescent protein
CIB1	calcium- and integrin- binding protein 1
CIN	Chronophin, independently identified as pyridoxal phosphate phosphatase (PLPP or Pdxp)
cppt	central polypurine tract
DAPI	4,6-diamidino-2-phenylindole
DEPC	diethylpyrocarbonate
DMSO	dimethylsulfoxide
DNA	deoxyribonucleic acid
DNase	deoxyribonuclease
dNTPs	desoxyribonucleosidtriphosphates
D-PBS	Dulbecco's phosphate-buffered saline
DTT	dithiothreitol
<i>E. coli</i>	<i>Escherichia coli</i>
ECL	enhanced chemiluminescence
EDTA	ethylenediamine-N,N,N',N'-tetra-acetate
EGF	epidermal growth factor
EGTA	ethyleneglycol-bis(β-aminoethyl)-N,N,N',N'-tetra-acetate
FCS	fetal calf serum
FRET	fluorescence resonance energy transfer
GBM	glioblastoma multiforme

GFP	green fluorescent protein
h	hour(s)
HBS	Hepes-buffered solution
Hepes	N-(2-hydroxyethyl)piperazine-N'-(2-ethanesulfonic acid)
HGF	hepatocyte growth factor
hPGK	human phosphoglycerate kinase eukaryotic promoter
HRP	horseradish peroxidase
LB medium	Luria-Bertani medium
LIMK	LIM (Lin-11/Isi-1/Mec-3)-domain-containing protein kinase
LSM	confocal laser scanning microscopy
LTR	long terminal repeat
mAb	monoclonal antibody
min	minute(s)
MTS	3-(4,5-dimethylthiazol-2-yl)-5-(3-carboxymethoxyphenyl)-2-(4-sulfophenyl)-2H-tetrazolium, inner salt
NFRET	normalised FRET
NGS	normal goat serum
NP-40	Nonidet™ P-40 (octylphenyl-polyethylene glycol)
pAb	polyclonal antibody
PAK	p21-activated kinase
PBS	phosphate-buffered saline
PCR	polymerase chain reaction
Pdpx	pyridoxal (pyridoxine, vitamin B ₆) phosphatase, independently identified as Chronophin (CIN)
PFA	paraformaldehyde
pH	negative decadic logarithm of the hydrogen ion concentration
P _i	inorganic phosphate
PLP	pyridoxal phosphate
PLPP	pyridoxal phosphate phosphatase, see also CIN and Pdpx

<i>p</i> -NPP	<i>para</i> -nitrophenylphosphate
puro ^R	puromycin resistance gene for the selection of mammalian cells
RIPA	radioimmunoprecipitation assay
RNA	ribonucleic acid
RT	room temperature
SD	standard deviation
SDS	sodium dodecyl sulfate
SDS-PAGE	SDS-polyacrylamide gel electrophoresis
shRNA	short hairpin RNA
siRNA	short interfering RNA
SOC	super optimal broth with catabolite repression
TBS	Tris-buffered saline
TEMED	N,N,N',N'-tetramethylethylenediamine
TESK	testis-specific protein kinase
Tris	tris(hydroxymethyl)-aminomethane
Triton X-100	<i>t</i> -octylphenoxy polyethoxyethanol
Tween-20	polyoxyethylen-(20)-monolaurate
UV	ultra violet (light)
v/v	volume per volume
w/v	weight per volume
WHO	World Health Organisation
<i>x g</i>	relative centrifugal force (RCF)
YFP	yellow fluorescent protein

1 Introduction

1.1 The eukaryotic cytoskeleton

The eukaryotic cytoskeleton provides the cell with structure and shape and is responsible for fundamental cellular processes such as cell migration (Le Clainche and Carlier, 2008), cell division and cell polarity (Li and Gundersen, 2008). Eukaryotic cells contain three different kinds of cytoskeletal filaments, which are microfilaments, microtubules and intermediate filaments.

Microfilaments (or actin filaments) are the thinnest filaments, approximately 7 nm in diameter, of the cytoskeleton of all eukaryotic cells. Microfilaments are most highly concentrated underneath the plasma membrane, where they form the cortical actin cytoskeleton that is responsible for the maintenance of cellular shape. Cortical actin dynamics regulate the morphological changes during mitotic cell division and cleavage furrow formation in the process of cytokinesis. Furthermore, they are of fundamental importance for cell migration and tumour cell invasion. Actin stress fibers traverse the cell cytosol and connect to focal adhesions, the sites of cell contact with the extracellular matrix through integrin receptors. The main function of stress fibers is therefore to resist tension (Pellegrin and Mellor, 2007).

Microtubules have a diameter of 25 nm and lengths varying from 200 nm to 25 μm . Microtubules serve as structural components within cells and are involved in many cellular processes including mitosis, cytokinesis, and vesicular transport (Zhu et al., 2009).

Together with microtubules and actin microfilaments, the intermediate filaments (which are approximately 11 nm in diameter) constitute the integrated, dynamic filament network present in the cytoplasm of eukaryotic cells. While the structures of microtubules and microfilaments are known in atomic detail, the intermediate filament architecture is much less understood (Strelkov et al., 2003). Different intermediate filaments are made of vimentins (the common structural support of many cells), keratins (found in skin cells, hair and nails), neurofilaments (found in neural cells) and lamins (giving the structural support to the nuclear envelope).

1.2 The regulation of actin cytoskeletal dynamics

Actin is one of the most abundant and highly conserved proteins among eukaryotes. There are three different isoforms of monomeric actin: α -, β -, and γ -isoforms. In response to different stimuli, actin monomers in the cells polymerise into helical filaments (also called filamentous actin or F-actin), which can be further assembled into a wide variety of higher-

order cellular structures ranging from lamellipodia to microvilli, each of which performs a wide range of cellular functions (Figure 1). Actin filaments are polarised, with a fast-growing barbed end and a slow-growing pointed end. The dynamics of actin filaments are essential for different cellular activities, such as cell migration, morphological changes and polarity formation. These events are regulated by a large variety of actin binding proteins, which cooperatively act in the assembly/disassembly and reorganisation of actin filaments in cells (dos Remedios et al., 2003; Revenu et al., 2004).

The first identified actin assembly factor was the Arp2/3 complex, composed of seven polypeptides (ARPC 1–5, Arp2 and Arp3). Arp2 and Arp3 are actin-related proteins, and are shown to mimic an actin dimer that can elongate towards the barbed end. The Arp2–Arp3 dimer thereby serves as a nucleation site, and the complex remains at the pointed end of the filament. In addition, the Arp2/3 complex binds to the side of pre-existing actin filaments, and its nucleation activity thereby produces a branched filament structure with an angle of 70° between the filaments. Repeated branching leads to ‘dendritic network’ formation, important for lamellipodia formation and cell migration (Chhabra and Higgs, 2007).

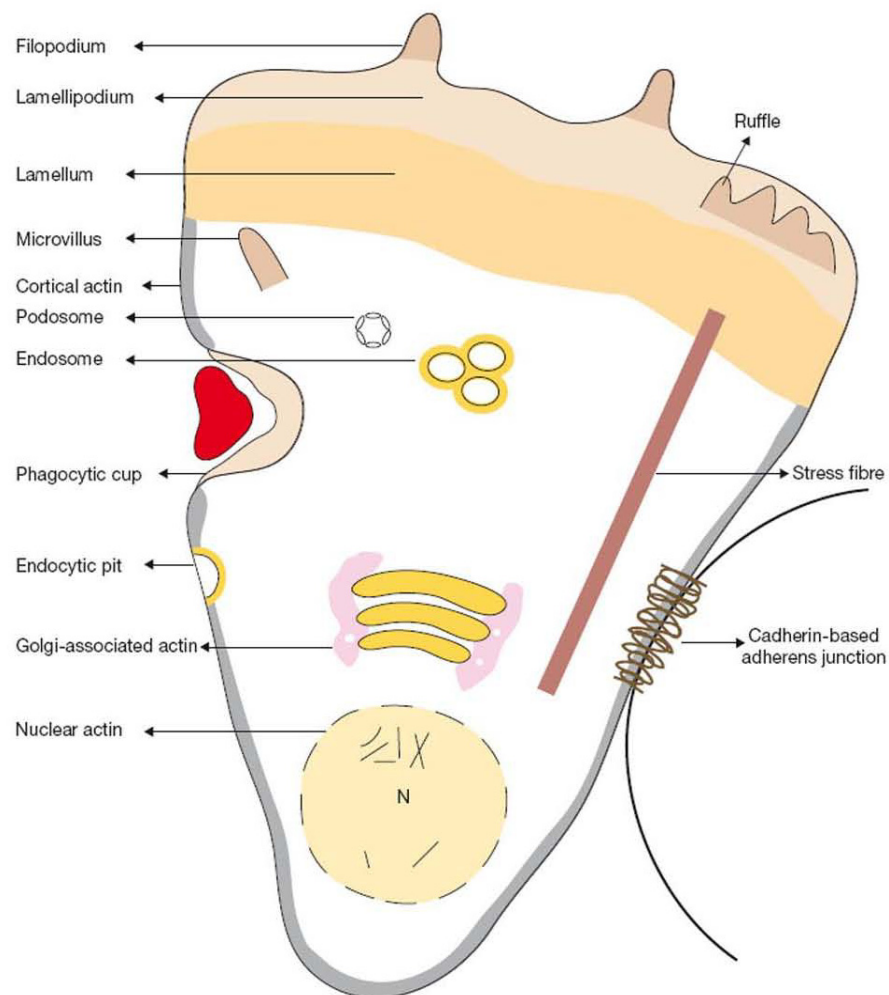


Figure 1: Actin-based structures in cells.

A hypothetical cell, migrating upwards and attached to a second cell on the right. Cellular structures known or strongly suspected to contain actin filaments are indicated. N, nucleus. From Chhabra and Higgs, 2007.

The ubiquitously expressed proteins of the cofilin family (consisting of the actin-depolymerising factor, ADF; the broadly expressed cofilin-1, and the non-neuronal cofilin-2 isoform; which are from now on collectively referred to as cofilin) are equally essential for actin cytoskeletal dynamics. Active cofilin stimulates actin filament disassembly and fragmentation and thereby accelerates actin filament turnover (Bamburg et al., 1999). These activities can cause several complex consequences in cells. Initially, active cofilin reduces the amount of polymerised actin by its depolymerisation and fragmentation activities. Provided that sufficient amounts of G-actin monomers are available for new filament formation, this can then lead to a local increase of F-actin, because fragmentation increases the number of free barbed ends, which are highly favoured sites for the formation of new filaments. Cofilin also plays an important role in stimulus-dependent actin filament assembly during lamellipodium formation and defines the direction of cell motility (Ghosh et al., 2004; Kiuchi et al., 2007). Thus, cofilin is an essential factor for fundamental actin-based process like cell cycle control, cell division and migration, endocytosis and phagocytosis (Bamburg, 1999; DesMarais et al., 2005). A tightly regulated cofilin activity is crucial for complex morphogenetic and developmental processes.

The opposing and synergistic activities of cofilin and Arp2/3 are shown schematically in Figure 2.

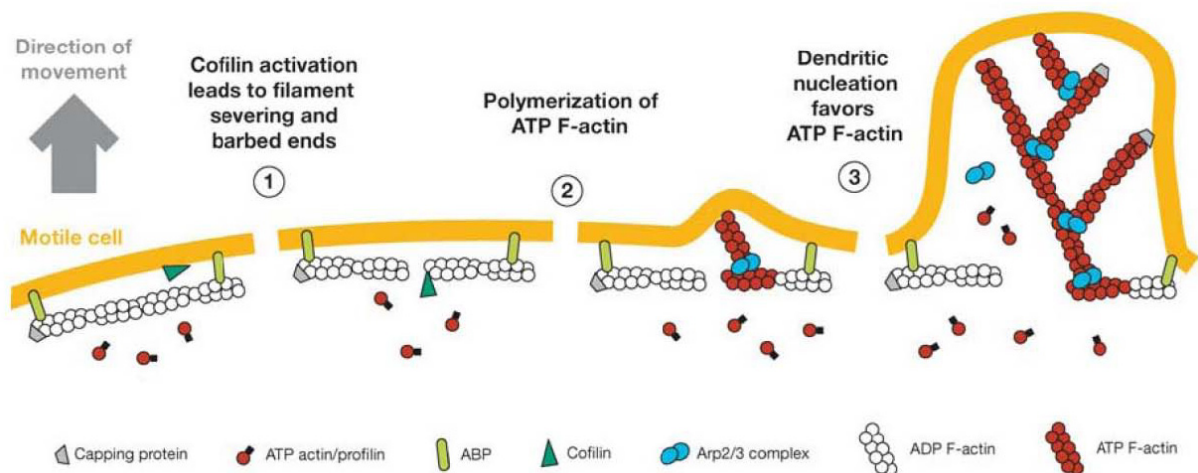


Figure 2: Interplay between Arp2/3-complex and cofilin functions.

The stimulated protrusion model showing the role of cofilin severing in determining the site of dendritic nucleation, protrusion, and cell direction. Severing of actin filaments in the cortical actin cytoskeleton by cofilin creates free barbed ends that bias the location and the amount of dendritic nucleation by the Arp2/3 complex. Polymerisation proceeds from a pool of pre-existing actin monomers, allowing the initiation of polymerisation to occur without being tightly coupled to depolymerisation. Taken from Condeelis et al., 2005.

1.3 The cofilin family of actin regulatory proteins

Cofilin activity is controlled by an inhibitory phosphorylation of a conserved, single serine residue (serine 3 in human and murine cofilin). The cellular balance between the active, non-phosphorylated form and the inactive, phosphorylated form of cofilin (phospho-cofilin or p-cofilin), is tightly regulated and shown schematically in Figure 3.

The signal transduction pathways leading to the phosphorylation and inactivation of cofilin are well characterised. It was shown that small GTPases of the Rho-family (in particular RhoA, Rac1, Cdc42), which are regulated through different G-protein coupled receptors (GPCRs) and receptor tyrosine kinases (RTKs), can induce a reorganisation of the actin cytoskeleton (Etienne-Manneville and Hall, 2002; Ridley, 2001). Rac1 and Cdc42 are known to activate the p21-activated kinases (PAKs), which phosphorylate and thereby activate LIM kinases (Edwards et al., 1999). LIM kinases, which include the two closely related isoforms LIMK1 and LIMK2, were identified as direct and specific cofilin-inactivating kinases (Arber et al., 1998; Yang et al., 1998). RhoA can activate the family of Rho-associated serine-threonine protein kinases (ROCKs), which can also activate LIM kinases (Maekawa et al., 1999). Other kinases known to directly phosphorylate and inactivate cofilin are the testicular protein kinases (TES kinases TESK1 and TESK2; (Toshima et al., 2001a; Toshima et al., 2001b). TESK activity is independent of ROCKs or PAKs and is regulated through integrin-mediated pathways (Toshima et al., 2001a). The result of cofilin phosphorylation is a block of cofilin activity in the assembly/disassembly and reorganisation of actin filaments. This typically leads to a net increase in the cellular filamentous actin (Agnew et al., 1995).

In addition to phosphorylation, other ways of cofilin inactivation include the binding of cofilin to phosphatidylinositol 4-phosphate or phosphatidylinositol 4,5-diphosphate. The lipid binding site of cofilin overlaps with its actin-binding domain and therefore inhibit cofilin binding to actin (Yonezawa et al., 1991). Phospho-cofilin can also associate with 14-3-3zeta proteins, which stabilise p-cofilin (Gohla and Bokoch, 2002). The depolymerisation of actin filaments by cofilin was shown to be pH-dependent and to occur over a physiologically relevant pH-range: localised increases in pH can enhance actin depolymerisation by cofilin, whereas the localised decreases in pH can inactivate the depolymerisation ability of cofilin (Bamburg et al., 1999; Ressad et al., 1998).

Whereas kinases that inactivate cofilin by phosphorylating it on serine 3 are well characterised, much less is known and understood about specific phosphatases that reactivate cofilin functions. The existence of specific cofilin phosphatases to counteract the functions of specific cofilin kinases for the appropriate balance between the active and inactive forms of cofilin has been long postulated in the literature, but such phosphatases were long elusive (Bamburg, 1999; Bamburg et al., 1999).

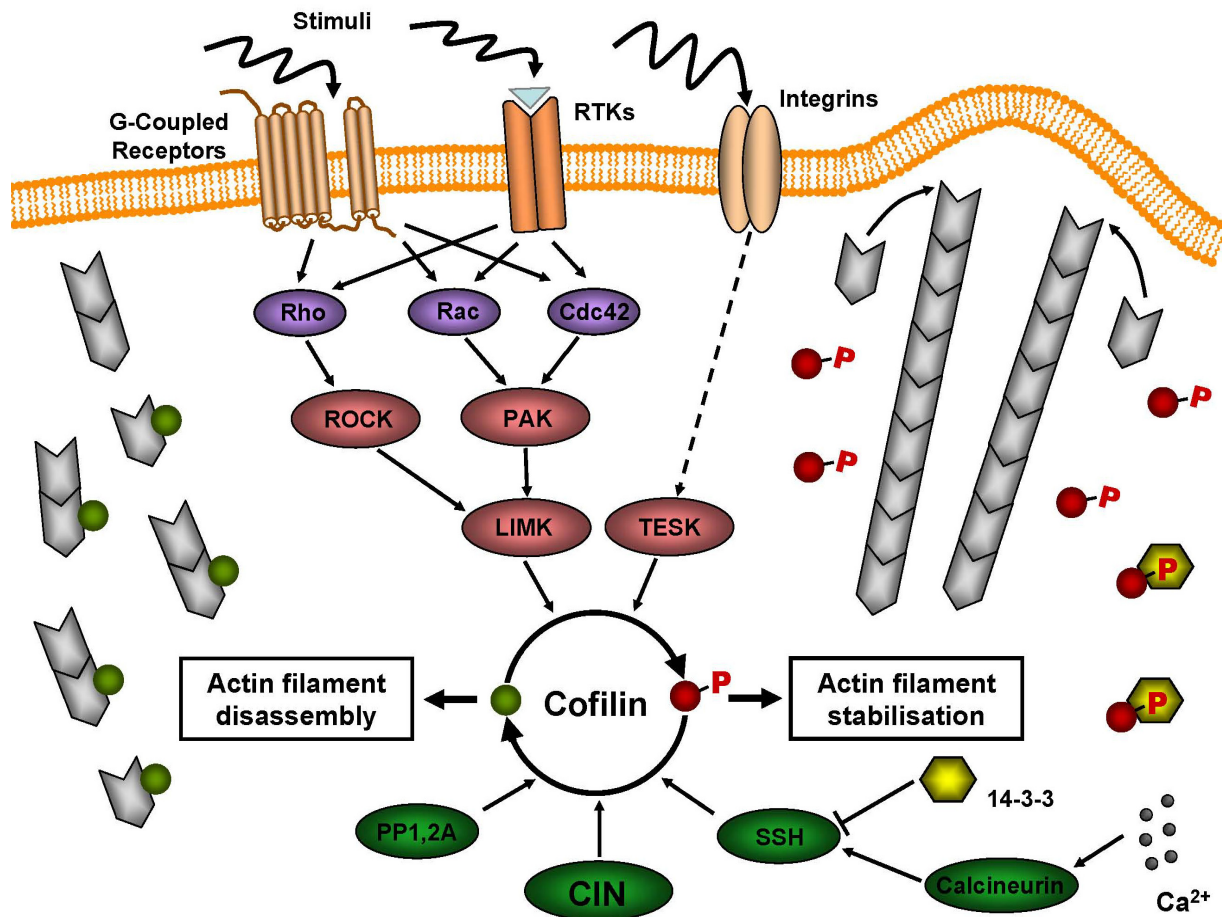


Figure 3: Regulation of cofilin activity.

In cells, cofilin exists in two different forms: an active nonphosphorylated form, and an inactive form phosphorylated at serine 3. Active cofilin binds to actin and induces a rapid depolymerisation of actin filaments. Cofilin activity is blocked by LIMK- or TESK-mediated phosphorylation at serine 3. Upon cell stimulation by various agonists acting through G protein-coupled receptors or receptor tyrosine kinases (RTKs), LIMKs are activated either by PAKs or through Rho-ROCK pathway. TESKs are activated in an integrin-dependent manner. Cofilin can be reactivated by specific phosphatases such as Slingshot (SSH) isoforms or Chronophin (CIN). Protein phosphatases PP1 and PP2A predominantly dephosphorylate cofilin in human T lymphocytes and *in vitro*. For more details, see text.

The serine/threonine protein phosphatases type 1 and type 2A (PP1 and PP2A) are able to associate with cofilin and also dephosphorylate this protein and thereby mediate cofilin activation in T lymphocytes (Ambach et al., 2000). However, the roles of PP1 and PP2A may be a cell type-specific, because the activation and dephosphorylation of cofilin in other cell types was shown to occur even in the presence of specific inhibitors of PP1 and PP2A.

The Slingshot (SSH) family of cofilin phosphatases was identified by genetic screens in flies (Niwa et al., 2002). The SSH enzymes contain a phosphatase domain with sequence similarity to mitogen-activated protein kinase (MAPK) phosphatases, have F-actin binding properties, and can dephosphorylate and thus reactivate cofilin in cultured cells and in cell-free assays. SSH was also shown to dephosphorylate other actin-regulatory proteins, such

as LIMK (Soosairajah et al., 2005) and Coronin 1B (Cai et al., 2007). Loss of SSH function in *D. melanogaster* dramatically increases the levels of both F-actin and p-cofilin and disorganises epidermal cell morphogenesis (Niwa et al., 2002). In mammalian cells, human SSH homologs suppress LIMK1-induced actin reorganisation. Slingshot phosphatases were also involved in the regulation of cytokinesis in animal cells (Kaji et al., 2003), in cell polarity and matrix assembly, which is important for epidermal cell migration (Kligys et al., 2007). The cofilin phosphatase activity of SSH increases ~10-fold by association of SSH with actin filaments (Nagata-Ohashi et al., 2004). SSH phosphatase activity is inhibited by PAK4-mediated phosphorylation (Soosairajah et al., 2005). PAK4-phosphorylated SSH is able to bind 14-3-3 proteins, which results in sequestering of SSH proteins into the cytoplasm and therefore in their inactivation (Nagata-Ohashi et al., 2004; Soosairajah et al., 2005). SSH phosphatase activity can be reactivated by dephosphorylation with calcineurin in Ca^{2+} -dependent manner (Wang et al., 2005). The activation of SSH by calcineurin is significant because cofilin undergoes dephosphorylation in response to extracellular stimuli that elevate intracellular Ca^{2+} concentrations. The Ca^{2+} /calcineurin-dependent SSH activation pathway is distinct from other known cofilin activation mechanisms, such as cAMP- or protein kinase C-dependent pathways (Meberg et al., 1998; Zhan et al., 2003).

Nevertheless, the expression of SSH phosphatases is largely restricted to epithelial cells (Niwa et al., 2002; Ohta et al., 2003), whereas its substrate cofilin is ubiquitously expressed. Also, some eukaryotic organisms can maintain functional actin reorganisation without SSH. For example, *C. elegans*, which has two cofilin isoforms, each of which is regulated by phosphorylation, has no gene encoding for a SSH-related phosphatase. As the regulation of F-actin by cofilin is essential for actin dynamics, other cofilin phosphatases must exist (Wiggin et al., 2005).

Chronophin (CIN) is a recently identified, ubiquitously expressed and evolutionarily conserved cofilin phosphatase, which belongs to the haloacid dehalogenase family of hydrolases and is structurally unrelated to SSH (Gohla et al., 2005). Currently, very little is known about physiological and potential pathophysiological functions and regulation of CIN.

1.4 Characterisation of CIN

CIN was isolated biochemically from bovine brain cytosol using sequential column chromatography (Gohla et al., 2005). Fractions were screened for an activity that could dephosphorylate purified p-cofilin. The fraction containing cofilin phosphatase activity was further analysed in an in-gel phosphatase assay, and relevant protein bands were sequenced by tandem mass spectrometry. This approach led to the identification of a putative serine phosphatase with an unconventional structure of the catalytic domain. In

contrast to SSH, CIN is a broadly expressed enzyme with highest expression found in brain (Gohla et al., 2005).

CIN is a member of the aspartate-dependent haloacid dehalogenase (HAD) family of phosphatases. HAD phosphatases are a subfamily within the large and ancient family of HAD hydrolases. The HAD superfamily includes more than 2000 different members from all species and comprises P-type ATPases, phosphatases, epoxide hydrolases and L-2-haloacid dehalogenases (Ridder and Dijkstra, 1999). All HAD enzymes are characterised by three short and highly conserved sequence motifs, called HAD domains, which line the catalytic pocket of the enzyme and determine its substrate specificity. HAD phosphatases are characterised by the first N-terminal HAD motif with the signature sequence DXDX(V/T), where X is any amino acid (Figure 4). The first aspartate residue is strictly conserved among phosphatases from different species and is catalytically essential. It was shown that mutation of this aspartate to asparagine in human CIN (D25N mutation) leads to inactivation of the catalytic activity of CIN phosphatase (Gohla et al., 2005). The second conserved aspartate in this domain stabilises the leaving phosphate group during the dephosphorylation step, and is thus an essential characteristic of HAD phosphatases.

All HAD phosphatases are Mg^{2+} -dependent enzymes that share a similar mechanism of substrate dephosphorylation by forming a phosphoaspartate intermediate (Ridder and Dijkstra, 1999). Thus, HAD phosphatases are insensitive to okadaic acid and calyculin A, which are typical inhibitors of cysteine-dependent phosphatases such as PP1 and PP2A. More than 20 human HAD phosphatases can be found by database searches, but until now, protein phosphatase activity has only been reported for a few of them: the magnesium-dependent phosphatase MDP1 (Selengut, 2001), the transcription factors Eyes absent (Eya) phosphatases (Li et al., 2003), and the cofilin phosphatase CIN (Gohla et al., 2005).

	Motif I	Motif II	Motif III	
H. sapiens	²¹ GVLFD CD GV L	⁵¹ GKAALFV S NN	²⁰³ LVV G KPS..... ²²⁴ LMV G DRLE T D	(NP_064711)
R. norvegicus	²¹ GVLFD CD GV L	⁵¹ GKATLFV S NN	²⁰⁵ LVV G KPS..... ²³⁰ LMV G DRLE T D	(XP_216983)
M. musculus	²¹ GVLFD CD GV L	⁵¹ GKNTLFV S NN	²⁰⁵ LVV G KPS..... ²³⁰ LMV G DRLE T D	(AAR12209)
D. rerio	²³ CVLFD CD GV I	⁵³ GKQV F FV T NN	²¹⁶ QVV G KPS..... ²⁴¹ LMV G DR L DTD	(AAH45860)
D. melanogaster	⁴¹ SV I FD CD GV L	⁷² GK S I F CT N NN	²³⁴ VV I G K PN..... ²⁵⁹ LM I GDR A NTD	(NP_649015)
C. elegans	⁵⁸ TF I FD AD GV L	⁸⁸ NK Q I I V L T N NN	²⁵⁹ LT V G K PC..... ²⁸⁴ MM I GDR T NTD	(NP_504511)
A. thaliana	²⁸ TF I FD CD GV I	⁵⁸ GK R LV F V T NN	²⁰⁴ LVV G KPS..... ²²⁹ CMV G DR L DTD	(BAA97552)
S. cerevisiae	²⁶ TF L FD CD GV L	⁵⁸ GK Q L I FV T NN	²²⁵ SY C G K PN..... ²⁵⁰ CMV G DR L NTD	(NP_010045)
S. pombe	²⁰ V F LFD CD GV L	⁵⁰ GK Q I I FV S NN	²¹⁶ K I L G K P Y..... ²⁴¹ CFV G DR L NTD	(NP_596255)
E. coli	⁵ N V I C D I DGV L	³⁵ GL P L V L L T N Y	¹⁷² F V Y G K P S..... ¹⁹⁷ V I V G DR L RTD	(NP_752680)
H. sapiens CIN(D25N)	²¹ G V L R NC D GV L	⁵¹ GKAALFV S NN	²⁰³ LVV G KPS..... ²²⁴ LMV G DRLE T D	
Consensus	ψψψDXDX(V/T)	ψψψS/T	K(X _n).....ψψψGD(X _n)(D/E)	

Figure 4: Alignment of the conserved HAD motifs in putative CIN orthologs.

All members of the HAD superfamily are characterised by three short and highly conserved sequence motifs. HAD phosphatases are characterised by the first HAD motif DXDX(V/T), where X is any amino acid. Black boxes show highly conserved residues, grey boxes indicate conserved hydrophobic residues (ψ). GenBank accession numbers of aligned proteins are given on the right. Taken from Gohla et al., 2005.

CIN was identified as an important regulator of cofilin-mediated actin cytoskeletal dynamics during cell migration and cell division (Gohla et al., 2005). It was shown that CIN directly dephosphorylates cofilin with high specificity and colocalises with its substrate cofilin in motile and dividing cells. Loss of CIN activity blocks cofilin phosphocycling, stabilises F-actin structures and causes massive cell division defects with a subsequent accumulation of multinuclear and aneuploid cells (Gohla et al., 2005). An altered cofilin activity has been causally linked to the initiation and progression of malignant tumours (Bamburg and Wiggan, 2002). Interestingly, the human CIN gene maps to chromosome 22q13.1, a region known to be affected in glial tumours (Ino et al., 1999; Nakamura et al., 2005; Nakamura et al., 2007). Genetic alterations found in glial tumours will be discussed further in chapter 1.6.

After the isolation and identification of CIN as a regulator of actin dynamics it became clear that this protein had been previously discovered as a protein with pyridoxal phosphate (PLP)-phosphatase activity that was referred to in the literature as PLPP or Pdxp. Fonda was the first who purified PLPP as an activity from human erythrocytes and characterised it as a phosphatase specific for phosphorylated vitamin B₆ compounds: pyridoxal-P, pyridoxine-P, pyridoxamine-P, 4-pyridoxic acid-P, and 4-deoxypyridoxine-P (Fonda, 1992). Fonda also demonstrated that PLPP requires Mg²⁺ for its activity and that it shows Michaelis-Menten kinetics with its substrates. Nevertheless, the molecular identity of "PLPP" was unknown at that time. Later on, using two tryptic peptide sequences derived from erythrocyte PLPP, BLAST searches of human EST databases were performed and a cDNA clone encoding PLPP was identified. Using this sequence information, PLPP was cloned by PCR amplification from a human brain cDNA library and catalytically active human PLPP was expressed in *E. coli* (Jang et al., 2003).

Interestingly, the non-protein CIN/PLPP substrate PLP is also known as a lysine-specific reagent, which can modify G-actin *in vitro*. It was shown that PLP reacts at pH 7.5 with 1.7-2 lysines on G-actin (Combeau and Carlier, 1992). PLP-actin can bind to the barbed ends of actin filaments and prevent dilution-induced depolymerisation like a capping protein. PLP-actin copolymerises with unmodified actin, and the stability of F-actin copolymers decreases with the fraction of PLP-actin incorporated, consistent with a model within which the actin-PLP-actin interactions in the copolymer are 50-fold weaker, and PLP-actin-PLP-actin interactions are 200-fold weaker than regular actin-actin interactions (Combeau and Carlier, 1992). If the interaction of PLP with G-actin also happens in cells, then the dual phosphatase activity of CIN may play an important role in the formation of new and more stable F-actin polymers: CIN dephosphorylates and activates cofilin, which leads to depolymerisation of F-actin and formation of the new pool of G-actin. At the same time, CIN dephosphorylates PLP, which decreases the number of PLP-actin complexes, and which will in turn increase the stability of the new F-actin polymers in cells.

1.5 Role of the cofilin pathway in tumours

Cofilin and its regulatory factors that tightly control the cofilin activity in cells are essential factors for fundamental actin-based processes like cell cycle control, cell division, cell motility, morphogenesis, endocytosis and phagocytosis (Bamburg, 1999; DesMarais et al., 2005; Wang et al., 2007a). Altered cofilin production, regulation or localisation have been linked to the initiation and progression of numerous human diseases, including Alzheimer's and ischemic kidney diseases, cognitive impairment, inflammation, infertility, immune deficiencies and different malignancies (Bamburg and Wiggan, 2002).

There are at least three general aspects of tumour biology in which cofilin and its phosphoregulation play a significant role: the initial process of cellular transformation (Pawlak and Helfman, 2002); cell division (Amano et al., 2002; Gunsalus et al., 1995; Kaji et al., 2003; Nagaoka et al., 1995; Yang et al., 2004); and enhanced cell motility during metastasis (Condeelis et al., 2001; Ghosh et al., 2004; Wang et al., 2007a).

Reduced cofilin activity has been shown to block the mitotic progression and cytokinesis, and to cause an accumulation of multinuclear and aneuploid cells (Abe et al., 1996; Amano et al., 2002; Gunsalus et al., 1995; Yang et al., 2004). Aneuploidy is a hallmark of most tumours and defects in the mitotic machinery leading to aneuploidy can also cause genetic instability and lead to tumour initiation and progression (Pihan and Doxsey, 1999; Ross, 1996). Aneuploidy is therefore often discussed in the literature as a causative mechanism of tumour formation (Pihan and Doxsey, 1999; Ross, 1996). On the contrary, other reports have shown that aneuploidy may prevent tumourigenesis (Weaver and Cleveland, 2007).

Cofilin and its regulatory kinases are dysregulated in different types of tumours. Cofilin itself is overexpressed at transcript level in the highly invasive C6 rat glioblastoma cell line (Gunnarsen et al., 2000), at protein level in A549 human lung cancer cells (Keshamouni et al., 2006) and in human pancreatic cancer cells (Sinha et al., 1999). The overexpression of cofilin at transcript level using a cDNA microarray approach has been shown for the invasive subpopulation of tumour cells in mammary tumours of rats (Wang et al., 2004) and in clinical samples of ovarian cancer (Martoglio et al., 2000). Furthermore, increased levels of cofilin expression are detected using proteomic analysis in clinical tumour samples of oral squamous-cell carcinoma (Turhani et al., 2006) and renal cell carcinoma (Unwin et al., 2003). In contrast, other studies showed a downregulation of cofilin in invasive tumour cells. The downregulation of cofilin was observed by proteomic analysis in highly metastatic MHCC97-H hepatocellular carcinoma cells (Ding et al., 2004), and in ovarian surface epithelium cells (Smith-Beckerman et al., 2005). Furthermore, cell lines derived from T-cell

lymphoma (Jurkat) and carcinomas from the cervix (HeLa), colon (KM12), liver (HepG2) and kidney (COS1) are characterised not by changes in the expression levels of cofilin, but by decreased amounts of phosphorylated cofilin and thus by an increase in potentially active cofilin (Nebi et al., 1996). Thus, determining the expression status of cofilin alone is insufficient to describe the characteristics of tumour cells, such as proliferation, migration and invasion. Rather, the balanced contribution of cofilin and other molecules in the cofilin regulatory pathways has to be taken into account (Wang et al., 2007a).

The family of LIM kinases, which inactivate cofilin by phosphorylation on serine-3, consists of two isoforms: LIM kinase 1 (LIMK1) and LIM kinase 2 (LIMK2). Both LIMK1 and LIMK2 are ubiquitously expressed proteins, but knockout studies in mice suggest a more predominant role for LIMK1 in the brain and for LIMK2 in testes (Bernard, 2007). In cells, LIMK1 localises mainly to focal adhesions, and LIMK2 is found in cytoplasmic punctae that resemble endosomes (Acevedo et al., 2006). This different subcellular localisation of LIMK1 and LIMK2 suggests that they may have different cellular functions (Bernard, 2007). The LIM kinases have been proposed to play an important role in tumour cell invasion and metastasis (Bernard, 2007; Scott and Olson, 2007). LIMK1 is overexpressed in melanoma, ovarian carcinoma, lung, breast, prostate cancer tumours and the corresponding cell lines (Davila et al., 2003; Davila et al., 2007; Wang et al., 2007a; Yoshioka et al., 2003). However, the initial reports on whether or not the overexpression of LIMK1 increases or decreases cell invasion are inconsistent (Wang et al., 2007a). It was shown that overexpression of a constitutively active LIMK1 in mammary carcinoma cells increases the amount of phospho-cofilin *in vivo* and inhibits actin polymerisation and cell motility in response to EGF (Zebda et al., 2000). In addition, the overexpression of LIMK1 inhibits cell motility in Ras-transformed fibroblasts (Sahai et al., 2001) and in neuroblastoma cell lines, whereas the expression of dominant-negative LIMK1 in neuroblastoma cell lines increases cell motility (Meyer et al., 2005). In contrast, the inhibition of LIMK1 expression by siRNA inhibits the motility of Jurkat T cells (Nishita et al., 2005). In addition to these findings, it was described that the overexpression of LIMK1 increases invasiveness of prostate epithelial cells, and that a reduction of LIMK1 expression levels in these cells decreases their ability to invade matrigel *in vitro* (Davila et al., 2003). Thus, differences in the expression level and activity of LIMK1 have major effects on tumour cell motility and invasion. However, the opposing conclusions from studies on the effects of LIMK1 expression on tumour invasion support the need of investigating not only single components of the cofilin pathway, but rather multiple key regulators and the final output of the cofilin pathway (Wang et al., 2007a).

Clinical studies of bladder, breast, and colorectal cancers have implicated Rho A and ROCK kinase, which phosphorylates and activates LIMK1, to be upregulated in these cancers (Condeelis et al., 2005). Other upstream activators of LIMKs, the p21 activated kinases (PAKs), are serine/threonine kinases important for a wide variety of cellular functions including cell morphogenesis, motility, survival, mitosis, and angiogenesis. Six different isoforms of the p21 activated kinases, PAK1 – PAK6, are now characterised. PAK1, PAK2 and PAK3 are structurally very similar but differ in their tissue distribution: PAK1 is expressed in the brain, muscle, and spleen; PAK2 is a ubiquitously expressed protein; and PAK3 is expressed only in the brain (Jaffer and Chernoff, 2002). Based on their conserved structure, PAK1, PAK2 and PAK3 are classed together as Group I PAKs. Three other isoforms PAK4, PAK5 and PAK6 are classed as Group II PAKs. PAK4 is expressed in most examined tissues, with the highest levels in the prostate, testis, and colon (Abo et al., 1998; Callow et al., 2002). PAK5 expression is brain-specific (Jaffer and Chernoff, 2002) and PAK6 has the highest expression in testis and prostate (Yang et al., 2001). PAKs of the Group I bind to and are stimulated by activated forms of the small GTPases Cdc42 and Rac1. In contrast, Group II PAKs are able to bind to, but are not stimulated by small GTPases (Jaffer and Chernoff, 2002). Interestingly, PAK4 is known to be particularly important for cell transformation and anchorage-independent cell growth (Callow et al., 2002; Qu et al., 2001).

Overexpression of PAK1 in epithelial cancer cells has been shown to increase migration potential and cause abnormalities in mitosis (Kumar and Vadlamudi, 2002; Vadlamudi and Kumar, 2003). The overexpression of PAK1 at the protein level or its gene amplification are shown for breast, colon, ovarian, bladder and brain cancers (Kumar et al., 2006). Additionally, gene amplification and protein overexpression of PAK4 isoform are shown in pancreatic cancer (Mahlamaki et al., 2004). A multitude of different PAK substrates have either been linked to tumourigenesis or may be potentially involved in tumour formation as reviewed by Kumar (Kumar et al., 2006) and shown in Table 1.

In contrast to the relatively well documented dysregulation of cofilin expression and its deactivating kinases in tumours, there is almost no information about the potential role of cofilin-activating phosphatases in tumours. Coordinated overexpression of cofilin itself, LIM kinase and SSH phosphatase has been shown by microarray studies of invasive mammary tumours (Wang et al., 2007a). Interestingly, UniGene and EST expression information indicates CIN phosphatase overexpression in neuroblastomas and germ cell seminomas (Gohla et al., 2005). Intriguingly, the human CIN gene localises to chromosome 22q13.1, a previously reported 'hot spot' in glial tumours (Ino et al., 1999; Nakamura et al., 2005; Nakamura et al., 2007). However, there is currently no information about CIN expression or its potential role in glial tumours.

Table 1: PAK substrates with a proven role in tumourigenesis or potentially involved in tumour formation (Kumar et al., 2006)

PAK isoform	PAK effectors	Cellular function	Associated tumour types
PAK1, PAK2	Merlin	Microfilament–membrane attachment and Rho signal-transduction pathways	Neurofibromatosis 2 (NF2)
PAK1	PGAM	Enzyme in glycolysis	Lung, colon, liver, prostate, breast, brain
PAK1	PGM	Enzyme at branch point of glycolysis and sucrose catabolism	Breast
PAK1, PAK2	p47 (phox)	Subunit of NADPH oxidase — production of ROS	Colon
PAK3	p67 (phox)	Subunit of NADPH oxidase — production of ROS	Neuroblastoma, melanoma
PAK1	RAF1	MAP3 kinase downstream of Ras	T-cell lymphoma
PAK1	NFκB	Transcriptional regulator	Breast, sarcoma, lymphoma, gastric
PAK1	FKHR	Forkhead family cofactors	Breast
PAK1, PAK2	BAD	Apoptosis	Leukaemia, breast
PAK1	DLC1	Component of dynein and myosin motor complexes	Breast
PAK1	Filamin	Cross links actin filaments and regulates cytoskeletal rearrangements	Melanoma, oesophageal
PAK1	TCoB	Chaperone involved in tubulin folding	Breast
PAK1, PAK2, PAK4	LIMK	Signalling molecule involved in cytoskeletal reorganisation	Prostate
PAK1	OP18 (stathmin)	Microtubule regulator and intracellular relay protein of stathmin family	Leukaemia, ovarian, lung, lymphoma, breast, prostate, neuroblastoma
PAK1	p41-ARC	A subunit of Arp2/3 complex with a role in actin reorganisation	Breast
PAK1	Vimentin	Intermediate filament protein	GBM, prostate, breast
PAK1	ESR1	Nuclear receptor activated by steroid hormone, oestrogen; functions as a transcriptional factor	Breast
PAK1	SHARP	Hormone-inducible corepressor	Breast
PAK1	CTBP1	Transcriptional corepressor that interacts with polycomb complex	Leukaemia, breast, lymphoma, melanoma
PAK1	SNAI1	Zinc-finger transcriptional repressor involved in EMT	Hepatocellular carcinoma, breast, ovarian, oesophageal

Abbreviations: CTBP1, C-terminal binding protein 1; ESR1, oestrogen receptor 1; NFκB, nuclear factor κB; PGM, phosphoglucomutase; PGAM, phosphoglycerate mutase; ROS, reactive oxygen species; FKHR, forkhead transcription factor; BAD, BCL2-antagonist of cell death; SNAI1, snail homologue 1.

1.6 Characterisation of glial tumours

The classification of different brain tumours according to the World Health Organisation (WHO) is based on the cell types that predominate within the tumour mass and is shown in Table 2. Astrocytic tumours, or astrocytomas, are the most common tumour type affecting the central nervous system. They originate from astrocytes, a type of glial cell, and are classified into increasing grades of malignancy with the most aggressive form being grade IV, the glioblastoma multiforme (GBM), which is almost invariably fatal.

The highly aggressive GBM tumours develop either as a result of the malignant progression from low-grade gliomas (secondary glioblastomas) or, more frequently, develop rapidly in a *de novo* manner (primary glioblastomas). Morphologically, primary and secondary glioblastomas cannot be distinguished (Reifenberger and Collins, 2004), but the examination of two molecular aberrations, TP53 mutations and epidermal growth factor receptor (EGFR) amplifications, has revealed correlations with the type of glioma as defined on a clinical basis. Specifically, tumours with TP53 mutations are more likely to be secondary GBMs, whereas primary GBMs are more likely to harbour EGFR amplifications (Reifenberger and Collins, 2004; Schwartzbaum et al., 2006). In both cases, prognosis is very poor, and the median survival of patients when radiotherapy and chemotherapy are combined is only 14.6 months. This is largely due to the fact that GBMs are characterised by a diffuse and extensive dissemination of tumour cells within the brain that prevents a complete surgical resection of the tumour mass (Vescovi et al., 2006). Molecular mechanisms that dictate this locally invasive behaviour of GBMs still remain very poorly understood (Hoelzinger et al., 2005). On a morphological level, GBMs are characterised by hypercellularity, the occurrence of mitotic figures, and nuclear abnormalities (Reifenberger and Collins, 2004; Schwartzbaum et al., 2006).

Table 2: WHO classification of brain tumours (Vescovi et al., 2006)

Group of tumours	Diseases
Astrocytic tumours	<ul style="list-style-type: none"> • Diffuse astrocytoma (grade II) • Anaplastic astrocytoma (grade III) • Glioblastoma (GBM; grade IV)
Oligodendroglial tumours	Oligodendroglioma
Mixed gliomas	Oligoastrocytoma
Ependymal tumours	Ependymoma
Neuronal and mixed tumours	Gangliocytoma
Neuronal/glial tumours	<ul style="list-style-type: none"> • Dysembryoplastic neuroepithelial tumour • Ganglioglioma
Embryonal tumours	<ul style="list-style-type: none"> • Medulloepithelioma • Ependymoblastoma • Neuroblastoma
Primitive neuroectodermal	Medulloblastoma

A number of genetic changes (deletions, amplifications, gains) in several chromosomal regions have been identified using classical cytogenetic and array-based comparative genomic hybridization studies of gliomas. Chromosomal amplifications and gains may point to genes involved in tumour initiation or progression (oncogenes), whereas chromosomal regions characterised by deletions and loss of heterozygosity in tumours might point to genes involved in tumour suppression. The chromosomal alterations that are most regularly observed in gliomas are summarised in Table 3 (Schwartzbaum et al., 2006). For example, inactivation of PTEN signalling, either by mutation, deletion, or loss of expression of PTEN itself or by alterations of the other genes involved in the PTEN/PI3K/Akt signalling pathway, has been linked to the malignant progression of glioblastomas. Aberrant PTEN/PI3K/Akt signaling may contribute to several characteristic biologic features of GBMs, such as loss of cell-cycle control and uncontrolled proliferation, escape from apoptosis, brain invasion, and aberrant neoangiogenesis (Knobbe et al., 2002).

Table 3: Common chromosomal alterations in gliomas (Schwartzbaum et al., 2006)

Chromosomal region	Type of alteration	Candidate glioma genes
1p36.31-pter	Gains and deletions	Not known
1p36.22-p36.31	Gains and deletions	Not known
1p34.2-p36.1	Gains and deletions	Not known
1q32	Gains	DSTYK, MDM4, PIK3C2B and
4q	Deletions	NEK1, NIMA
7p11.2-p12	Amplifications or gains	EGFR
9p21-p24	Deletions	CDKN2
10q23	Deletions	PTEN
10q25-q26	Deletions	MGMT
11p	Deletions	Between CDKN1C and RRAS2
12q13.3-q15	Amplifications	MDM2, CDK4 and others
13p11-p13 and 13q14-	Loss	Retinoblastoma 1
19q13	Loss	GLTSCR1, GLTSCR2, LIG1, PSCD2 and many others
22q11.21-q12.2	Loss	28 genes, including SMARCB1
22q13.1-q13.3	Loss	Not known

Abbreviations: DSTYK, dual serine/threonine and tyrosine protein kinase; MDM2, 4, Mdm2, 4 p53 binding protein homolog (mouse); PIK3C2B, phosphoinositide-3-kinase, class 2, beta polypeptide; NEK1, NIMA (never in mitosis gene a)-related kinase 1; CDKN, cyclin-dependent kinase inhibitor; PTEN, phosphatase and tensin homolog; MGMT, O-6-methylguanine-DNA methyltransferase; RRAS2, related RAS viral (r-ras) oncogene homolog 2; CDK4, cyclin-dependent kinase 4; GLTSCR, glioma tumour suppressor candidate of unknown function; LIG1, ligase I, DNA, ATP-dependent; PSCD2, pleckstrin homology, Sec7 and coiled/coiled domains 2; SMARCB1, SWI/SNF related, matrix associated, actin dependent regulator of chromatin, subfamily b, member 1.

Although several well-known tumour suppressor genes and oncogenes are located in the regions affected by alterations known for glioblastoma and shown in Table 3, many other genes located in these regions have yet to be examined for their specific relationship with gliomagenesis (Schwartzbaum et al., 2006). One interesting chromosomal alteration is the loss of heterozygosity on chromosome 22q13.1, *i.e.*, the region where the CIN gene is located. Characterisation of the 22q deletions in primary glioblastomas has identified a minimally deleted region of 957 kb at 22q12.3-13.2. This short region shows a loss of heterozygosity in 41% of primary and in about 82% of secondary glioblastomas (Nakamura et al., 2005), indicating that this alteration is related to glioma progression (Laigle-Donadey et al., 2006). These data may indicate the presence of unidentified tumour suppressor genes at this location. Other hallmark features of most GBMs are a deregulation of the cell cycle (Schwartzbaum et al., 2006), the presence of multinucleated, giant cells with accompanying alterations of the actin cytoskeleton, and the occurrence of other nuclear abnormalities which often serve as diagnostic markers (Reifenberger and Collins, 2004).

The known role of the cofilin-activating phosphatase CIN in the regulation of actin cytoskeletal dynamics during cell division together with the established involvement of the cofilin pathway in tumour invasion and metastasis and the intriguing localisation of the CIN gene to a region frequently deleted in glioblastomas has led us to investigate the possible function of CIN in glioblastomas.

2 Aims of the study

Proteins of the cofilin family of actin reorganising proteins are essential regulators of cell migration, -invasion and -division. Chronophin (CIN) is a recently identified cofilin activating phosphatase that is highly expressed in brain. The loss of CIN-mediated cofilin activation leads to massive cell division defects with a subsequent accumulation of aneuploid cells. Aneuploidy is a hallmark of most tumours, and an altered cofilin activity has been causally linked to the initiation and progression of malignant tumours. Reduced cofilin activation (due to increased activity of cofilin kinases and/or reduced activity of cofilin phosphatases) has also been implicated in changes in the motile and invasive behaviour of tumour cells. The CIN gene maps to human chromosome 22q13.1 in a short region that is frequently deleted in astrocytic tumours. The frequency of loss of heterozygosity on chromosome 22q13.1 strongly increases with the tumour malignancy grade, suggesting the presence of thus far unidentified tumour suppressor genes.

The aim of this thesis was to analyse the potential role of CIN for astrocytoma pathogenesis. Therefore, we

- investigated the protein expression of key components of the cofilin pathway in tumour samples from astrocytomas with different grades of malignancy
- established a glioblastoma model cell line to analyse the consequences of CIN depletion for actin cytoskeletal dynamics, cell transformation and cell invasion, and
- analysed the role of CIB1, a newly identified CIN regulatory protein, for CIN activity.

A better understanding of the cellular pathways and molecular mechanisms involved in the initiation and progression of astrocytic tumours is expected to contribute to the development of new molecular targets for the treatment and prevention of this disease.

3 Materials

3.1 List of manufacturers and distributors

- (1) AppliChem, Darmstadt
- (2) Amersham Biosciences, Little Chalfont, UK
- (3) ATCC, Manassas/VA, USA
- (4) BD Becton Dickinson GmbH, Heidelberg
- (5) Beckman Coulter, Krefeld
- (6) Bio-Rad, München
- (7) Biomol (brand of Enzo life sciences), Lössrach
- (8) BMG Labtech, Offenburg
- (9) Carl Zeiss AG, Jena
- (10) Calbiochem, Darmstadt
- (11) Cell Signaling Technologies, Danvers/MA, USA
- (12) Cytoskeleton Inc., Denver/CO, USA
- (13) Dako, Glostrup, Denmark
- (14) Dharmacon RNAi Technologies (part of Thermo Fisher Scientific), Schwerte
- (15) Fermentas, St. Leon-Rot
- (16) Fujifilm, Düsseldorf
- (17) GATC Biotech, Konstanz
- (18) Genaxxon Bioscience, Biberach
- (19) Invitrogen, Karlsruhe
- (20) Leica Microsystems, Wetzlar
- (21) Menzel, Braunschweig
- (22) Merck, Darmstadt
- (23) MP Biomedicals, Eschwege
- (24) Nikon GmbH, Düsseldorf
- (25) Operon Biotechnologies, Köln
- (26) Pierce, Rockford/MA USA
- (27) Promega, Heidelberg
- (28) Qiagen, Hilden
- (29) Raytest, Straubenhardt
- (30) R&D Systems, Wiesbaden-Nordenstadt
- (31) Roche Applied Science, Mannheim
- (32) Roth, Karlsruhe
- (33) Sakura Finetek, Zoeterwoude, Holland

-
- (34) Santa Cruz, Heidelberg
(35) Serva, Heidelberg
(36) Schleicher & Schuell, Dassel
(37) Sigma-Aldrich, Deisenhofen
(38) Takara Bio Europe, Saint-Germain-en-Laye, France
(39) TPP, Trasadingen, Switzerland
(40) Upstate/Millipore, Schwalbach
(41) Vector Laboratories, Burlingame/CA, USA

3.2 Chemicals

Acetic acid	(22)
Acrylamide/bisacrylamide (37.5:1)	(32)
Agarose, "low-melting"	(18), (37)
Ampicillin	(32)
Aprotinin	(37)
APS	(37)
BES	(10)
BSA	(1), (32)
BSA, receptor grade (for immunohistochemistry)	(35)
Bromophenol blue	(35)
Calcium chloride (CaCl ₂ ·6H ₂ O)	(22)
Crystal violet	(37)
dATP, dCTP, dGTP, dTTP	(18)
Difco Agar Noble	(4)
DMSO	(1)
DTT	(37)
DNase	(37)
EDTA	(37)
EGTA	(10)
Ethanol	(32)
Ethidium bromide	(37)
Gelatine	(22)
Glycerol	(1)
Glycine	(22)
HCl	(32)
Hepes	(37)

LB Agar (powder)	(1)
LB Medium (powder)	(1)
Leupeptin	(37)
Magnesium chloride (MgCl ₂)	(37)
Magnesium acetate (Mg(CH ₃ COO) ₂ ·4H ₂ O)	(37)
β-Mercaptoethanol	(1)
Methanol	(32)
MG132	(7)
TEMED	(37)
Na-azide (NaN ₃)	(22)
NaCl	(1), (22)
Na-deoxycholate	(22)
Na-orthovanadate (Na ₃ VO ₄)	(22)
Ni-sulfate (NiSO ₄)	(37)
Nocodazole	(37)
NP-40	(10)
Pepstatin	(1)
PFA	(37)
Phosphatase inhibitor cocktail 1 and 2	(37)
PLP	(37)
p-NPP	(10)
Polybrene (1,5-dimethyl-1,5-diazaundecamethylene polymethobromide)	(37)
Ponceau S	(37)
Potassium acetate (CH ₃ COOK)	(37)
2-Propanol (C ₃ H ₈ O)	(32)
Protease inhibitor cocktail tablets (complete, EDTA-free)	(31)
Puromycin	(23)
RNase A	(37)
SDS	(35)
Saponine	(1)
Thymidine	(1)
Tris, Tris-base	(32)
Triton X-100	(37)
Tween-20	(1)
Water (PCR quality)	(22)

3.3 Reagents for immunoblotting

Micro BCA Protein Assay kit	(26)
Milk powder	(32)
ECL Western Blotting Detection System	(2), (26)
Electrophoresis equipment	(6)
Horseradish peroxidase (HRP) anti-goat IgG	(26)
Horseradish peroxidase (HRP) anti-mouse IgG	(13)
Horseradish peroxidase (HRP) anti-rabbit IgG	(26)
Hybond-C Extra (nitrocellulose membrane optimised for protein transfer)	(2)
Whatman GF/B paper	(36)
X-ray films	(16)

3.4 Reagents for immunohistochemistry

Anti-rabbit IgG HRP-linked antibody	(11)
DAB	(13)
Entellan	(22)
NGS	(13)
Polysine slides	(21)
Rabbit IgG, isotype control antibody	(26)
Tissue-Tek	(33)
Vectastain ABC Kits	(41)
Xylene	(22)

3.5 Cell culture, cell culture media and supplements

Cell culture plastic consumables	(39)
DMEM cell culture medium	(19)
DMEM-F12 medium	(19)
D-PBS	(18), (19)
EGF (human, recombinant, E. coli)	(10)
HGF (human, recombinant)	(30)
FCS origin EU approved, catalog #10270106	(19)
L-Glutamine	(18)
Lipofectamine 2000 (reagent for transfection of mammalian cells)	(19)

OptiMEM medium	(19)
Penicillin/streptomycin (10,000 U/ml / 10,000 µg/ml)	(18)
SOC medium	(19)
Trypsin/EDTA (0.5/0.2%, 10x solution in PBS)	(18), (19)

3.6 Cell lines

All cell lines used in this work have been obtained from ATCC	(3)
---	-----

3.7 Protein and DNA standards

PageRuler prestained protein ladder	(15)
GeneRuler DNA ladder	(15)

3.8 Kits

AQueous One Solution Cell Proliferation Assay Kit	(27)
BD BioCoat Matrigel Invasion Chambers	(4)
High Fidelity RNA PCR kit	(38)
Micro BCA Protein Assay Kit	(26)
PiPer Phosphate Assay Kit	(19)
Qiagen Plasmid Maxi Kit	(28)
Qiagen Plasmid Mini Kit	(28)
QIAquick Gel Extraction Kit	(28)
Qiazol Reagent	(28)

3.9 Enzymes

Platinum Pfx DNA polymerase	(19)
Restriction enzymes	(15)
T4 DNA polymerase	(15)
T4 DNA ligase 5 U/µl	(15)

3.10 Reagents for microscopy

Alexa 488 goat anti-mouse IgG (H+L), highly cross-absorbed	(19)
Alexa 488 goat anti-rabbit IgG (H+L), highly cross-absorbed	(19)
Alexa 546 goat anti-mouse IgG (H+L), highly cross-absorbed	(19)
Alexa 546 goat anti-rabbit IgG (H+L), highly cross-absorbed	(19)
Alexa 568 goat anti-mouse IgG (H+L), highly cross-absorbed	(19)
Alexa 568 goat anti-rabbit IgG (H+L), highly cross-absorbed	(19)
Alexa 633 goat anti-mouse IgG (H+L), highly cross-absorbed	(19)
Alexa 633 goat anti-rabbit IgG (H+L), highly cross-absorbed	(19)
Alexa Fluor 488 Phalloidin	(19)
Alexa Fluor 546 Phalloidin	(19)
Alexa Fluor 633 Phalloidin	(19)
DAPI	(37)
Fluorescent mounting medium	(13)
Prolong Gold Antifade mounting medium	(19)

All other chemicals and standard buffer components used in this work were purchased either from Roth (32) or Sigma-Aldrich (37) with “pro analysi” (p.a.) grade. Confocal microscopy and FRET experiments were performed on a Zeiss LSM 510 Meta confocal microscope (9). Epifluorescence microscopy was conducted on a Nikon TE2000 Eclipse microscope (24). Tissue slices for immunohistochemistry were done using a Cryostat Leica CM 3050S (20) or a Microtom Leica SM 2000R (20). Oligonucleotides and primers were synthesised by Operon (25), and DNA sequencing was performed by GATC (17). A DIANA III Camera System (29) was used for the quantification of DNA bands in agarose gels, as well as for the chemiluminescence quantification of Western blot signals. The photometrical analysis DNA and RNA was performed on a DU800 spectrophotometer (5). A FLUOstar OPTIMA microplate reader (8) was employed for the measurement of protein concentration in BCA-assays and for the analysis of *in vitro* phosphatase assays.

3.11 Solutions and buffers

(in alphabetical order)

Antibody Diluent (for immunoblotting)	10 mM	Hepes, pH 7.4
	0.5 M	NaCl
	1%	BSA
	0.2%	Tween-20
	0.02%	NaN ₃
Blocking Buffer (for immunohistochemistry)	1 x	TBS
	2%	BSA receptor grade
	3%	NGS
BLOTTO Buffer (for immunoblotting)	50 mM	Tris, pH 8.0
	2 mM	CaCl ₂
	80 mM	NaCl
	5% (w/v)	milk powder
	0.2%	NP-40
DAB Solution (for immunohistochemistry)	50 ml	0.05 M Tris-HCl, pH 7.6
	1 tablet	DAB (10 mg)
	50 µl	nickel sulfate (13 mg/ml)
	6.5 µl	30% H ₂ O ₂
dNTP stock solutions (for PCR)	25 mM	of dATP, dCTP, dGTP, dTTP (each)
Hepes-Buffered Solution (HBS) (for FRET and live cell imaging)	10 mM	Hepes, pH 7.5
	5.5 mM	glucose
	138 mM	NaCl
	6 mM	KCl
	1 mM	MgCl ₂
	1 mM	CaCl ₂
	0.2% (w/v)	BSA

Laemmli Buffer (1x) (SDS-PAGE sample buffer)	62.5 mM	Tris-HCl, pH 6.8
	10% (v/v)	glycerol
	5% (v/v)	β -mercaptoethanol
	2% (w/v)	SDS
	0.02% (w/v)	bromophenol blue
Lysis Buffer I (for lysis of mouse tissues)	50 mM	Tris-HCl, pH 7.4
	150 mM	NaCl
	1% (v/v)	Triton X-100
	0.1% (w/v)	SDS
	1% (w/v)	Na-deoxycholate
	1 mM	EDTA
	0.5 mM	Na_3VO_4
	1 mM	NaF
1x	protease inhibitor cocktail	
Lysis Buffer II (for lysis of brain cancer samples)	50 mM	Tris-HCl, pH 7.4
	150 mM	NaCl
	1% (v/v)	Triton X-100
	1% (v/v)	NP-40
	0.1% (w/v)	SDS
	1x	phosphatase inhibitor cocktail 1
	1x	phosphatase inhibitor cocktail 2
1x	protease inhibitor cocktail	
RIPA Buffer (for lysis of cultured cells)	50 mM	Tris-HCl, pH 8.0
	150 mM	NaCl
	1% (v/v)	NP-40
	0.1% (w/v)	SDS
	0.5% (w/v)	Na-deoxycholate
	1x	protease inhibitor cocktail
Running Buffer (10x), pH 8.7 (for SDS-PAGE)	250 mM	Tris-base
	2 M	glycine
	10%	SDS

Stripping Buffer (for reprobing of immunoblots)	62.5 mM 2% 100 mM	Tris-HCl, pH 6.7 SDS β -mercaptoethanol (added immediately before use)
--	-------------------------	---

TAE (50x) (for DNA gels)	2 M 100 mM	Tris-acetate, pH 8.0 EDTA
-----------------------------	---------------	------------------------------

TBS (10x) (for immunoassays)	0.5 M 1.5 M	Tris-HCl, pH 7.5 NaCl
---------------------------------	----------------	--------------------------

TBS-T (for immunoblotting)	50 mM 150 mM 0.1%	Tris-HCl, pH 7.5 NaCl Tween 20
-------------------------------	-------------------------	--------------------------------------

Transfer Buffers for semi-dry blotting:

Anode Buffer I	0.3 M 40%	Tris-base Methanol
----------------	--------------	-----------------------

Anode Buffer II	25 mM 40%	Tris-base Methanol
-----------------	--------------	-----------------------

Cathode Buffer	25 mM 40 mM 10%	Tris-base glycine methanol
----------------	-----------------------	----------------------------------

3.12 RNA interference tools

All siRNA oligoribonucleotides were obtained from Dharmacon (14). Four different synthetic siRNA oligoribonucleotides for human CIN were ordered as ON-TARGET plus Set of 4, (catalog # LQ-017120-00-0002). The ON-TARGET plus siCONTROL pool of 4 non-targeting siRNAs (catalog # D-001810-01-05) was used as a control in all siRNA experiments.

A functional human CIB1 siRNA has been published (Leisner et al., 2005). This CIB1 siRNA was synthesised as a duplex with the sense sequence 5'-GCAGGAGAUCUCCUAGCCUU, and the antisense sequence 5'-GGCUAGGAGGAUCUCCUGCUU.

To establish stably CIN-depleted cell lines, we employed a lentiviral system with CIN-directed shRNAs derived from the MISSION shRNA Program. Lentiviral plasmids (pLKO.1-puro) containing corresponding shRNAs were purchased from Sigma-Aldrich (37) as bacterial glycerol stocks (catalog # SHCLNG-NM_020271). Control shRNA plasmid (catalog # SHC002) was ordered as a DNA stock from Sigma-Aldrich (37).

Table 4: siRNA sequences used to downregulate CIN protein expression

Construct	Sense Sequence	Antisense Sequence
J-017120-05	CGGCAAGGCGGCUCUGUUUUU	5'-PAAACAGAGCCGCCUUGCCGUU
J-017120-06	GAGCAUCGCAGACUUGACAUU	5'-PUGUCAAGUCUGCGAUGCUCUU
J-017120-07	GCACGCUUAUGGUGGGUGAUU	5'-PUCACCCACCAUAAGCGUGCUU
J-017120-08	UCGAGUGCAUCACGGAGAAUU	5'-PUUCUCCGUGAUGCACUCGAUU
D-001810-01-05 mix of four control siRNAs	UGGUUUACAUGUCGACUAA	5'-PUUAGUCGACAUGUAAACCA
	UGGUUUACAUGUUUUCUGA	5'-PUCAGAAAACAUGUAAACCA
	UGGUUUACAUGUUUCCUA	5'-PUAGGAAAACAUGUAAACCA
	UGGUUUACAUGUUGUGUGA	5'-PUCACACCAACAUGUAAACCA

Table 5: Sequences of shRNA used to specifically down-regulate CIN expression

Construct	Insert sequence
TRCN0000050043	CCGGCCATTACTATGTGGAGAGCATCTCGAGATGCTCTCCACATAGTAATGGTTTTTG
TRCN0000050044	CCGGCATCACGGAGAACTTCAGCATCTCGAGATGCTGAAGTTCTCCGTGATGTTTTTG
TRCN0000050045	CCGGGCTCTGTTTGTGAGCAACAACCTCGAGGTTGTTGCTCACAAACAGAGCTTTTTG
TRCN0000050046	CCGGCCTACATGTTTCGAGTGCATCACTCGAGTGCCTCGAACATGTAGGTTTTTG
TRCN0000050047	CCGGTGTGGGCTACGACGAGCACTTCTCGAGAAGTGCTCGTCGTAGCCCACATTTTTG
SHC002, control	CCGGCAACAAGATGAAGAGCACCAACTCGAGTTGGTGCTCTTCATCTTGTGTTTTT

3.13 List of primary antibodies

Directed against	Type of Ab	Source
α -tubulin (clone DM1A)	mouse mAb	(37)
β -actin (clone C4)	mouse mAb	(23)
Calmyrin (CIB1)	mouse mAb	(19)
CIB1 (clone D-15)	goat pAb	(34)
CIN	rabbit mAb	(11)
cofilin	rabbit pAb	(12)
p-cofilin	rabbit pAb	(11)
p-cofilin	rabbit mAb	(11)
GFP	rabbit pAb	(19)
LimK1	rabbit pAb	(11)
LimK2	rabbit pAb	(11)
Myc Tag	mouse mAb	(10)
Myc Tag	rabbit pAb	(40)
PAK4	rabbit pAb	(11)
Phospho-PAK4(Ser474)/ PAK5(Ser602)/ PAK6(Ser560)	rabbit pAb	(11)

4 Experimental procedures

Standard molecular biology techniques were performed as described in “A Laboratory Manual”, Cold Spring Harbor Laboratory Press, NY, Vol 1-3 (Sambrook et al., 1989).

4.1 Transformation of bacteria

Fifty ng of plasmid DNA or 5 µl of a ligation reaction were mixed with 50 µl of chemically competent DH5α bacteria and incubated on ice for 30 min. After a brief heat shock (42°C for 1 min in a waterbath) and subsequent cooling on ice (2 min), 500 µl of SOC medium was added, and bacteria were incubated in shaker at 37°C for 30 – 60 min. The use of SOC medium in the final step of bacterial transformation maximises the transformation efficiency of *E. coli* (Hanahan, 1983). Cells were then centrifuged (10,000 x *g*, 1 min, RT) and the supernatant was discarded. Finally, cells were resuspended in 100 µl of LB medium and plated on LB plates containing the appropriate antibiotics. Plates were then incubated overnight at 37°C. The obtained antibiotic-resistant colonies were screened for the expression of the desired plasmids by isolating and digesting the DNA as described below (4.2, 4.3), and positive strains were either stored as glycerol stocks (in LB medium supplemented with 25 % (v/v) glycerol) at –70°C, or were expanded to isolate the DNA and were stored as DNA stocks at –20°C.

4.2 Plasmid isolation from *E. coli*

The *Qiagen Plasmid Mini Kit* (Qiagen) was used for the preparation of small amounts of DNA and for the screening of colonies. Briefly, 3 ml of LB medium supplemented with the appropriate antibiotic was inoculated with a single colony and was incubated overnight at 37°C with constant agitation. Cultures were transferred into 2 ml Eppendorf tubes and bacteria were pelleted by a brief centrifugation (12,000 rpm, 1 min, RT). Plasmids were then isolated from the bacteria according to the manufacturer’s instructions. The DNA was eluted from the columns by the addition of 50 µl of elution buffer (Tris-HCl 10 mM, pH 8.0) and was collected by centrifugation (12,000 rpm, 2 min, RT).

For the preparation of larger quantities of DNA, the *Qiagen Plasmid Maxi Kit* (Qiagen) was used. A single colony was inoculated in 2 ml of LB medium containing the appropriate antibiotic, and bacteria were grown at 37°C for 6-8 h with constant agitation. Afterwards, this culture was diluted in 100 ml of LB medium supplemented with the appropriate antibiotic and the culture was expanded overnight at 37°C with constant agitation. Bacteria were pelleted by centrifugation (6,000 x *g*, 15 min, 4°C) and the DNA was isolated as described in the manufacturer’s protocol. The DNA pellet was resuspended in 500 µl of Tris-HCl buffer (10 mM, pH 8.0) and the DNA concentration was determined. The DNA was diluted to a concentration of 0.5 – 1 µg/ml, aliquoted and stored at –20°C.

4.3 DNA gel electrophoresis and DNA preparation from gels

Restriction analysis and cloning was performed with restriction enzymes and buffers from Fermentas. The DNA was incubated with the recommended amounts of the appropriate restriction enzymes (1 U of enzyme per 1 mg of DNA) in a suitable buffer for 1 h at 37°C. Restriction was terminated by the addition of DNA loading buffer (Qiagen), and samples were subjected to agarose gel electrophoresis. Agarose gels were prepared by heating 1% (w/v) agarose (Sigma or Genaxxon) in 1xTAE buffer, followed by the addition of ethidium bromide (final concentration of approximately 0.5 µg/ml). The gels with DNA probes were run at constant voltage (100 – 120 V). Afterwards, DNA bands were detected using the DIANA III Camera System (Raytest).

The isolation and purification of DNA fragments from agarose gels was done using the *QIAquick Gel Extraction Kit* (Qiagen). Ethidium bromide-labelled DNA was visualised using UV-light, and the appropriate DNA band was excised from the gel with a scalpel and transferred into an Eppendorf tube. The gel slices were weighed, three volumes of the supplied buffer were added, and the gel slice was incubated for 10 min at 50°C to solubilise the agarose. Afterwards, one volume of isopropanol was added to the samples, and the DNA was separated from the obtained mixture by binding it to the supplied columns followed by a washing step with wash buffer. Afterwards, the DNA was eluted from the columns by the addition of 20 – 30 µl of elution buffer (Tris-HCl 10 mM, pH 8.0) and recovered by centrifugation (12,000 rpm, 1 min, RT). The obtained DNA fragments were further analysed by DNA agarose gel electrophoresis and were then used for cloning.

4.4 Isolation of total RNA

Total RNA from glioma cell lines, brain cancer samples or mouse tissues was isolated using *Qiazol Reagent* (Qiagen). This single-step RNA isolation procedure has been adapted from the original method as described by Chomczynski and Sacchi (Chomczynski and Sacchi, 1987). Briefly, an appropriate amount of *Qiazol Reagent* (1 ml of *Qiazol Reagent* per 50 - 100 mg of tissue or per 3.5 cm dish with adherent cells) was added to the samples. Samples were homogenised by pipetting, chloroform was added (0.2 ml per 1 ml of *Qiazol Reagent*), and samples were centrifuged (15,000 rpm, 30 min, +4°C) to separate the organic phase from the RNA-containing aqueous phase. RNA was then precipitated from the aqueous phase by mixing it with isopropyl alcohol (0.5 ml of isopropyl alcohol per 1 ml of *Qiazol Reagent* used for the initial homogenisation). The RNA pellet was washed once with 1 ml of 75% ethanol and redissolved in 20 µl of DEPC-water. After spectrophotometric determination of the RNA concentration and purity, total RNA was used in further experiments.

4.5 DNA constructs and cloning procedures

Full length murine CIN cDNA was cloned from mouse brain by RT-PCR. Total RNA was isolated from the whole brain of an adult C57/Bl6 mouse (as described under 4.4), and mouse brain cDNAs were generated by RT-PCR using the *High Fidelity RNA PCR Kit* (Takara), with Oligo dT primers (65°C for 1 min, 30°C for 1 min, 30°C for 30 s, with +1°C/cycle, 17 cycles). Full length CIN cDNA was amplified using Platinum Pfx Polymerase (PCR conditions: 5 min at 95°C, 25 cycles at 95°C for 1 min, 60°C for 1 min, and at 68°C for 1.5 min followed by 30 sec at 68°C) and the forward primer 5'-GAATTCGGATCCATGGCGCGCGCTGCGAGC-3' and the reverse primer 5'-CTGCAGTCATCTCGAGTAGTCCTCCAGCCCCTCCATC-3'. The PCR product was cloned into the pCRII-TOPO vector and sequenced.

CIN was subcloned from pCRII-TOPO into pcDNA3 and pTrcHis A *via* BamHI – EcoRI sites. For the construction of C-terminally tagged, fluorescent versions of CIN for FRET analysis, the mouse CIN coding sequence lacking the stop codon was cut from pCRII-TOPO using BamHI and XhoI, and was subcloned into pcDNA3-CFP or pcDNA3-YFP vectors. For the generation of a myc/His₆-tagged CIN, the same fragment was subcloned into pcDNA4-myc/His₆ with subsequent linearising of the obtained plasmid with XhoI, blunting it with T4 DNA polymerase, and ligating it with T4 ligase.

The phosphatase-dead point mutant of CIN, murine CIN-D25N (Gohla et al., 2005), was derived from murine CIN-WT by site directed mutagenesis. Briefly, 100 ng of pTrcHis-mCIN plasmid were used as a template in the mutagenesis reaction with the forward primer 5'-CGCAGGGAGTCCTGTTCAACTGCGACGGAGTGC-3' and its corresponding reverse complement primer. The PCR reaction was performed with Platinum Pfx Polymerase (5 min at 94°C, 12 cycles at 94°C for 30 sec, 58°C for 1 min, and 5 min at 68°C, followed by 1 min at 68°C). One µl of DpnI enzyme was added to the PCR mix for the digestion of the methylated template. The obtained PCR-product was transformed into chemically competent DH5α cells (see chapter 4.1), and resulting colonies were screened for the presence of the desired mutation by sequencing. Murine CIN-D25N was afterwards subcloned into pcDNA3 and into pcDNA4-myc/His₆ analogous to CIN-WT.

Mouse CIB1 was amplified by PCR using pcDNA3-CIB1 as a template, Native Pfu Polymerase and the forward primer 5'-GCAGGATCCGCCACCATGGGAGGTTTCGGGCAG-3' and reverse primer 5'-GGTGAATTCGCCAGGACAATCTTAAAGGAG-3'. The resulting CIB1 cDNA was directly cut from the obtained PCR product using BamHI and EcoRI, and was subcloned into pcDNA3-CFP and pcDNA3-YFP. To improve CIB1 expression levels, the CIB1 coding region was cloned together with the Kozak consensus sequence. The Kozak sequence is a short recognition sequence contained in most eukaryotic mRNAs which

enhances the initial binding of mRNA to the small subunit of the ribosome and thus facilitates the initiation of translation. In vertebrates, this sequence is (GCC)RCCATGG, where R is a purine (A or G) (Kozak, 1986, 1987).

The packaging vector psPAX2 and the envelope vector pCR-VSV-G were used for the production of lentiviruses as described previously (Schneider et al., 2007).

Positive (Schmid et al., 2001; Sunesen et al., 2003) and negative controls (Mielke et al., 2000) for FRET experiments have been published and were kindly provided by Dr. Christian Mielke, Zentralinstitut für Klinische Chemie und Laboratoriumsdiagnostik der Universität Düsseldorf. Briefly, CFP fused to YFP was employed as a FRET positive control, whereas CFP, YFP and the puromycin resistance gene subcloned into a tricistronic expression vector allowed the coexpression of CFP and YFP that functioned as FRET negative control.

All generated constructs were verified by sequencing (GATC Biotech).

4.6 Cell culture

All cell lines used in this work (GBM6840, HEK293T, HeLa) were cultured in Dulbecco's modified Eagle's Medium (DMEM) supplemented with 10% FCS, 2 mM L-glutamine, 100 U/ml penicillin and 100 µg/ml streptomycin at 5% CO₂ and 37°C in a humidified atmosphere in a standard cell culture incubator. Cells were grown under subconfluent conditions and were passaged every 3-4 days at a ratio of 1:5 to 1:10. In brief, culture medium was removed, cells were washed with calcium- and magnesium-free D-PBS and incubated with trypsin-EDTA for 5 min at 37°C. Trypsin was neutralised by the addition of FCS-containing cell culture medium. A single cell suspension was obtained by repeated pipetting. Cell counting was performed with a Neubauer chamber under a Zeiss Axiovert 25 inverted microscope (Carl Zeiss). Average cell numbers per square of the Neubauer chamber were multiplied with 10⁴ in order to determine the number of cells per millilitre of cell suspension.

4.7 Transient transfection of cells

The day preceding the transfection, cells were seeded in 6-well plates. For immunofluorescence experiments, cells were seeded at a density of 1 – 1.5 x 10⁶ cells on round 22 mm glass coverslips placed in 6-well plates. For overexpression experiments with subsequent immunoblotting, cells were seeded at a density of 4 – 4.5 x 10⁶ cells. For RNAi experiments, cells were seeded at a density of 2 – 2.5 x 10⁶ cells per well.

For transfection, plasmids or siRNA oligoribonucleotides and the Lipofectamine 2000 reagent were first mixed separately with OptiMEM in polystyrene tubes. Per well of a 6-well plate, 3 μ l of Lipofectamine 2000 reagent and 0.05 – 0.5 μ g of the respective plasmids or 7.5 nM of siRNA oligoribonucleotides were mixed with 250 μ l of OptiMEM medium and incubated for 5 min at room temperature. Afterwards, the DNA (or siRNA) and Lipofectamine 2000 solutions were combined and incubated for another 20 min at room temperature to form transfection complexes. Meanwhile, cells were washed 3 times with DMEM without any additives and the medium was replaced with 1 ml of OptiMEM. The transfection mix (500 μ l total volume per well of a 6-well plate) was added to the washed cells, which were then incubated in a cell culture incubator for 4 hours. Afterwards, the transfection medium was removed and replaced by 2 ml of standard growth medium. Twentyfour h after transfection (for overexpression experiments) or 48 – 72 h (for RNAi experiments), cells were either fixed for immunofluorescence (see 4.17), lysed for immunoblotting (see 4.14), or used for further functional experiments (see 4.18 - 4.21).

When cells were transfected in larger plates, the cell number was increased proportionally to the effective growth area of the employed plates. The volume of the transfection solutions was also increased proportionally to the effective growth area (from 1 ml for a 6 cm plate to 2 ml for a 10 cm plate), but the molarity of the transfection complexes was left unchanged. In other words, the amounts of DNA (or siRNA) and Lipofectamine 2000 used for transfection were increased proportionally to the increase in the volume of the transfection mix, and not proportionally to the cell numbers.

4.8 RNA interference as a tool for gene silencing

In the past years, the suppression of protein expression by RNA interference (RNAi) has developed into a widely used method for specific gene silencing. When double-stranded RNA (dsRNA) whose antisense strand is complementary to the transcript of a target gene is introduced into cells, it results in the specific degradation of the targeted mRNA and in the subsequent silencing of the targeted gene. Two distinct steps are involved in this process. In the first step, the enzyme Dicer recognises and cleaves long dsRNA into siRNA molecules, which are between 21 and 23 nucleotides in length. In the second step, these oligoribonucleotides become incorporated into a multicomponent RNA-induced silencing complex (RISC), which uses these siRNAs to guide the sequence-specific cleavage of the RNA transcripts of the target gene at sites homologous to siRNA sequences (Stewart et al., 2003). As a result, the synthesis of the encoded protein is largely suppressed, without its gene being affected (Tuschl and Borkhardt, 2002).

For experimental purposes, siRNA oligoribonucleotides can either be directly transfected into cells, or they can be generated from short hairpin RNA (shRNA) oligoribonucleotide precursors, which can be introduced into cells by transfection or *via* expression vectors. ShRNAs consist of single RNA strands with a sense and an antisense sequence that are connected by a short loop of several nucleotides, which allows complementary base-pairing and the formation of a hairpin structure. The shRNAs are then processed by cellular enzymes into active siRNA oligoribonucleotides through removal of the loop sequence (Figure 5).

Thus, RNAi offers a simple, fast, and cost-effective method of gene silencing compared to existing gene targeting technologies, such as knockout genetics. Synthetic siRNA and retroviral shRNA libraries covering most of the known and predicted human and mouse genes are commercially available.

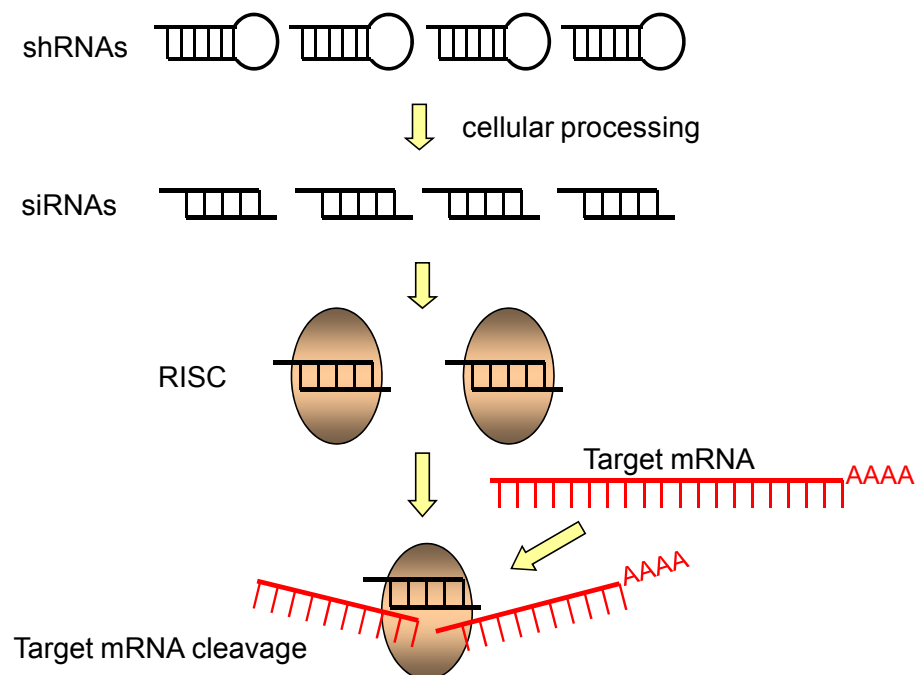


Figure 5: A model for gene inactivation by RNA interference.

shRNA oligoribonucleotides are processed to 21-23-nt long siRNA duplexes by intracellular enzymes. The siRNA duplexes are incorporated into a siRNA-containing ribonucleoprotein complex, forming the RNA-induced silencing complex (RISC). The RISC mediates sequence-specific target RNA degradation by targeting homologous mRNAs for degradation due to its endonuclease activity. After Tuschl and Borkhardt, 2002.

4.9 Production of shRNA-containing lentivirus and viral transduction

For the expression of shRNAs in cultured cells, we used the MISSION lentiviral shRNA expression system developed by the RNAi consortium (TRC). The structure of the lentiviral plasmid pLKO.1-Puro (Moffat et al., 2006), which carries the puromycin-resistance gene and drives shRNA expression from a human U6 promoter, is shown in Figure 6. This system allows the delivery of shRNA expression cassettes into the target cells using transient or stable transfection, as well as the production of lentiviral particles and the transduction of target cells.

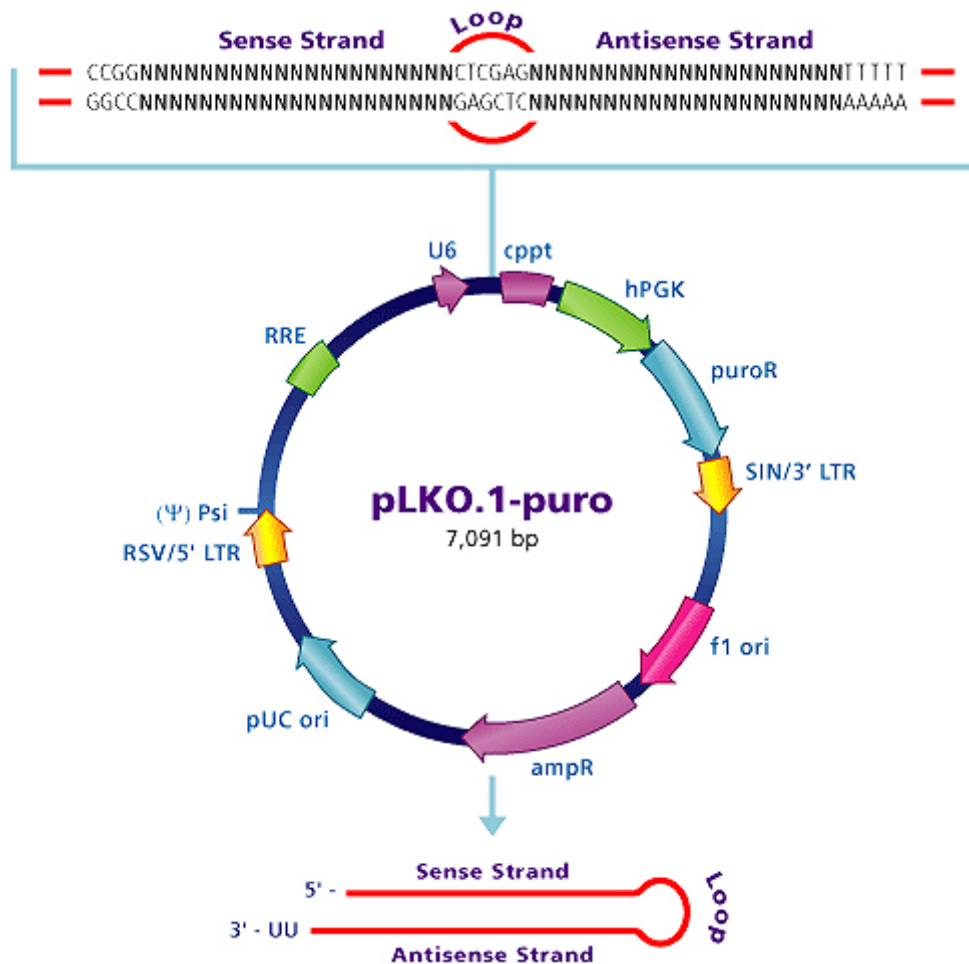


Figure 6: pLKO.1-Puro vector map.

The pLKO.1-Puro vector can be used for transient or stable transfection of shRNAs, as well as for the production of lentiviral particles and the subsequent transduction of target cells. A human U6 promoter is used for the expression of shRNAs. Stable expression of shRNAs and long-term gene silencing can be achieved by puromycin selection. Cppt, the central polypurine tract; hPGK, human phosphoglycerate kinase eukaryotic promoter; puroR, puromycin resistance gene for the selection of mammalian cells; SIN/3' LTR, 3' self inactivating long terminal repeat; f1 ori, f1 origin of replication; ampR, ampicillin resistance gene for bacterial selection; pUC ori, pUC origin of replication, 5' LTR, 5' long terminal repeat; Psi, RNA packaging signal; RRE, Rev response element; U6, mouse U6 RNA polymerase III promoter for expression of shRNA. From Moffat et al., 2006.

The lentivirus used here is derived from human immunodeficiency virus (HIV). The unique infectious capacity of this retrovirus is due to the fact that it can permeate the nucleus of the target cell, and is therefore capable of delivering its genetic information even to non-dividing or primary cells.

Several shRNA sequences of 21 nucleotides in length targeting human CIN (see Figure 7, Table 5) were tested for their ability to downregulate CIN protein expression levels in GBM6840 cells, either after transient transfection (see 4.7) or after lentiviral transduction (see below). The MISSION non-targeting shRNA control SHC002 was used as a control (see Table 5). This shRNA control displays a minimum of four base pair mismatches to any known human or mouse gene and therefore does not target any known human or mouse gene (www.sigmaaldrich.com).

Lentiviruses were generated by transient transfection of human embryonic kidney 293T cells (these are HEK293 cells constitutively expressing the simian virus-40 (SV-40) large T antigen). HEK293T cells were seeded the day before transfection at a density of 4.5×10^6 cells per 10 cm dish. The different shRNAs contained in pLKO.1-puro were co-transfected together with the packaging vector psPAX2 and the envelope vector pCR-VSV-G at a concentration of 10 μ g each per 10 cm dish. The respective DNAs (at a concentration of 1 μ g/ μ l) were diluted in 533 μ l of H₂O, and 62.5 μ l of a 2.5 M calcium chloride solution was added. The formation of DNA-containing calcium phosphate precipitates was induced by the addition of 625 μ l of 2x BES-buffered saline solution (50 mM BES, 280 mM NaCl, 1.5 mM Na₂HPO₄, pH 7.02). Transfection mixtures were incubated at room temperature for 5 min and pipetted into the culture medium of 293T cells. Cells were then incubated for approximately 16 hours. Afterwards, the medium was replaced by fresh medium supplemented with 10 mM sodium butyrate for 6 hours in order to enhance lentivirus production. Sodium butyrate is known to increase protein expression from CMV promoter-containing vectors (packaging and envelope vectors) by stimulating the enhancer element of the promoter and was shown to increase lentivirus titer even under suboptimal transfection conditions (Kolokoltsov et al., 2005). The medium with sodium butyrate was replaced with 10 ml fresh growth medium, and recombinant lentiviral particles were allowed to form for 24 h. The cellular supernatant containing the viral particles was collected with a 20 ml syringe, and cellular debris was removed by filtration through a sterile 0.45 μ m filter. Virus-containing supernatants were then directly used to transduce target cells.

Target cells were seeded on the day before transduction at a density of 1×10^6 cells per 10 cm dish. For viral transduction, the growth medium of target cells was removed, virus-containing medium was added, and cells were incubated in a cell culture incubator for 24 h. Afterwards, cells were subjected to selection medium containing 1 μ g/ml puromycin for 2 – 3 days.

```

1ATGGCGCGCTGCGAGAGGCTGCGCGGAGCGGCCCTGCGCGACGTGCTGGGCCGGGCGCAGGGGGTCTG
TTCGACTGTGACGGGGTCTGTGGAACGGCGAGCGCGCCGTGCCGGGCGCCCCGGAGCTGCTGGAGCGGCT
GGCGCGGGCCGGCAAGGCGGCTCTGTTTGTGAGCAACAACAGCCGGCGCGCGCGGGCCGAGCTGGCCCTG
CGCTTCGCGCGCCTCGGCTTCGGGGGGCTGCGCGCCGAGCAGCTCTTCAGCTCCGCGCTGTGCGCCGCGC
GCCTGCTGCGCCAGCGCCTGCCGGGCTCCGGACGCGCCGGGCGCCGTGTTGCTGCTGGGCGGGCAGGG
GCTGCGCGCCGAGCTGCGCGCCGCGGGGCTGCGCCTGGCCGGGACCCGAGCGCGGGGGACGGCGCGGCC
CCGCGCGTGCAGCGCCGTGCTTGTGGGCTACGACGACACTTCTCCTTCGCCAAGCTGAGGGAGGCGTGCG
CGCACCTGCGGACCCCGAGTGCCTACTCGTGCCACCGACCGTGACCCATGGCACCCGCTGAGCGACGG
CAGCCGGACCCCTGGCACCGGGAGCCTGGCCGCTGCACTGGAGACAGCCTCGGGACGCCAGGCCCTGGTG
GTGGGCAAGCCAGCCCTACATGTTTCGAGTGCATCACGGAGAATTGAGCATCGACCCGCGACGCACGC
TTATGGTGGGTGACCGCCTGGAGACCGACATCCTCTTTGGCCACCGCTGCGGCATGACCACTGTGCTCAC
GCTCACAGGAGTCTCCCGCTAGAAGAGGCCAGGCTACCTAGCGGCCGGCCAGCACGACCTCGTGCC
CCATACTATGTGGAGAGCATCGCAGACTTGACAGAGGGGTTGGAGGACTGA891

```

Figure 7: Localisation of the used siRNA/shRNA in open reading frame of human CIN. Targeting regions of used siRNA and shRNA oligoribonucleotides in open reading frame of human CIN are signed and shown in gray boxes.

Puromycin-resistant cells were stored as cryostocks. To do so, cells were harvested by trypsinisation (see 4.6). Cell suspensions were supplemented with 10% (v/v) DMSO and were slowly frozen down to -80°C . Cells were subsequently stored in liquid nitrogen. To bring cells back in culture, cryostocks were quickly thawed at 37°C , diluted 1:10 with prewarmed (37°C) growth medium, and centrifuged for 5 min at $1000 \times g$. Cell pellets were then resuspended in prewarmed growth medium and cells were seeded into culture dishes.

4.10 Validation of shRNA/siRNA-mediated protein knockdown

Individual MISSION shRNAs (Table 1) were initially screened for efficiency of CIN knockdown by transient transfection of the respective plasmids in GBM6840 cells (see chapter 4.7). Fourtyeight – 72 h after transfection, cells were lysed in RIPA buffer and lysates were tested for CIN downregulation by immunoblotting with CIN-specific antibodies (see chapter 4.14). Those shRNA sequences that showed sufficient knockdown in transient transfection experiments were then used for the production of lentiviruses and for the transduction of GBM6840 cells (see chapter 4.9). This approach led to the establishment of a stably CIN-depleted GBM6840 cell line together with a corresponding GBM6840 cell line stably expressing the MISSION control shRNA.

Alternatively, a transient transfection of synthetic siRNA oligoribonucleotides into host cells was used. The sequences of the employed oligoribonucleotides are presented in

Table 4 and their localisation in open reading frame of human CIN is shown in Figure 7. Host cells were seeded at low density on the day before transfection (see chapter 4.7). Next day, the cells were transfected as described in chapter 4.7 either with the different individual siRNA oligoribonucleotides or with a combination of two of them.

4.11 Acetone precipitation of proteins

To remove salts, detergents and soluble lipid contaminants from protein samples and also to concentrate the protein content, proteins can be precipitated from lysates. For this purpose we used the acetone precipitation method (Jiang et al., 2004). For that, four times the volume of acetone (precooled at -20°C) was added to the tube with the sample extract. The samples were vortexed and incubated for 60 minutes at -20°C . After that, samples were centrifuged for 10 minutes at $15,000 \times g$. Obtained protein pellets were air-dried at room temperature and then redissolved in an appropriate volume of lysis buffer.

4.12 Determination of protein concentration

The protein concentration of cell- or tissue lysates was measured using the Micro BCA Protein Assay Kit (Pierce). This assay allows the sensitive and selective colorimetric detection and quantification of the total protein content. The assay is based on the reduction of Cu^{2+} to Cu^{1+} by the proteins in the lysate under alkaline conditions (the Biuret reaction) and the colorimetric detection of the generated Cu^{1+} by a reagent containing bicinchoninic acid (BCA) (Smith et al., 1985). Chelation of two molecules of BCA with one cuprous cation (Cu^{1+}) leads to the formation of a water-soluble, purple-coloured product with maximal absorbance at 562 nm.

The BCA solution was prepared by mixing the components of the Micro BCA Protein Assay Kit according to manufacturer's instructions. The protein sample (2.5 μl) was diluted with water in a 96-microtiter plate well to give a volume of 150 μl of protein solution. Then 150 μl of BCA solution was added to each sample, and samples were incubated for 2 h at 37°C . A BSA standard curve ranging from 1 to 5 μg of BSA per well was tested in parallel. The samples of the BSA standard curve contained 2.5 μl of lysis buffer, to take into account the absorbance of compounds of the lysis buffer on the total absorbance of the sample. The extinction of the samples was determined in a FLUOstar OPTIMA microplate reader at 560 nm.

4.13 SDS-polyacrylamide gel electrophoresis

SDS-PAGE is a commonly used method for separating proteins according to their molecular masses using polyacrylamide gels as a support medium and sodium dodecyl sulfate (SDS) for protein denaturation and charge (Laemmli, 1970). The technique of SDS-PAGE followed by immunoblotting (see 4.14) is a commonly used method for protein expression analysis.

Protein samples were adjusted to equal protein concentrations, mixed with Laemmli buffer, denatured at 95°C for 5 min and loaded onto SDS-PAGE gels. The electrophoresis was carried out in running buffer at a constant current (25 – 30 mA). Proteins were first run in a stacking gel (4.5% (v/v) acrylamide solution) to concentrate them, and were then separated in a running gel (12.5% (v/v) acrylamide solution). To resolve lower molecular weight proteins, running gels with 15% (v/v) acrylamide solution were used. SDS-PAGE was performed on the Bio-Rad mini gel apparatus.

4.14 Immunoblotting

Immunoblotting is an analytical technique commonly used for the semiquantitative detection of specific proteins in a given sample of a cell lysate or of a tissue homogenate. The technique is based on the electrotransfer of proteins resolved by SDS-PAGE from polyacrylamide gels onto nitrocellulose membranes (Towbin et al., 1979). Blotted samples are analysed using primary antibodies raised against a protein of interest. Bound primary antibodies can be detected by using enzyme-coupled secondary antibodies directed against the primary antibody. The protein of interest can thus be visualised in an enzymatic reaction based on substrate turnover of bound secondary antibodies, where the intensity of the signal is proportional to the abundance of the protein of interest.

Proteins were transferred from the SDS-PAGE gels onto nitrocellulose membranes using a TRANSBLOT – semidry blotting apparatus (Bio-Rad). After equilibration of the SDS-PAGE gel in Cathode Buffer for 5 min, the blotting sandwich was prepared. For that, two sheets of Whatman paper were equilibrated in Anode Buffer I, one sheet of Whatman paper was equilibrated together with the nitrocellulose membrane in Anode Buffer II and three other sheets of Whatman paper were equilibrated in Cathode Buffer. The blotting sandwich was assembled, and proteins were transferred electrophoretically at constant current (70 mA for 1 mini-gel, 1 h). A prestained molecular weight marker was used to monitor the efficiency of protein transfer. After electrotransfer, Western blot membranes were stained with Ponceau S (0.2% in 5% acetic acid) to test for equal protein loading and homogeneity of transfer, and blots were photocopied for documentation purposes.

For immunodetection, non-specific binding sites on membranes were first blocked in BLOTTO Buffer for 30 min at room temperature under constant agitation. Primary antibodies

(see chapter 3.13) were applied at dilutions of 1:500-1:1,000 (or 1:10,000 for α -tubulin and β -actin) in Antibody Diluent, and membranes were incubated overnight at 4°C under constant agitation. Membranes were then washed with TBS-T (3 x 5 min) and probed for 1 – 2 h with HRP (horseradish peroxidase)-labelled secondary antibodies, diluted 1:10000 in BLOTTO Buffer. After washing with TBS-T (3 x 5 min), Western blot membranes were incubated with the ECL Western Blotting Detection System and exposed to X-ray films. Films were developed on Agfa Curix 60 developing machine. For semiquantative Western blot analysis, Western blot signals from the membranes were directly detected on the DIANA III Camera System. In some cases, exposed films were scanned and obtained images were densitometrically evaluated using the “Aida” software (Raytest).

4.15 Reprobing of Western blot membranes

In some cases, the same membranes were probed for several different antigens. For this purpose, nitrocellulose membranes were placed in Stripping Buffer and incubated at 55°C for 30 min under constant agitation to remove the associated primary and secondary antibodies. After that, membranes were washed three times in a large excess of TBS-T, blotted again with BLOTTO Buffer for 30 min at room temperature under constant agitation, and were then reprobed with other primary antibodies to detect other antigens of interest.

4.16 Immunohistochemistry

Immunohistochemical analysis allows the visualisation of a protein of interest in tissues with the help of specific antibodies. Antigen-bound primary antibodies are detected with biotinylated secondary antibodies. The biotinylated secondary antibody can then be detected with HRP-labelled avidin in the Avidin-Biotin Complex (ABC)-reaction. This complex formation can be visualised using a HRP-substrate such as DAB.

Paraffin-embedded or frozen mouse tissues or mouse embryos were cut into 5-14 μ m thick sections and were mounted on Polysine slides (Menzel/Thermo Scientific). To block the endogenous peroxidase activity of the tissues, sections were incubated for 10 min at RT with H₂O₂ (0.3% in TBS). To prevent nonspecific binding of the primary antibodies, sections were incubated in Blocking Buffer for 30 min at RT. Sections were incubated with primary antibodies (1:400 dilution in TBS with 3% NGS) in a humidified chamber at 4°C overnight. All further steps were done at RT. Sections were washed with TBS (3 x 5 min) to remove unbound primary antibodies and were then incubated with biotinylated secondary antibodies (1:200 dilution in TBS with 2% NGS) for 1 h. Sections were washed with TBS (3 x 5 min) to remove unbound secondary antibodies and were incubated with freshly prepared

ABC Mix for 1 h. After washing with TBS (3 x 5 min), sections were placed for 3 – 15 min in DAB Solution, and the reaction was stopped in water when colour development was appropriate. After that, sections were washed again in TBS (3 x 5 min) and dehydrated (2 x 70% EtOH for 2 min, 80% EtOH – 2 min, 90% EtOH – 2 min, 100% EtOH – 2 min, Xylene – 2 min, Xylene – 15 min). Dehydrated sections were mounted with Entellan.

4.17 Immunofluorescence microscopy

To visualise the actin cytoskeleton, cells were seeded on round 22 mm glass coverslips at low densities (1×10^5 cells per well in 6-well plates). The next day, cells were treated or not as described in the respective experiments, and were fixed with 4% PFA for 20 min and permeabilised with 0.1% Triton X-100 in PBS for 10 min. Polymerised, filamentous F-actin was visualised by staining cells for 30 min with Alexa Fluor 488 Phalloidin (1:400 dilution in PBS) and cell nuclei were visualised by staining with DAPI (1:6,000 in PBS, 5 min). After washing with PBS (3 x 5 min) stained cells were mounted on glass coverslips in ProLong Antifade medium.

To analyse the turnover rates of the actin cytoskeleton, cells were starved by serum withdrawal in DMEM medium without any additives for 24 h. After that, the medium was changed to fresh DMEM without any additives and cells were starved for another 3 – 4 h, fixed and processed as described above. Images were taken using a 40 x objective on a Nikon ECLIPSE TE2000-E inverted fluorescence microscope. Image analysis (such as cell area determination, insertion of scale bars etc.) was done using the Nikon software NIS – ELEMENTS AR 3.0, SP3, Hotfix2 (Build 469).

To determine the average cell area, images of more than 50 cells per condition were obtained, the circumference of the phalloidin-labelled cells was traced manually using the NIS – ELEMENTS software, and the cell area was calculated from the measured cell circumference.

4.18 Proliferation assay

The Aqueous One Solution Cell Proliferation Assay (Promega) was employed to compare the growth characteristics of cells. This colorimetric cell proliferation and cell viability assay is based on the bioreduction by cells of the tetrazolium compound MTS. MTS is stabilised with the electron coupling reagent phenazine ethosulfate. After addition of this solution to viable cells, a colored formazan product is formed due to the action of cellular reductases. The formation of the formazan product can be measured as an increase in absorbance at 492 nm, and it is directly proportional to the number of living cells in culture.

Equal amounts of cells (1000 cells per well) were seeded in triplicates in several 96-well plates (one plate for each day of experiment, since the measurements are not in steril conditions) and viable cell numbers were determined every day for several consecutive days. Twenty μl of the AQueous One Solution Reagent was added directly to the culture wells with cells, incubated for 1 hour in a standard humidified cell culture incubator (5% CO_2 , 37°C), and the absorbance was measured in a FLUOstar OPTIMA microplate reader at 492 nm.

4.19 *In vitro* invasion assay

To study the invasive potential of GBM6840 cells *in vitro*, we employed matrigel-coated Transwell chambers (BD Matrigel Invasion Chambers, BD Biosciences). These chambers are cell culture inserts with 8 μm pore-size membranes that are coated with matrigel. Matrigel is a solubilised basement membrane preparation containing extracellular matrix molecules such as laminin and collagen type IV, heparan sulfate proteoglycans, entactin, growth factors and other components. The principle of the invasion assay is that a cell suspension is introduced into the cell culture insert containing the porous membrane. The matrigel layer covers the membrane and occludes the membrane pores, such that non-invasive cells are prevented from migrating through the membrane in response to a chemotactic factor present in the bottom chamber of the well. Thus, only cells which are able to migrate directionally in response to a chemoattractant and that are able to degrade the matrigel can cross the membrane pores and will be present on the underside of the porous membrane.

Cells were harvested as described in 4.6, and were subsequently resuspended in DMEM medium without serum and any other additives. Cell numbers were determined by counting in a Neubauer chamber, cell suspensions were adjusted to a concentration of 5×10^5 cells/ml, and 500 μl were added to each insert. EGF (100 ng/ml) was used as a chemoattractant in the bottom chamber of the transwell. Twentyfour h later, cells on the bottom of the insert were fixed with 4% PFA, and non-invasive cells were removed from the upper surface of the membranes by "scrubbing" the membranes with a cotton swab. The invaded cells on the bottom sides of the inserts were stained with Crystal Violet (0.005% in PBS). One to two pictures from each insert were taken on a Zeiss Axiovert 40C inverted microscope using a 5x objective using an AxioCam MRc5 (Carl Zeiss, Jena). The number of invaded cells was determined by counting and expressed as average cell number per field of vision.

4.20 *In vitro* cell transformation assay

The ability of transformed cells to grow in an anchorage-independent manner in soft agar is frequently used to measure cellular transformation and tumorigenic potential, because a general correlation exists between the *in vitro* ability of cells to grow anchorage-independently with their *in vivo* tumorigenic potential (Freedman and Shin, 1974). In this assay, single cells are suspended at low densities in soft agar and are allowed to grow for 10 – 14 days in an anchorage-independent manner, since they lack a solid substratum under these conditions.

The colony formation experiments in soft agar were done in 6 cm plates (Di Tomaso et al., 2000). For this, 2% agar was suspended in water, melted in a microwave, and was then diluted in DMEM-F12 medium to give 0.5% base agar. Three ml of base agar were added to each 6 cm plate. For the top agar, 0.6% agar was prepared in DMEM-F12 with 20% FCS and was then cooled down to 45°C in a waterbath. Cells were trypsinised and counted, and a single cell suspension of 3×10^5 cells/ml was prepared in DMEM-F12 with 20% FCS. One hundred μ l of this suspension (3×10^4 cells) were added to 3 ml of DMEM-F12 with 20% FCS (prewarmed to 37°C), and 3 ml of 0.6% agar was added to the tube (giving the final concentration of the top agar 0.3%), mixed gently by inverting the tubes with cells 4 – 5 times, and 2 ml of this suspension was placed on top of the base agar. Plates were incubated in a standard humidified cell culture incubator (5% CO₂, 37°C), and the cells were fed every 2 days by carefully adding 300 μ l of DMEM medium with 10% FCS on the top of the agar. After 2 weeks, cells were stained with Crystal Violet (0.005% in PBS, 1 ml per dish) for 1 h at 37°C. Plates were scanned using a hp scanjet 5530 photosmart scanner (Hewlett Packard) and all macroscopically visible colonies were counted from the obtained pictures.

4.21 Sensitised emission FRET

Förster or fluorescence resonance energy transfer (FRET) is an imaging technique widely used to study protein – protein interactions in living as well as in fixed cells (Vogel et al., 2006). FRET is a mechanism by which energy is transferred directly from one fluorescent molecule, which is called the Donor, to another fluorescent molecule, the Acceptor. FRET can occur only over a very short distance, usually less than 10 nm, which is on the order of the size of an average protein. Thus, FRET between two proteins labelled with appropriate fluorophores can occur only when these two fluorophores -and thus the proteins- are in close proximity (1 – 10 nm) to each other. The requirements for FRET are shown in Figure 8. Therefore, the occurrence of FRET between two labeled proteins is generally accepted as a proof that these two proteins interact with each other.

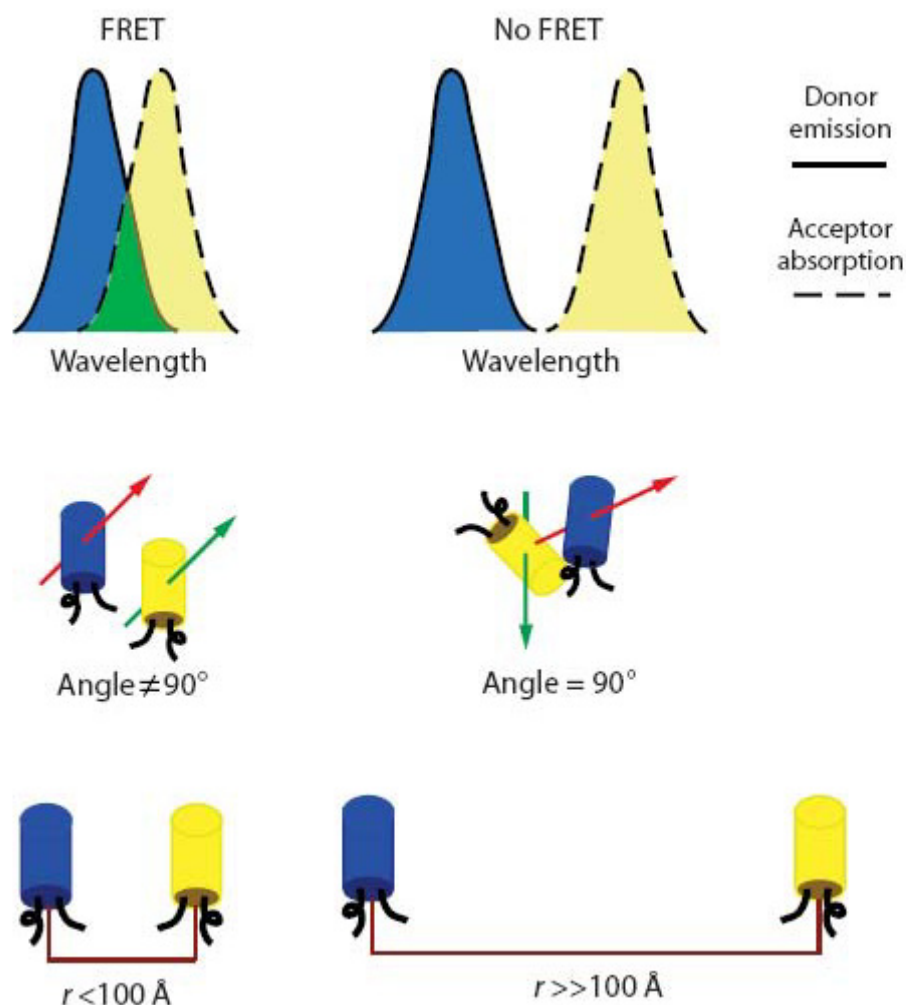


Figure 8: Principle and requirements for FRET.

FRET can occur only if the emission spectrum of the donor (solid line) overlaps the absorption spectrum of the acceptor (dashed line). The overlapping region is shown in green. If the emission dipole (red arrow) of a donor (blue cylinder) forms a 90° angle with the absorption dipole (green arrow) of the acceptor (yellow cylinder), FRET cannot occur. Dipole-dipole angles other than 90° will support FRET with a range of efficacies. Resonance energy transfer is observed only when the distance separating the two fluorophores (r) is typically less than 100 \AA . Modified from Vogel et al., 2006.

FRET experiments to study the CIN – CIB1 interaction were performed with living HeLa cells. The day before transfection, cells were trypsinised and seeded on round 22 mm glass coverslips in 6-well plates ($\sim 1.5 \times 10^6$ of cells per well). Cells were transfected with 75 ng of pcDNA3-CIN-YFP and 375 ng of pcDNA3-CIB1-CFP plasmids using the Lipofectamine-2000 transfection reagent (see 4.7). The constructs were either co-transfected to measure FRET efficiency, or they were transfected separately to determine spectral bleed-through coefficients for each fluorophore. As a positive control, a plasmid expressing YFP fused to CFP (YFP-CFP tandem) was used (Schmid et al., 2001; Sunesen et al., 2003). A plasmid simultaneously expressing CFP and YFP from a tricistronic mRNA, but not as a fusion protein, was used as a negative control (Mielke et al., 2000).

The day following the transfection, glass coverslips were placed in live-imaging chambers and cells were covered with HBS. For each transfection condition, groups of images were taken on a Zeiss LSM 510 Meta confocal microscope: the first one in the FRET setting (excitation of the Donor, detection of the Acceptor), the second one in the Donor setting (excitation of the Donor, detection of the Donor) and the third one in the Acceptor setting (excitation of the Acceptor, detection of the Acceptor). All microscope settings (laser power, detector gain, amplifier offset, amplifier gain, optical slice thickness of 1 μm) were kept constant during image acquisition for all experiments.

FRET analysis and calculations were done with the ImageJ software (<http://rsb.info.nih.gov/ij/>) using the PixFRET plug-in. PixFRET allows the determination of spectral bleed-through parameters, the display of normalised FRET (NFRET) images, and the calculation of FRET efficiency (Feige et al., 2005). FRET efficiency was determined for each cell from 10 different images (~ 30 cells), and the average FRET efficiency was calculated.

4.22 *In vitro* phosphatase activity assays

CIN was independently identified as a specific pyridoxal 5'-phosphate (PLP) phosphatase (Gao and Fonda, 1994; Jang et al., 2003). Since PLP is stoichiometrically phosphorylated, whereas cofilin can only be phosphorylated to ~20% *in vitro* (Gohla and Bokoch, 2002), PLP was used as a CIN substrate to analyse the regulation of CIN activity. To detect free inorganic phosphate (P_i) generated by PLP dephosphorylation, we employed the *PiPer Phosphatase Assay Kit* (Molecular Probes/Invitrogen).

The detection of P_i in this assay is based on a cascade of coupled enzymatic reactions, which are shown schematically in Figure 9. In the presence of P_i , maltose phosphorylase converts maltose to glucose 1-phosphate and glucose. Glucose is converted by glucose oxidase to gluconolactone and hydrogen peroxide. Catalysed by horseradish peroxidase, the generated H_2O_2 reacts with Amplex Red to the highly fluorescent product, resorufin. Thus, the resulting resorufin fluorescence is proportional to the amount of P_i generated by substrate dephosphorylation.

PLP dephosphorylation (final concentration, 5 μM) was conducted in a total reaction volume of 100 μl at pH 7.5 and 37°C. The amount of CIN protein for one reaction was 1 μg , and CIB1 was used in twofold-molar excess over CIN (1.4 μg of CIB1 per reaction). The concentration of free Ca^{2+} ions in the reaction was adjusted with 0.1 mM EGTA and calculated using the MaxChelator program (<http://www.stanford.edu/~cpatton/maxc.html>). Dephosphorylation reactions were done in the Ca^{2+} concentration range of 0.1 μM – 2 mM or without Ca^{2+} . All experiments were done in triplicates in 96-well plates and the kinetics of

resorufin formation were monitored for up to 2 h using the FLUOstar OPTIMA microplate reader (BMG Labtech) using excitation and emission wavelengths of 544 and 590 nm.

For the analysis of the effect of CIB1 on CIN phosphatase activity, the initial slopes of the kinetic curves were calculated (taking into account the first 15 min of the reaction after a 30 min pre-incubation time). The activity of CIN in the absence of Ca^{2+} and CIB1 was defined as 100%.

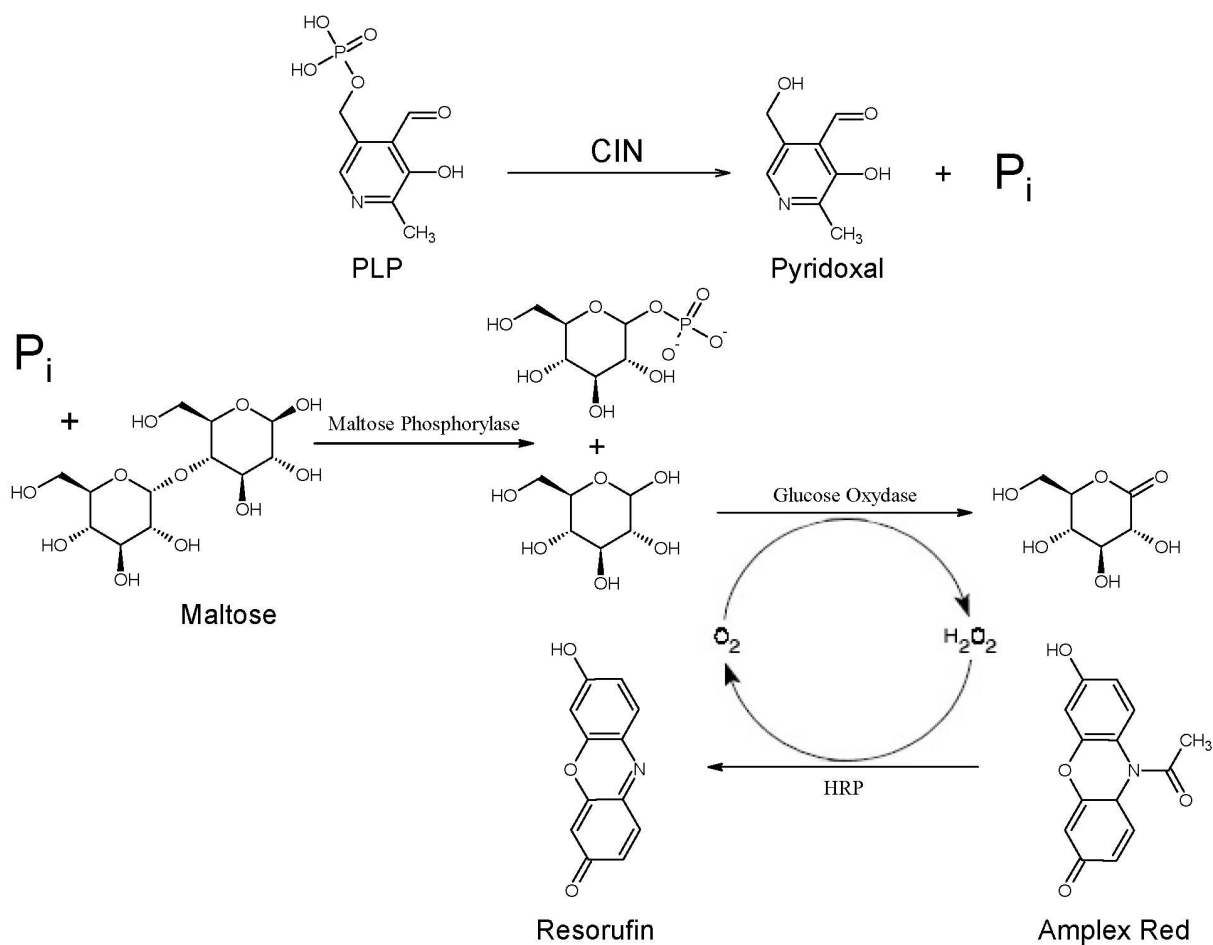


Figure 9. Principle of the *in vitro* phosphatase activity assay.

The formation of free inorganic phosphate (P_i) due to CIN-mediated PLP dephosphorylation is detected by a cascade of coupled enzymatic reactions, resulting in the formation of fluorescent resorufin. For details, see text. HRP, horseradish peroxidase. Adopted from www.invitrogen.com.

5 Results

5.1 CIN expression in mouse tissues

In previous work, CIN was shown to be a ubiquitously expressed protein found in all human tissues with the highest expression in brain (Gohla et al., 2005; Jang et al., 2003). To analyse CIN protein expression and the cellular and subcellular level, a rabbit α -CIN monoclonal antibody was generated in collaboration with Cell Signaling Technology (Danvers, MA, USA). This antibody can detect as little as 150 pg of recombinant CIN by Western blot analysis (Figure 10A) and shows very high specificity. CIN antibody detects only one specific band corresponding to endogenous CIN protein in a whole mouse brain lysate (Figure 10B).

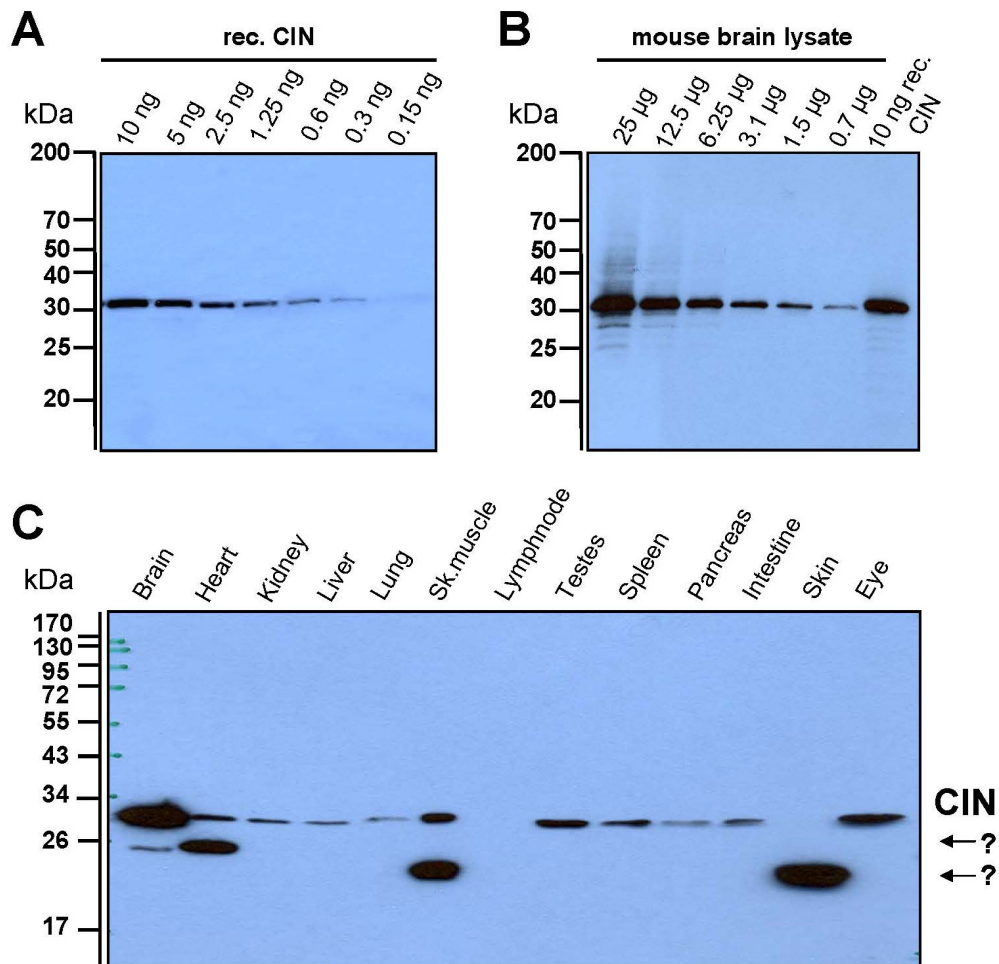


Figure 10: Characterisation of CIN antibody and analysis of CIN expression.

(A) Different amounts of recombinant CIN protein were tested by immunoblotting with a CIN rabbit monoclonal antibody. (B) 25 μ g of total protein from a whole mouse brain lysate were serially diluted and immunoblotted with a CIN rabbit monoclonal antibody. Recombinant CIN was used as a control. (C) Different mouse tissues were lysed in Lysis Buffer I and equal protein amounts (20 μ g) of each tissue lysate were separated by SDS-PAGE, transferred onto nitrocellulose membrane and then analysed by immunoblotting for CIN expression. Possible degradation/cleavage products, isoforms or splice variants of CIN detected in brain, muscle and skin are indicated with question marks.

We could confirm previous observations (Gohla et al., 2005; Jang et al., 2003) about different expression levels of CIN in various tissues and the highest expression level in brain (Figure 10C). The observed CIN antibody-reactive bands at approximately 25 and 20 kDa detected in brain, muscle and skin may indicate possible degradation/cleavage products, isoforms or splice variants of CIN.

For further characterisation of CIN expression in tissues, we performed immunohistochemical analysis of murine embryos and of adult mouse brain (Figure 11). We found that CIN is already highly expressed in mouse brain during organism development. The age of embryos used for immunohistochemical analysis was defined using images and comments from the digital Atlas of mouse embryonic development (<http://genex.hgu.mrc.ac.uk>).

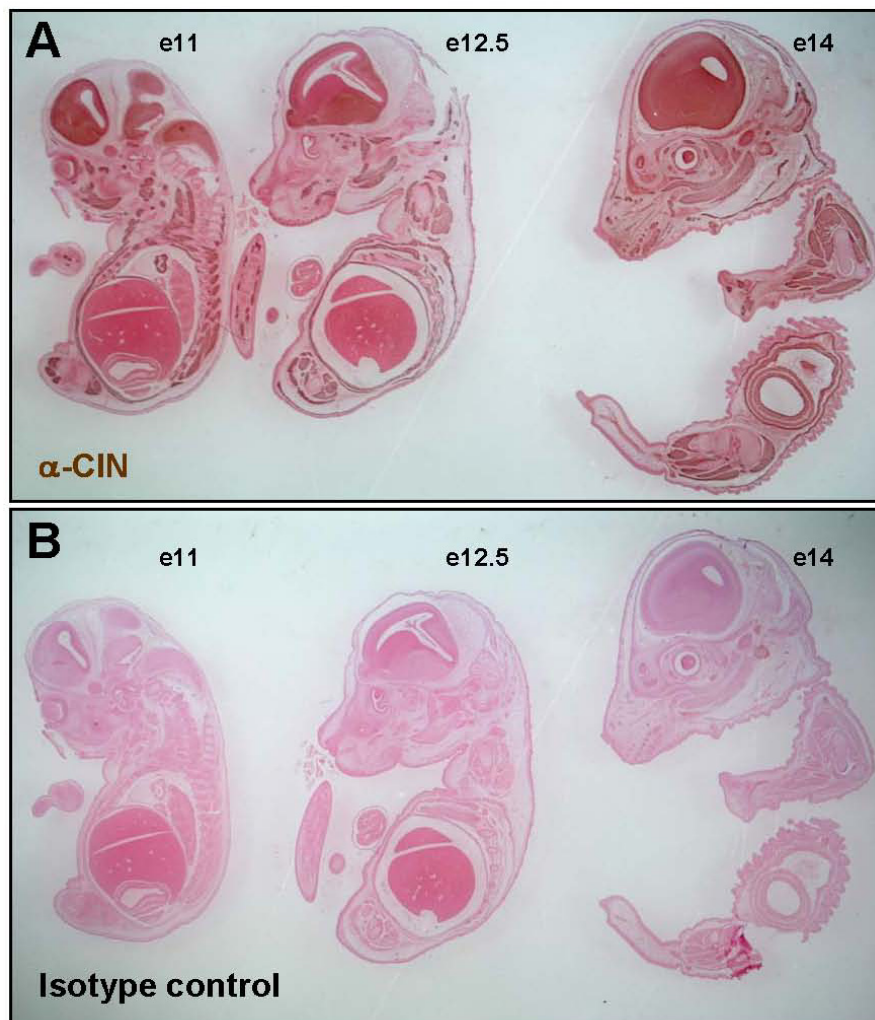


Figure 11: Immunohistological analysis of CIN expression in murine embryos.

Murine embryos of several developmental stages (e11, e12.5 and e14) were embedded in paraffin and 5 μ m paraffin-slices were cut. Distribution of CIN expression is shown in brown colour and was analysed using the CIN-specific rabbit monoclonal Ab at a dilution of 1:800 (A). The control staining (B) was performed in the same way but using an isotype-matched rabbit control antibody. CIN phosphatase is expressed in various tissues and is detected at high levels in brain.

CIN was detected with variable intensities in different regions of adult mouse brain. Interestingly, in the dentate gyrus (a part of the hippocampal formation), CIN is expressed at very high levels (Figure 12A and B) as compared to other regions of the mouse brain. The dentate gyrus is one of the few brain structures currently known to have high rates of neurogenesis in adult humans (Cameron and McKay, 2001). Other known sites of neurogenesis include the olfactory bulb (Graziadei and Monti Graziadei, 1985) and the cerebellum (Ponti et al., 2008).

Taken together, these results demonstrate that the cofilin-specific phosphatase CIN is a broadly expressed enzyme with the highest expression level in brain.

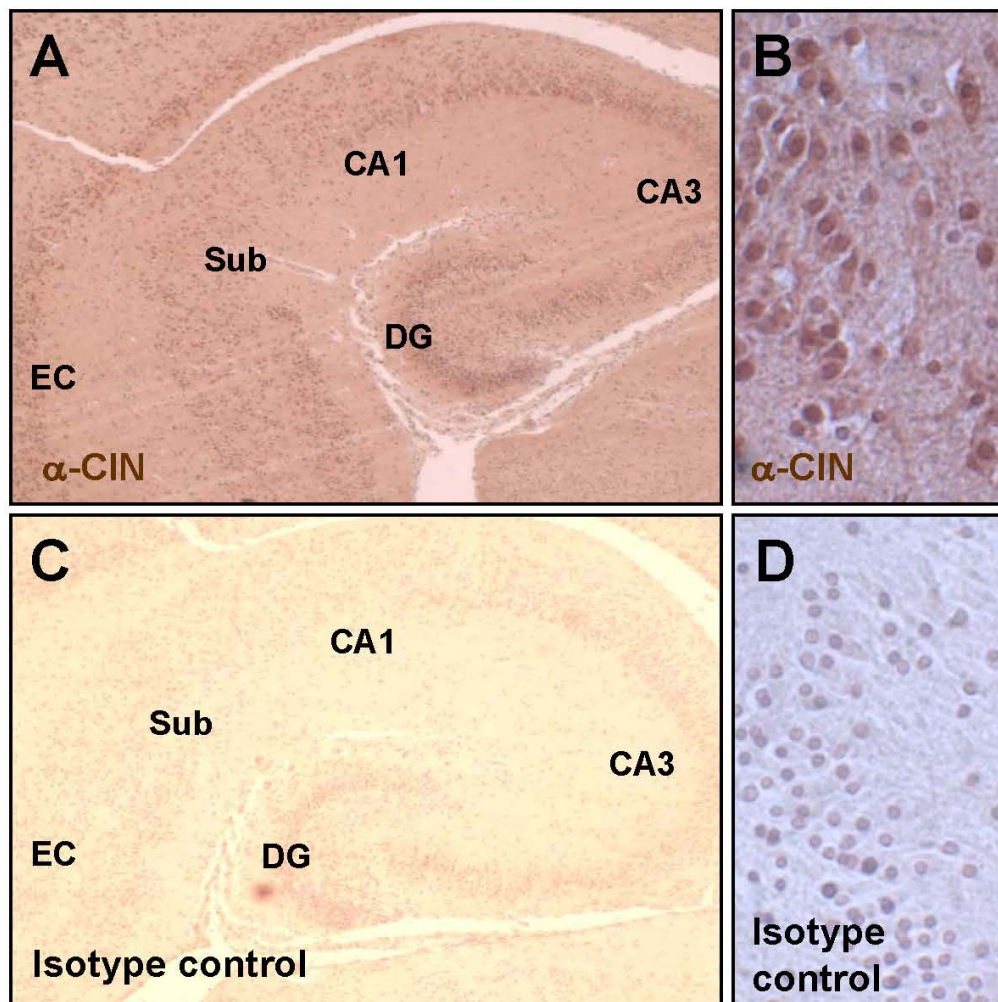


Figure 12: CIN expression in the adult mouse brain.

(A) Immunohistochemical analysis of CIN protein expression in mouse hippocampus using the CIN-specific rabbit monoclonal antibody. Brown color shows positive signal. CIN phosphatase is expressed at high levels in the hippocampus, particularly in the dentate gyrus (DG). Images were taken using a 2.5x objective. (B) Higher resolution imaging of the dentate gyrus was done using a 40x objective. (C) and (D) are isotype controls corresponding to (A) and (B). DG: dentate gyrus. Sub: subiculum. EC: entorhinal cortex. CA1, CA3: *Cornu Ammonis* areas.

5.2 CIN expression in human brain and astrocytic gliomas

CIN maps to a region of chromosome 22q that is known to be affected by deletions in glial tumours (Ino et al., 1999; Nakamura et al., 2005; Nakamura et al., 2007). Loss of chromosome 22q was related to glioma progression (Laigle-Donadey et al., 2006), but until now tumour suppressor genes located in this region have been elusive (Schwartzbaum et al., 2006). To analyse if CIN expression is indeed affected in gliomas, we first performed immunohistological analysis of CIN protein expression in human brain tumour samples. Histological analysis of CIN protein expression in these samples revealed that CIN is expressed at high levels in normal human brain, where it is found in neurons as well as in glial cells (Figure 13A). Interestingly, the expression level of CIN protein in glioblastoma multiforme is dramatically reduced as compared to the neighboring, non-tumourous areas (Figure 13B and C).

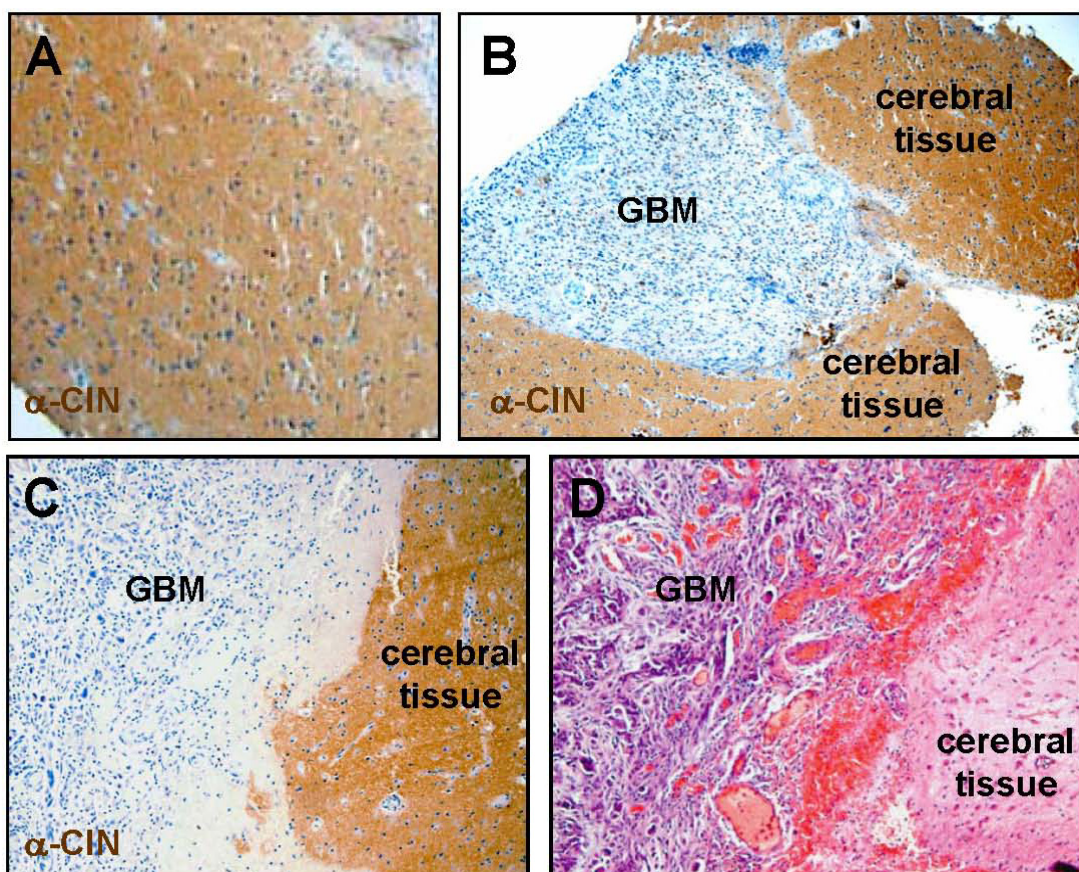


Figure 13: Histological analysis of CIN expression in human brain samples.

Immunohistochemical analysis of CIN expression was done in (A) normal human brain and (B, C) human brain samples from patients with glioblastoma multiforme. Brown color shows positive signal for CIN expression. (D) Hematoxylin and eosin staining corresponding to (C). Analysis was performed and images were kindly provided by Dr. B. Klink from the Department of Neuropathology (University Hospital Düsseldorf, Germany).

5.3 Deregulation of the Cofilin pathway in glial tumour samples

In order to verify our finding that CIN expression is downregulated in glioblastoma multiforme and to investigate CIN expression in other astrocytic tumours, we performed quantitative real-time (qRT)-PCR analysis of human brain tumour samples. We analysed the expression levels of CIN mRNA in more than 70 tumour samples from patients with astrocytic gliomas of different malignancy grades, including astrocytoma grades II and III and glioblastoma grade IV. This analysis was performed in collaboration with the Department of Neuropathology at the University Hospital Düsseldorf.

Five normal brain tissue samples from two different age-matched patients were used as reference tissues and the average expression levels of tested genes in these tissues were defined as 1 as indicated by a red line in Figure 14. Interestingly, CIN mRNA was downregulated in almost all tested tumour samples, as compared to normal brain controls (Figure 14). CIN was identified as a cofilin-regulatory phosphatase (Gohla et al., 2005). Cofilin is an essential factor for stimulus-dependent actin remodelling (Bamburg, 1999; Bamburg et al., 1999; Gurniak et al., 2005), and altered cofilin activity and alterations of cofilin-regulatory proteins were linked to the initiation and progression of malignant tumours, particularly breast cancer (Condeelis et al., 2005; Wang et al., 2007a). Because we observed a downregulation of CIN, our next goal was to test the expression levels of the other major players of the cofilin pathway in tumour samples from patients with different types of glial tumours.

Slingshot SSH1L was the first reported cofilin-specific phosphatase (Niwa et al., 2002). Interestingly, and in contrast to CIN, the relative mRNA levels of SSH1L phosphatase were almost unchanged and comparable to the expression levels of SSH-1L in normal brain control samples (Figure 14).

The members of the LIM kinase (LIMK) family, which includes LIMK1 and LIMK2, are serine protein kinases involved in the regulation of actin polymerisation by phosphorylating and inactivating cofilin (Bernard, 2007). The qRT-PCR experiments showed a massive upregulation of LIMK2, whereas LIMK1 appeared to be downregulated in the majority of the tested brain tumour samples (Figure 14).

Upstream activators of LIM kinases are p21-activated kinases (PAKs). The qRT-PCR experiments clearly showed a massive upregulation of PAK4 mRNA, in contrast to a loss of PAK5 and PAK6 mRNA. These findings are in good correlation with previous data from the literature on PAK4 expression at the messenger RNA level. It was shown per Northern blot that PAK4 is expressed at very low levels in most adult tissues and that it is upregulated in

almost all of the tested human tumour cell lines of various tissue origins (Callow et al., 2002; Mahlamaki et al., 2004). The upregulation of PAK4 expression levels has also been shown in some primary tumours, including colon, esophageal, and mammary tumours (Liu et al., 2008).

The mRNA levels of cofilin itself were elevated in grade II astrocytomas, but not significantly changed in grade III astrocytomas or in glioblastomas (Figure 14).

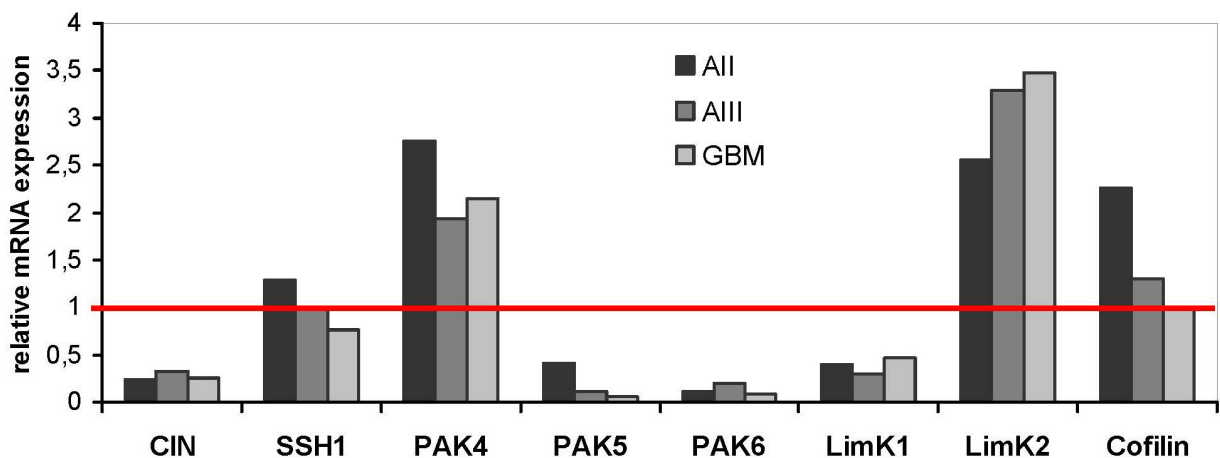


Figure 14: Expression analysis of the cofilin pathway by real-time PCR.

The transcript level of each gene was normalised to ARF1 (ADP ribosylation factor 1). Five normal brain tissue samples from two different patients were used as reference tissues. Obtained median expression levels of indicated genes are shown for different stages of astrocytic tumours. The cofilin pathway is dysregulated in glial tumours, with an upregulation of cofilin-inactivating kinases LIMK2 and PAK4 and a downregulation of a cofilin reactivating phosphatase CIN. Shown are median results of 69 tumour samples (6 All, 8 AIII, 55 GBM samples). Real-time PCR experiments were done at the Department of Neuropathology by Dr. Christiane Knobbe and Dr. Barbara Klink (University Hospital Düsseldorf, Germany). All, AIII, astrocytoma grade II or III; GBM, glioblastoma multiforme.

To compare these real-time PCR results with the expression of proteins in the cofilin pathway at the protein level, we performed immunoblot analysis of representative tumour samples using commercially available antibodies. All antibodies employed were first tested for specificity using lysates from glioblastoma cell lines endogenously expressing and / or transfected with the proteins of interest (data not shown).

Consistent with our immunohistochemical and real-time PCR data, CIN was massively downregulated at the protein level in astrocytic tumour samples (Figure 15A).

Interestingly, CIN protein expression appeared to be inversely correlated with glial tumour malignancy grade. In particular, CIN expression decreases from astrocytoma grade II to astrocytoma grade III as compared to normal cerebrum. And in grade IV glioblastoma multiforme, CIN expression is massively reduced and hardly detectable (Figure 15A, B and C). These findings are in good correlation with reported data about the increasing loss of chromosome 22q in gliomas with increasing grades of malignancy (Laigle-Donadey et al., 2006).

Concerning cofilin-inactivating kinases, we found by immunoblotting assay that both isoforms of LIM kinase (LIMK1 and LIMK2) are markedly upregulated in the majority of tested brain tumour samples (Figure 15B). We suppose that the difference in LIMK1 expression by RT-PCR and immunoblotting assays is due to the existence of two possible splice variants of human LIMK1 (Ott et al., 2007; Scott and Olson, 2007), which can not be differentiated by the employed primers. PAK4, an upstream activator of LIMKs, was also massively upregulated in GBM samples (Figure 15B), while in normal brain it was hardly detectable.

The median values obtained from the densitometrical evaluation of at least three independent experiments of immunoblotting analysis of glioblastoma samples show a ~70% decrease of CIN phosphatase, a ~two-fold increase of LIMK1, and at least an 11-fold increase of PAK4 kinase expression in these samples (see diagram in Figure 15D).

To summarise, these data on the expression levels (RT-PCR and immunoblotting) of proteins involved in the regulation of cofilin activity clearly indicate a dysregulation of the cofilin pathway in glioblastomas, with an upregulation of the cofilin-inactivating kinase LIMK1 and its upstream activator PAK4 and a downregulation of the cofilin reactivating phosphatase CIN.

To our knowledge, this is the first description of the expression of proteins of the cofilin pathway in astrocytic tumour samples, and the first report of CIN downregulation and PAK4 upregulation on the protein level in glioblastoma multiforme.

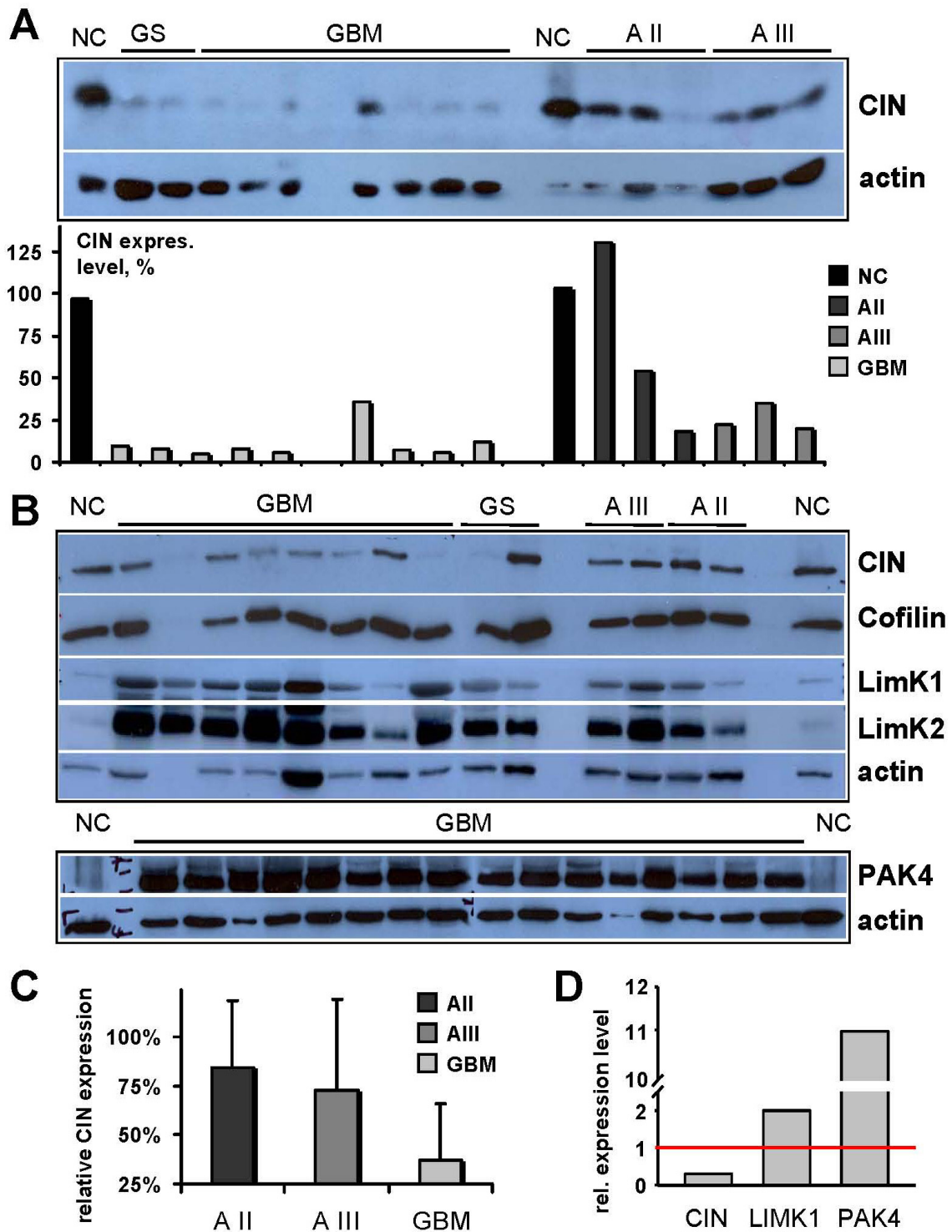


Figure 15: Dysregulation of the cofilin pathway in human brain tumour samples.

(A) and (B) Representative immunoblots showing dysregulation of the cofilin pathway. Lysates of tumour samples from patients with different types of glial tumours: gliosarcoma (GS), glioblastoma multiforme (GBM), astrocytoma grade II (A II), and astrocytoma grade III (A III) were tested by immunoblot analysis for expression levels of main players of the cofilin pathway compared to normal cerebrum (NC). The cofilin pathway is deregulated in glial tumour samples, with an upregulation of cofilin-inactivating kinases LIMK1, LIMK2 and PAK4 and a downregulation of a cofilin reactivating phosphatase CIN. Actin was used as a loading control. (C) Relative CIN expression levels in different stages of astrocytoma were determined from immunoblots by densitometry. Shown are mean values \pm SD of four independent experiments. (D) Relative expression levels of CIN, LIMK1 and PAK4 in glioblastoma were determined from immunoblots by densitometrical evaluation. Shown are median values of at least three independent experiments. The red line indicates the expression level of these genes in normal brain control sample.

5.4 CIN knock-down

5.4.1 Choosing of appropriate cell line

Because CIN expression is inversely correlated with glial tumour malignancy grade (see chapter 5.1) and, as mentioned above, loss of heterozygosity at chromosome 22, on which CIN is located, was shown in 41% of primary and in about 82% of secondary glioblastomas (Nakamura et al., 2005), we decided to investigate a possible role of CIN phosphatase in gliomagenesis. To investigate if there is a causal connection between CIN depletion and tumour initiation and progression, it was decided to knock-down CIN in an astrocytic tumour cell line. For this, an appropriate cell line had to be selected from a number of available glioma cell lines. Most of the available glioma cell lines have been established from biopsies of patients with different types of glial tumours. Because we wanted to manipulate the expression of CIN by RNA interference, we required a model cell line with detectable CIN expression levels. We therefore tested all glioma cell lines available in our laboratory for CIN expression levels by RT-PCR and immunoblotting analysis. The maximum CIN expression at the protein level was found for GBM6840 and U118 cell lines (Figure 16A). Maximum CIN expression in GBM6840 was also confirmed by RT-PCR experiments, which were done in collaboration with Department of Neuropathology at the University Hospital Düsseldorf. The GBM6840 cell line shows almost the same expression level of CIN at mRNA level as normal human brain, used as a control in RT-PCR experiments and defined as 1 in Figure 16B. These results are consistent with published data on this cell line. The glioblastoma line GBM6840 has been originally derived from a biopsy of a paediatric cerebellar glioblastoma multiforme and karyotypic analysis of this cell line revealed that chromosome 22 is not affected (Di Tomaso et al., 2000). Based on these data, GBM6840 cell line was selected for further experiments.

5.4.2 CIN downregulation using siRNA

To reduce CIN expression levels in the GBM6840 cell line, four different CIN-specific synthetic siRNA oligoribonucleotides targeting different regions of human CIN were tested. Different concentrations (5 – 75 nM) of each siRNA oligoribonucleotide were tested in transfection experiments and it was found that the best knockdown efficiency was achieved by using siRNA oligoribonucleotides at the concentration of 50 nM. The best efficiency was found for two of the four tested siRNA constructs: J-017120-07 (CIN siRNA #1) and J-017120-08 (CIN siRNA #2). The sequences of these siRNA oligoribonucleotides are shown in chapter 3.12. The maximum knock-down efficiency using siRNA oligoribonucleotides was achieved by the co-transfection of these two siRNA oligoribonucleotides (Figure 17). The knock-down efficiency in the transfection experiments employing a 1:1 mixture of these two oligoribonucleotides was about 75%, as evaluated densitometrically from the obtained Western blots (Figure 17B).

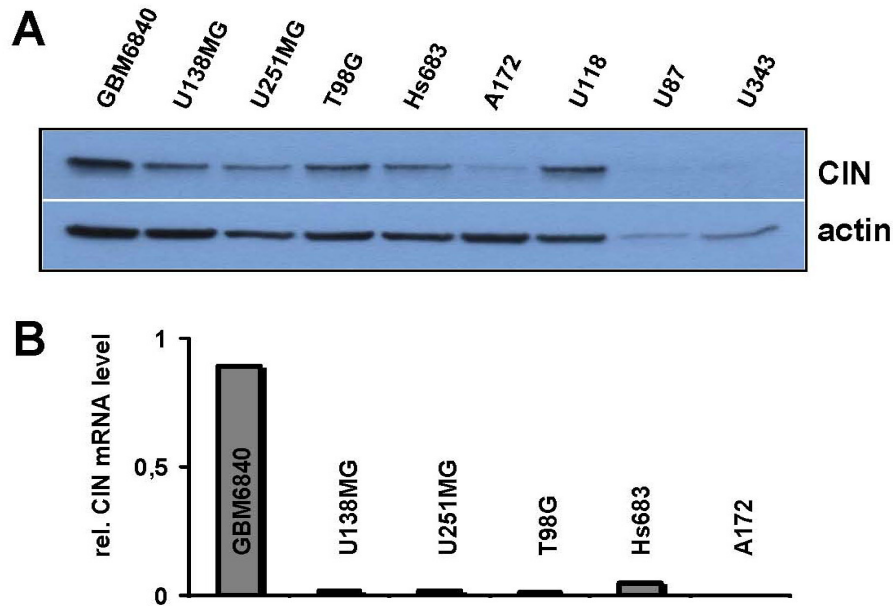


Figure 16: CIN expression in different glioma model cell lines.

(A) CIN protein expression levels were tested in different glioma cell lines by immunoblotting with a CIN-specific rabbit monoclonal antibody. (B) CIN mRNA expression levels were tested by RT-PCR. Five normal brain tissue samples from two different patients were used as reference tissues and CIN mRNA expression level in these tissues was defined as 1. RT-PCR experiments were performed by Dr. B. Klink at the Department of Neuropathology (University Hospital Düsseldorf, Germany).

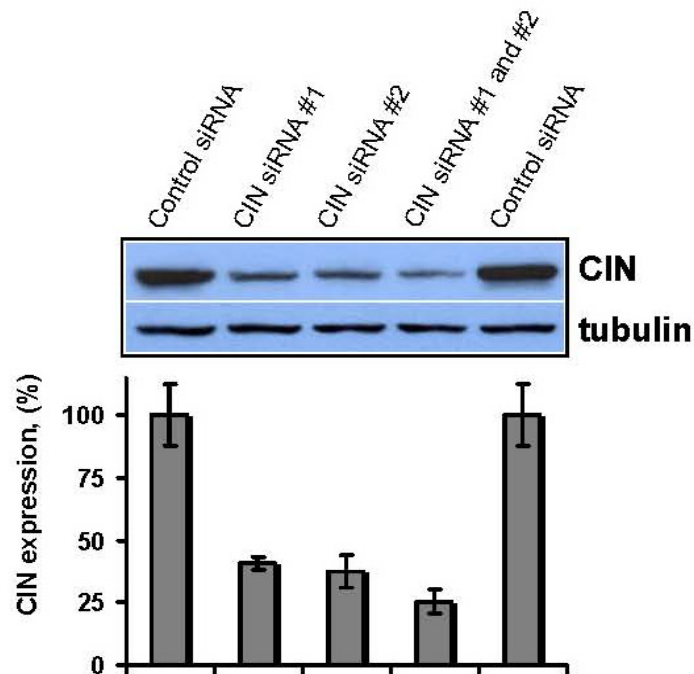


Figure 17: CIN knockdown in glioma cell line GBM6840 with siRNA.

GBM6840 cells were transfected with 50 nM control siRNA or CIN siRNA #1, CIN siRNA #2 or CIN siRNA #1 and #2 (25 nM of each). Cells were lysed 48 to 72 hours after transfection. Equal protein amounts (20 μ g) from lysates were separated by SDS-PAGE, transferred onto nitrocellulose membranes and CIN levels were analysed by immunoblotting with CIN rabbit monoclonal antibody. Densitometrical evaluation of CIN knock-down efficiency from Western blots was performed from 3 independent experiments. CIN signals were normalised to actin and/or tubulin signals.

5.4.3 CIN downregulation by shRNA

Despite the fact that transient transfection of siRNA oligoribonucleotides often achieves good knock-down efficiency in cells, these experiments would allow only a transient suppression of CIN protein expression. Thus, this approach is not feasible for long-term experiments. To solve this problem, it was decided to use a vector-based system to express CIN-directed shRNA in cells. Vector-based systems allow the establishment of the stable cell lines which are likely to be useful in long-term experiments.

For a long-term suppression of CIN protein expression in GBM6840 cells, five different human CIN-specific shRNA sequences targeting different regions of CIN were tested. The sequences of these shRNA constructs are shown in chapter 3.12. In preliminary experiments using transient transfections of these constructs in GBM6840 cells, we found three constructs (TRCN0000050045, TRCN0000050046 and TRCN0000050047), which downregulate CIN protein level in this glioma cell line and show good knock-down efficiency (Figure 18A). It was decided to use these three constructs for establishing stable cell lines. Stable GBM6840 cell line, expressing shRNA for depletion of CIN protein, as well as control GBM6840 cell line, expressing control shRNA, were generated using lentiviruses, produced as described in chapter 4.9. We observed that only one of three shRNA constructs (TRCN0000050046), which showed good results in transient transfection experiments, also very yielded a good CIN knock-down efficiency after transduction. All further experiments were performed using stable GBM6840 cell lines, received after the transduction of TRCN0000050046 for CIN depletion and of SHC002 as a control shRNA.

5.5 Dysregulation of the cofilin pathway in CIN depleted GBM6840

In the generated stable cell lines, we first analysed the expression levels of proteins involved in actin regulation by regulating cofilin activity, because we observed a dysregulation of this pathway in CIN-deficient glioma tumour samples (Figures 13-15). Interestingly, RNAi-mediated CIN depletion in GBM6840 cells causes similar effects to those observed in samples from patients with glioblastoma. We found some upregulation of LIMK2 and a massive upregulation of PAK4 (Figure 18B).

CIN activates cofilin by dephosphorylation, and this function is antagonised by LIMKs and the upstream regulator PAK4, which deactivate cofilin by phosphorylation on serine-3. We therefore tested if the decrease in CIN and increase in LIMK and PAK4 levels would increase P-cofilin levels in CIN-depleted GBM6840 cells. Indeed, we found a robust increase in P-cofilin levels in CIN-depleted GBM6840 cells. Indeed, we found a robust increase in P-cofilin levels in CIN-depleted cells, whereas the overall cofilin levels were unchanged (Figure 18B).

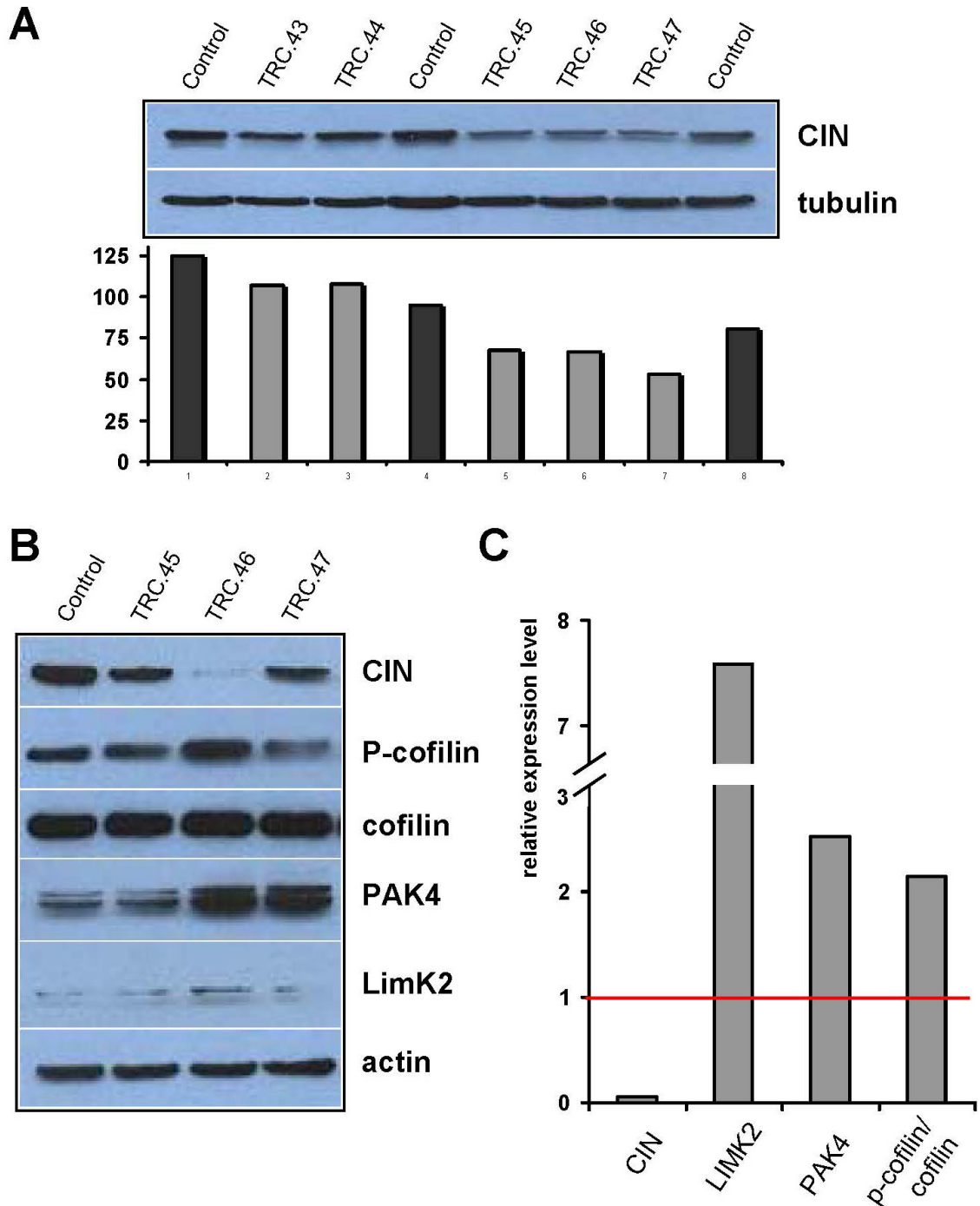


Figure 18: CIN knock-down in GBM6840 using MISSION shRNA constructs.

(A) MISSION shRNA constructs were transfected in GBM6840 and CIN expression level was analysed per immunoblot in received lysates 72 h after transfection. Densitometrical evaluation of obtained immunoblots shows that three shRNA constructs, TRC.45, 46 and 47 have an effect on CIN expression levels in GBM6840 cells. (B) Representative immunoblot analysis of cofilin pathway members in a stably CIN-depleted cell line, generated by transduction of GBM6840 with MISSION shRNA constructs. For convenience, the names of the constructs were abbreviated as follows: TRC.43 for TRCN0000050043, TRC.44 for TRCN0000050044, etc. (C) The mean values from densitometrical evaluation of immunoblot from (B) show a dysregulation of the cofilin pathway in the stably CIN-depleted clone TRC.46. Depletion of CIN phosphatase in GBM6840 cells shows a phenotype similar to the observed alterations in samples from patients with glioblastoma, with an upregulation of the cofilin-activating kinases LIMK2 and PAK4. The dysregulation of the cofilin pathway leads to increased amounts of p-cofilin level in CIN depleted cells. The red line shows the expression levels of these proteins in GBM6840 cells expressing control shRNA.

Taken together, these results suggest a causal connection between CIN downregulation and the upregulation of LIMK and PAK4, both in cells and in glial tumours. A dysregulation of the balance between the cofilin-activating phosphatase CIN and the cofilin-inactivating kinases LIMKs and PAK4 leads to a marked increase in p-cofilin levels. Such elevated p-cofilin levels are expected to cause a number of morphological and functional aberrations in cells, as a tightly regulated cofilin activity is well known to be essential for proper actin dynamics (Bamburg, 1999; DesMarais et al., 2005).

5.6 Effect of CIN depletion on nuclear morphology

The depletion of cofilin-activating phosphatase CIN with the resulting upregulation of cofilin-inactivating kinases LIMKs and PAK4 and the subsequent increase in p-cofilin levels should lead to a stabilisation of F-actin structures in cells and cause changes in the cell morphology. To analyse cellular morphology, we stained CIN depleted and control cells with phalloidin (to visualise F-actin) and DAPI (to visualise the nuclei) and analysed cells under an epifluorescence microscope.

The typical cellular and nuclear morphology for control siRNA-treated GBM6940 cells, which is similar to non-treated cells, is shown in Figure 19A. CIN knockdown using single siRNA oligoribonucleotides or their mixture in GBM6840 cells leads to a drastic increase in the number of deformed nuclei, as well as to a stabilisation of F-actin-rich structures. Typical images of deformed and lobulated nuclei observed after CIN siRNA transfections are shown in Figure 19B. These results are likely of high relevance for astrocytic tumours. In the histopathology of glial tumours, nuclear deformities are taken as a robust indicator of malignancy grade. GBM are characterised by an abundance of cells with nuclear deformities and the presence of multinucleated giant cells (Reifenberger and Collins, 2004).

To quantify number of aneuploid cells with deformed and abnormal nuclear morphology, cells were treated with CIN or control siRNA. 72 h after transfection, cells were fixed and stained with phalloidin and DAPI, and were analysed under an epifluorescence microscope. The analysis of the nuclear phenotype-distribution in over 300 cells per condition shows that CIN depletion increases the number of deformed and lobulated nuclei from 10% in control treated cells to 45% in CIN-depleted cells (Figure 19C). In contrast, the proportion of CIN-depleted cells with micronuclei or multinucleated cells is comparable to control treated cells.

In previous work it was shown that the phosphoregulation of cofilin by CIN is important during mitosis and cytokinesis. CIN knockdown or loss of CIN function in HeLa cells triggers cell division defects and results in a subsequent accumulation of aneuploid cells (Gohla et al., 2005). Our data confirm these findings and show that siRNA-mediated depletion of CIN phosphatase in the glioma cell line GBM6840 also leads to the accumulation of deformed and lobulated nuclei. Defects in the mitotic machinery, which lead to aneuploidy, can also cause genetic instability and trigger tumour initiation and progression (Pihan and Doxsey, 1999; Ross, 1996). To better understand the role of CIN in mitosis and cytokinesis, we next analysed endogenous CIN localisation during cell division in GBM6840 and HeLa cells.

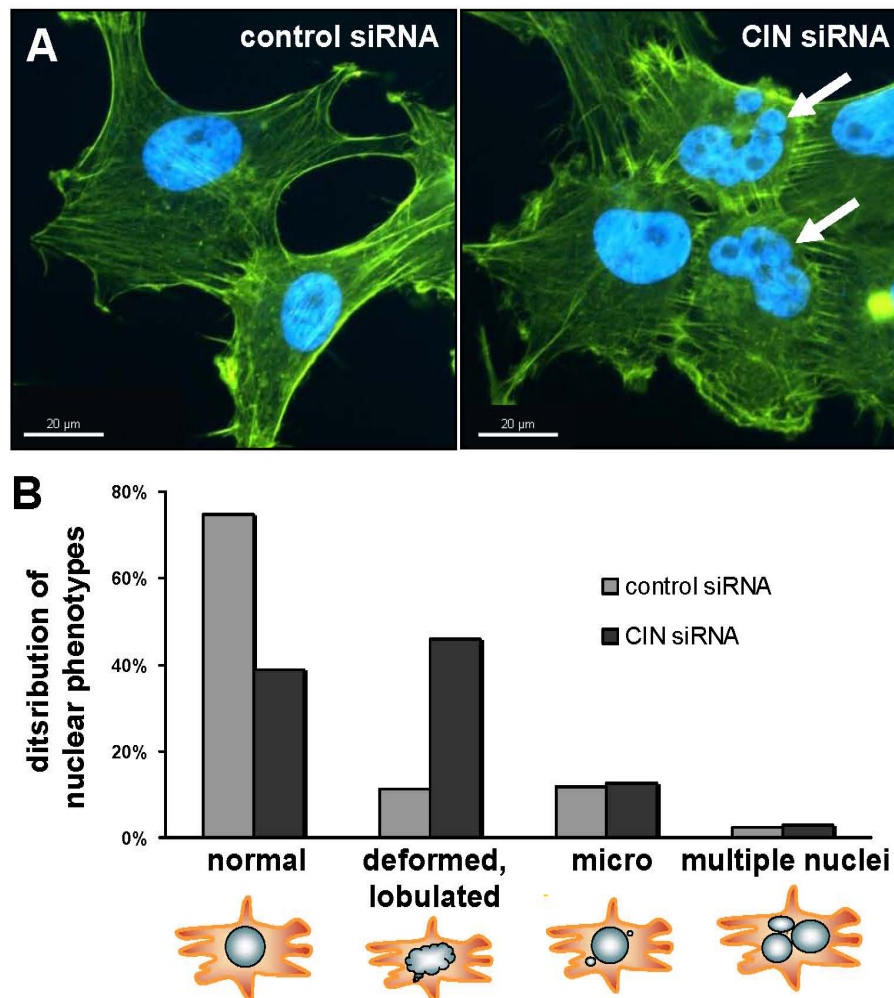


Figure 19: Analysis of nuclear morphologies in CIN-deficient glioblastoma cells.

(A) Typical cell and nuclear morphology of GBM6840 cells, transfected with control siRNA or with CIN siRNA. Depletion of CIN phosphatase in GBM6840 cells leads to increased number of deformed and lobulated nuclei. Nuclei are shown in blue and actin cytoskeleton in green colors. Scale bars represent 20 μm . **(B)** Distribution of different nuclear phenotypes in CIN-depleted cells compared to control siRNA-treated cells. Images were obtained from one transfection experiment of 3 slides with cells transfected with CIN siRNA or control siRNA and nuclear phenotypes were scored for more than 300 cells.

5.7 Subcellular CIN localisation during mitosis and cytokinesis

Analysis of endogenous CIN localisation in GBM6840 and HeLa cells during different stages of mitosis revealed an accumulation of CIN phosphatase on the mitotic spindle apparatus, in the cleavage furrow, and also in the plasma membrane during the late stages of cytokinesis (Figure 20). The localisation of CIN in the cleavage furrow of GBM6840 cells indicates a role for CIN during cytokinesis, as previously reported (Gohla et al., 2005). Another cofilin-specific phosphatase, Slingshot-1L, was also shown to be involved in cytokinesis in HeLa cells and to accumulate in the cleavage furrow. Slingshot depletion *via* RNA interference causes a prominent accumulation of multinucleated cells (Kaji et al., 2003). As shown in Figure 19, the number of multinucleated GBM6840 cells is similar in the presence or in the absence of CIN, suggesting that Slingshot and CIN may perform redundant functions in the regulation of actin dynamics during cytokinesis.

Actin dynamics were recently shown to be very important not only in the process of cytokinesis, but also in mitosis (Walczak and Heald, 2008). Previous work has shown the accumulation of actin filaments on the microtubule-based mitotic apparatus and has demonstrated an essential role of actin for mitotic spindle function (Woolner et al., 2008; Yasuda et al., 2005). The essential role of CIN for actin dynamics and the observed accumulation of CIN on the mitotic spindle points to multiple important roles for CIN phosphatase in mitotic cell division. These combined functions may explain the increased number of deformed and lobulated nuclei in CIN depleted cells (see Figure 19).

5.8 Effect of CIN depletion on the actin cytoskeleton

CIN-depleted GBM6840 cells are characterised by a dysregulation of the cofilin pathway, similar to the altered protein expression pattern seen in samples from patients with astrocytic tumours (for more details see chapters 5.1 and 5.5). The CIN depletion-mediated upregulation of LIMKs and PAK4 leads to an increased pool of p-cofilin in GBM6840 cells (Figure 18B). Increased p-cofilin levels generally stabilise F-actin-based structures in cells. We have therefore analysed the cell morphology and actin stress fiber formation of CIN depleted cells as compared to control GBM6840 cells. Interestingly, under normal growth conditions (in the presence of FCS), we were unable to detect significant differences in the actin cytoskeletons between CIN depleted and control cells. However, when CIN depleted and control GBM6840 cells were grown under starvation conditions (without serum), we observed massive changes in actin structures (Figure 21).

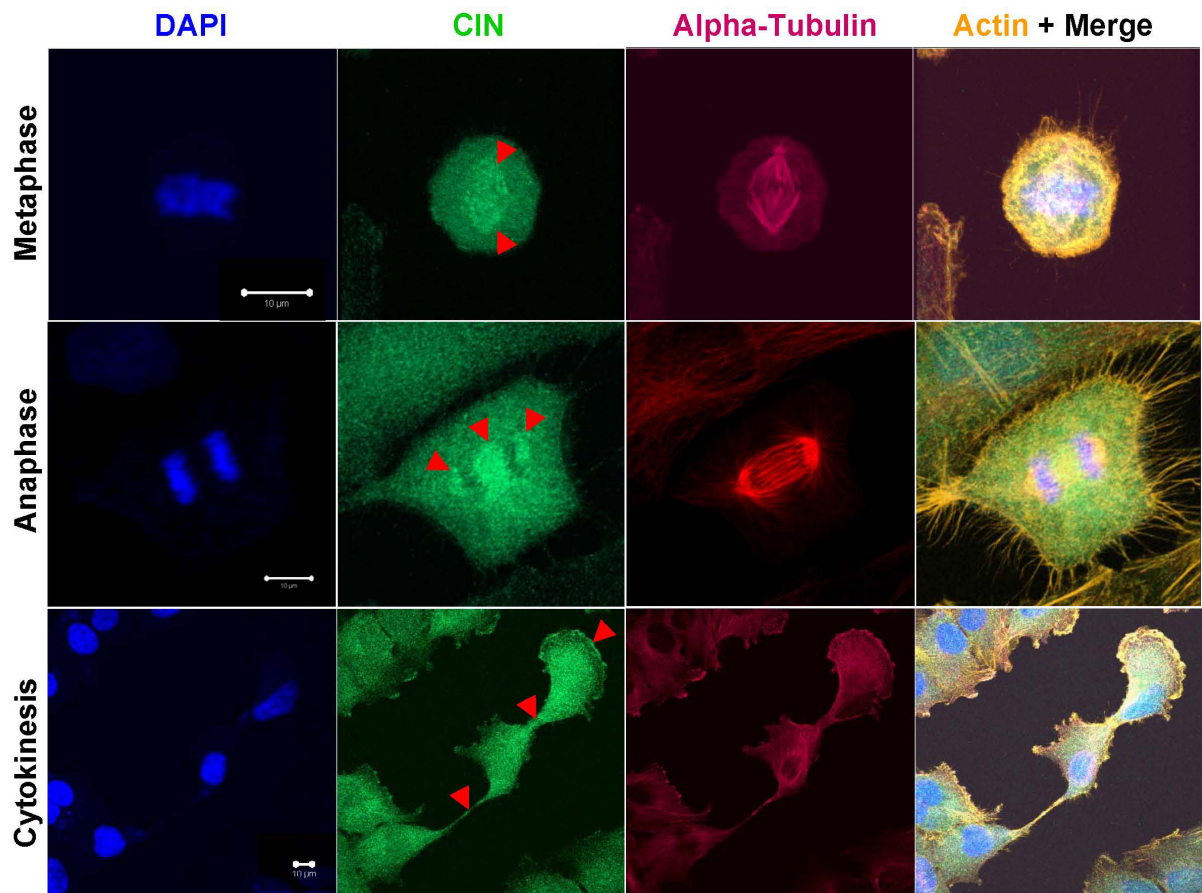


Figure 20: Endogenous CIN localisation in cells during mitotic cell division.

Nuclei and DNA (chromosomes) are shown in blue, endogenous CIN in green, tubulin in red and actin in yellow colors. CIN is targeted to sites of cofilin-dependent actin dynamics during mitosis. The localisation of endogenous CIN is shown in a panel of different mitotic GBM6840 and Hela cells. Arrows indicate CIN targeted to the mitotic spindle apparatus in metaphase and anaphase and to the plasma membrane and cleavage furrow in later stages of cytokinesis. GBM6840 cells are shown in metaphase and cytokinesis and Hela cells are shown in anaphase. Scale bars represent 10 μm .

We found that starvation of control shRNA cells leads to a depolymerisation of actin structures in GBM6840 cells (Figure 21A). In contrast, starvation of CIN depleted GBM6840 cells under the same conditions has no significant effect on F-actin. Actin structures remain polymerised and actin stress fibers are still present in starved CIN depleted GBM6840 cells, as shown in Figure 21B. These results indicate a CIN-dependent difference in the turnover rates of the dynamic actin cytoskeletons, which are revealed upon growth factor withdrawal. This finding is consistent with the role of CIN as a cofilin activator that leads to increased actin dynamics.

Another interesting observation is that CIN depleted GBM6840 cells are clearly bigger in size, compared to cells expressing the control shRNA construct. We analysed cell areas of almost 100 cells after starvation for each condition (CIN shRNA versus control shRNA). We found that the average cell area of control cells is about $1400 \mu\text{m}^2$. CIN depletion leads to stress fiber stabilisation and increases the average cell area by more than 60% to an average value of $2300 \mu\text{m}^2$ (see diagram in Figure 21C).

Taken together, the effects of CIN depletion in GBM6840 cells on nuclear deformities (see Figure 19) and on cell size (Figure 21C) are consistent with the observed occurrence of aneuploid, giant cells in glioblastoma multiforme (Reifenberger and Collins, 2004).

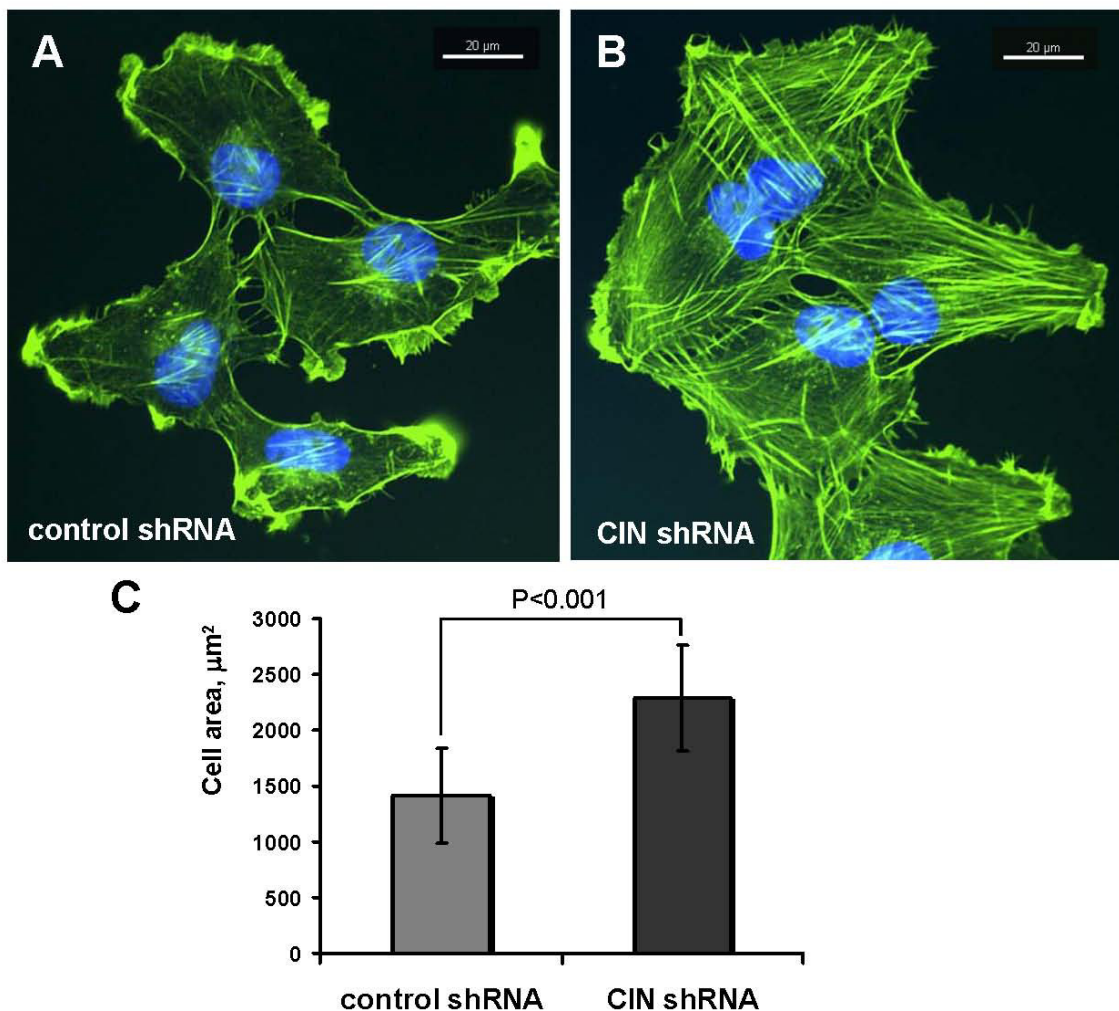


Figure 21: Effect of CIN depletion on cell morphology.

Different cell morphologies after overnight starvation of GBM6840 cells stably expressing control shRNA (A) and CIN shRNA constructs (B). Nuclei are shown in blue and the actin cytoskeleton in green colors. Scale bars represent $20 \mu\text{m}$. (C) Analysis of the cell areas after starvation. Indicated are mean values \pm SD of two independent experiments. Cell areas were determined from more than 100 cells.

5.9 Effect of CIN depletion on anchorage-independent growth

Downregulation of CIN phosphatase causes massive changes in cellular cofilin phosphocycling and in actin dynamics (see Figures 18, 19 & 21). Altered cofilin activity has been linked to the initiation and progression of malignancies, particularly in breast cancer (Wang et al., 2007a), and it is well established that the process of cell transformation depends on alterations in the cytoskeleton, which decrease adhesion-dependent growth requirements (Bamburg and Wiggan, 2002). To test if CIN depletion plays a role in transformation, and thus potentially in tumourigenicity, we performed soft-agar assays.

First, we compared the ability of GBM6840 cells transfected either with CIN siRNA oligoribonucleotides or with control siRNA to grow in soft agar. Downregulation of CIN, mediated by siRNA oligoribonucleotide transfection, increased the anchorage-independent growth of CIN-depleted cells by approximately 40% as compared to control siRNA-transfected cells (Figure 22C). Importantly, the stable, shRNA-mediated downregulation of CIN phosphatase increased the colony formation ability of GBM6840 cells in soft agar more than two-fold as compared to cells expressing control shRNA constructs (Figure 22E).

To test if this effect was due to an increased growth or viability of CIN-depleted cells, we performed proliferation assays in parallel with soft agar assays for both siRNA- and shRNA-based experiments. As shown in the diagram in Figure 22D, CIN depleted cells proliferate at the same rate as control cells (for siRNA). In case of stable depletion of CIN by shRNA, CIN-deficient cells even tend to grow a little slower than the control cells.

These results suggest a possible role of CIN phosphatase in glial tumour initiation.

5.10 Increased EGF signalling and invasion of CIN depleted cells

Our results indicate that CIN phosphatase may play a role in glial tumour initiation. All glial tumours are characterised by a high local invasive potential with unknown molecular mechanism of such behavior (Hoelzinger et al., 2005; Vescovi et al., 2006). CIN depleted cells are characterised by a dysregulation of the cofilin pathway with upregulation of LIMKs, PAK4 and an increased amount of p-cofilin. Interestingly, LIMKs are shown to play an important role in tumour-cell invasion and metastasis with overexpression of LIMKs in melanoma, ovarian carcinoma, lung, breast, prostate cancer cell lines and tumours (Davila et al., 2003; Davila et al., 2007; Scott and Olson, 2007; Wang et al., 2007a; Yoshioka et al., 2003). The cofilin pathway itself was also linked to enhanced cell motility during metastasis (Condeelis et al., 2001; Ghosh et al., 2004; Wang et al., 2007a).

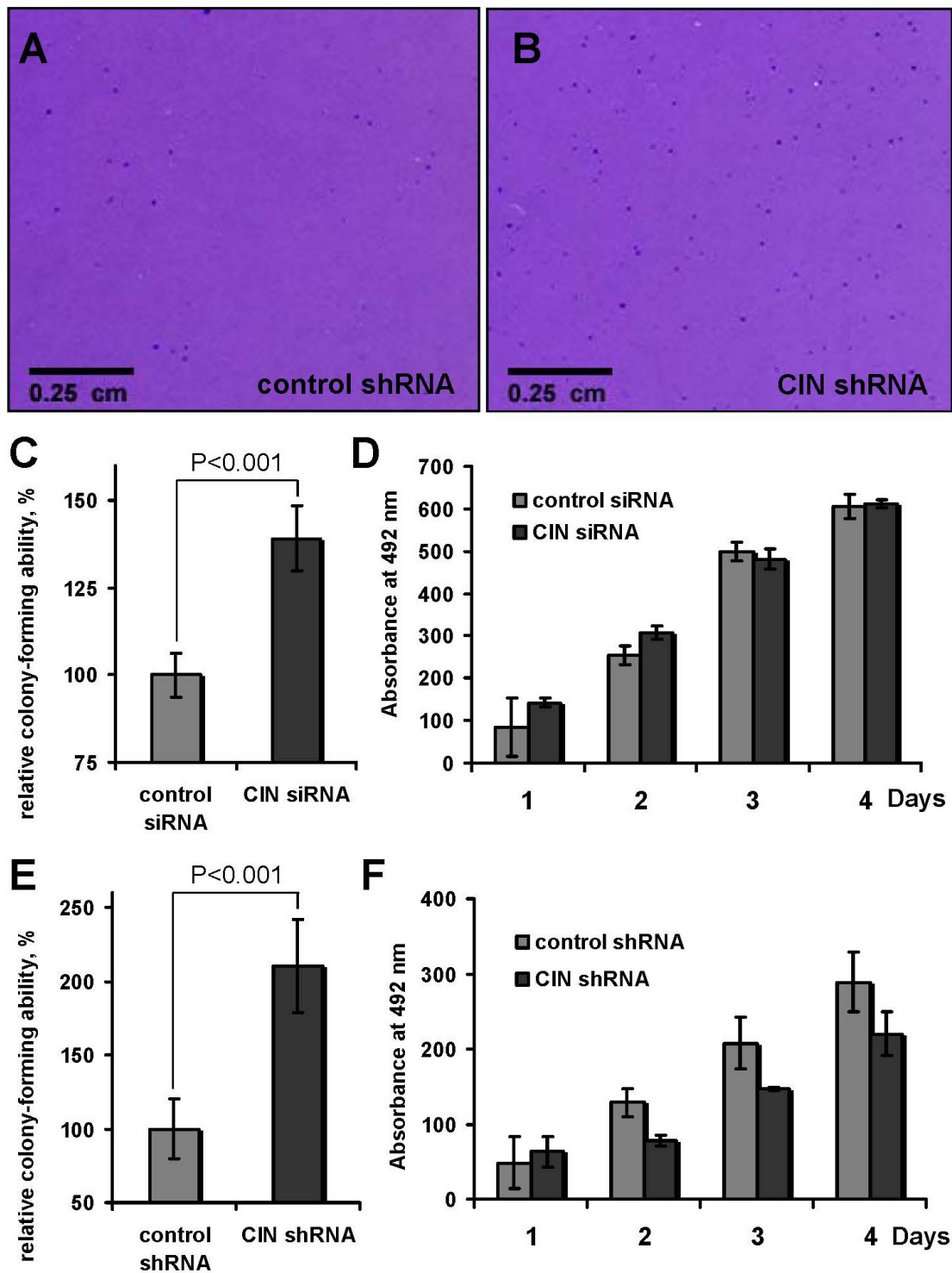


Figure 22: Effect of CIN depletion on cell growth.

Anchorage-independent growth of GBM6840 cells stably expressing control shRNA (A) or CIN shRNA (B) constructs. Cells transfected with siRNA or stably expressing shRNA constructs were seeded in soft agar. After 2 weeks, the formed colonies were visualised by staining with Crystal Violet. Plates were scanned and colonies were counted visually. The average number of colonies per plate with control constructs was set as 100% and the results are shown in diagram (C) for siRNA (2 independent experiments performed in triplicates, more than 200 colonies per plate) and on (E) for shRNA (3 independent experiments performed in triplicates, more than 3,000 colonies per plate). CIN depletion increases anchorage-independent growth of GBM6840 cells. (D) GBM6840 cells, transfected with control or CIN siRNA oligos, were seeded in 96-well plates and the Aqueous One Solution Cell Proliferation Assay was performed for 4 days, because after that time cells became confluent. (F) Proliferation assay as in (D), but for cells stably expressing shRNA constructs.

To measure the invasive potential of CIN-depleted GBM6840 cells compared to control cells we performed *in vitro* invasion assays. We first tested which chemoattractant may be used in this assay. Hepatocyte growth factor (HGF) was shown to activate PAK4 in prostate cancer cells. PAK4 binds to and phosphorylates LIMK1, and increases cell migration speed (Ahmed et al., 2008). Epidermal growth factor (EGF) was shown to activate kinases that phosphorylate cofilin and is often used to study cell migration (Condeelis et al., 2005; Wang et al., 2007a). Moreover, strong overexpression/amplification of epidermal growth factor receptor is found in about 60% of primary glioblastomas (Hoelzinger et al., 2005; Reifenberger and Collins, 2004; Schwartzbaum et al., 2006). We therefore compared the stimulation ability of EGF and HGF on CIN depleted and control GBM6840 cells. As a readout we used p-cofilin levels in these cells upon stimulation. As shown in Figure 23A, HGF has no significant effect on p-cofilin levels. In contrast, EGF stimulation of both control and CIN depleted GBM6840 cells leads to increased p-cofilin levels. Interestingly, p-cofilin levels in CIN depleted cells are clearly higher than in control GBM6840 cells upon EGF stimulation (Figure 23A and B). Based on these findings, we decided to use EGF as a chemoattractant in the *in vitro* invasion assay.

As shown in the diagram in Figure 23C, depletion of CIN phosphatase in GBM6840 cells increases the invasive behaviour of these cells more than two-fold. Together with our findings so far, the data suggest that the CIN depletion-mediated dysregulation of the cofilin pathway triggers this cellular behaviour.

5.11 CIN regulation

CIN is an important regulator of cofilin-mediated actin cytoskeletal dynamics during cell migration and cell division (Gohla et al., 2005). Here, we show that CIN protein is strongly reduced in astrocytic tumours, and that the depletion of CIN phosphatase in GBM6840 cells has dramatic effects on the cofilin pathway and increases the tumorigenic and invasive potential of these cells. However, there is currently very little information on the regulation of CIN phosphatase activity. Recently, an inhibitory interaction between CIN and Hsp90 protein was reported (Huang et al., 2008). It was shown that the ATP-depletion-mediated loss of this interaction enables CIN-dependent cofilin dephosphorylation with consequent actin/cofilin rod assembly, which explains a mechanism for the formation of pathological actin/cofilin aggregates during neurodegenerative energy flux (Huang et al., 2008).

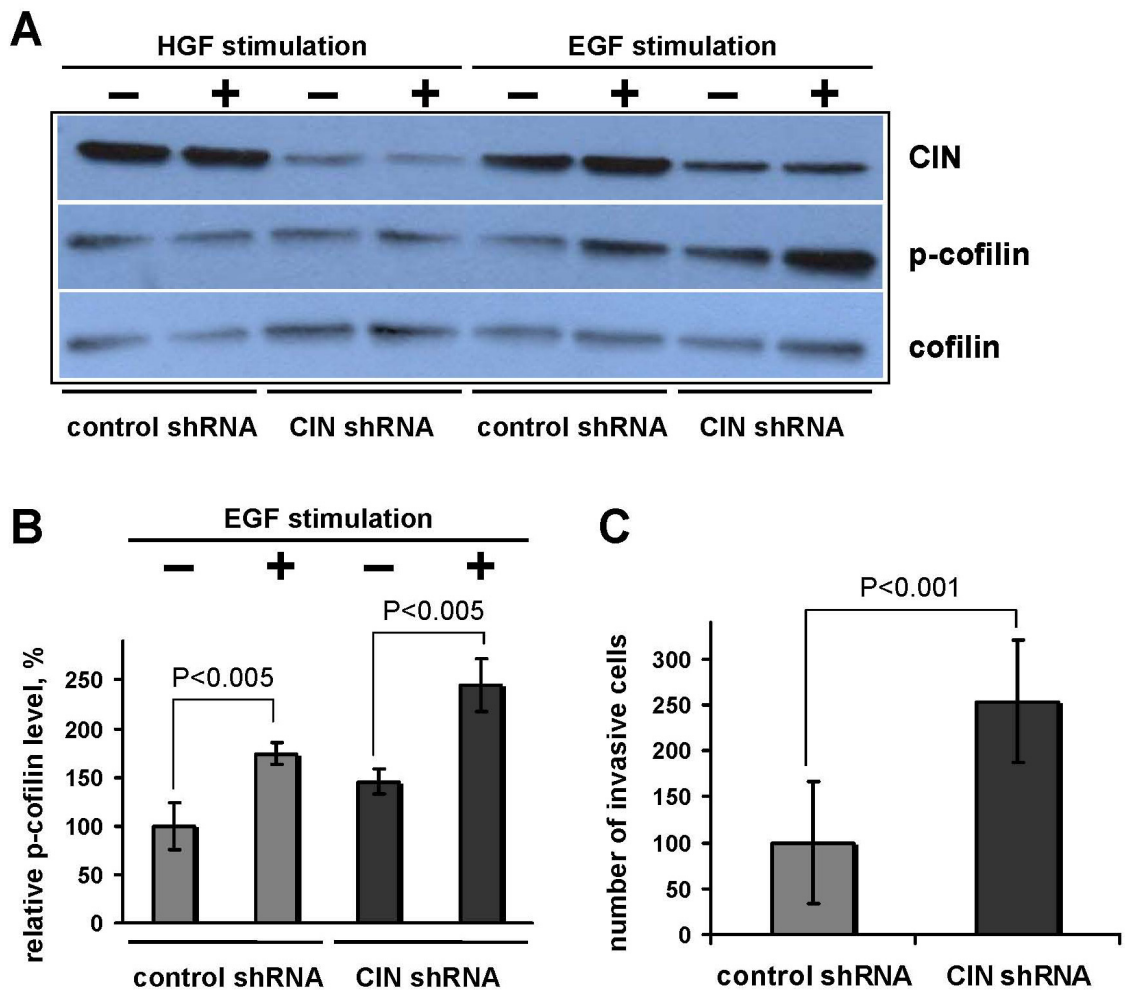


Figure 23: Effect of HGF and EGF on p-cofilin levels and invasive behaviour of CIN depleted and control GBM6840 cells.

(A) CIN depleted and control GBM6840 cells were starved for 4 hours in DMEM medium without any additives and were then stimulated for 5 min with HGF or EGF. After that, cells were lysed and cell lysates were analysed by immunoblotting. (B) Densitometrical evaluation of p-cofilin levels in GBM6840 cells upon EGF stimulation of three independent experiments. P-cofilin signals were normalised to cofilin signals. CIN depleted GBM6840 cells are characterised by increased EGF signalling. Shown are mean values \pm SD. (C) *In vitro* invasion assay of CIN depleted and control GBM6840 cells. CIN depleted cells show higher invasive potential, compared to control cells. Indicated are mean values \pm SD of three independent experiments done in triplicates.

The identification of new CIN interacting partners will provide more information about the regulation of cofilin-mediated actin dynamics. One ongoing project in our group has identified the calcium- and integrin- binding protein 1 (CIB1) as an interaction partner of CIN in yeast two-hybrid screens (Hoffmann, Fedorchenko, Jeanclos, Gohla; data not shown).

CIB1 is an evolutionarily conserved and NH₂-terminally myristoylated protein, which contains two functional calcium-binding EF hand motifs that can bind calcium or magnesium (Naik et al., 1997; Yamniuk et al., 2007). CIB1 shows relatively high homology to other EF hand proteins such as Calmodulin (54%) and Calcineurin B (57%). Interestingly, Calcineurin B is known as the regulatory subunit of Ca²⁺-dependent protein phosphatase 2B (Guerini et

al., 1989), suggesting that CIN may exist in a similar complex, consisting of a catalytic subunit CIN and a structural subunit CIB1. CIB1 is able to bind different proteins and modify their function and/or localisation (Leisner et al., 2007). In the context of this work, the interaction of CIB1 with PAK1 is most interesting. It was demonstrated that CIB1 interacts in a calcium-stimulated fashion with PAK1, leading to an increase in PAK-induced cytoskeletal dynamics (Leisner et al., 2005).

To analyse the interaction between CIN and CIB1, we performed colocalisation experiments and FRET analyses.

5.11.1 CIN – CIB1 colocalisation in HeLa cells

We first investigated the subcellular localisation of CIN and CIB1 in HeLa cells. For that, we overexpressed CIB1-GFP and tested the localisation of the overexpressed CIB1-GFP fusion protein and simultaneously analysed the localisation of endogenously expressed CIN using confocal laser scanning microscopy.

We found that endogenous CIN strongly co-localises with CIB1-GFP in the nucleus, in dynamic membrane areas involved in cell motility, as well as in the cytokinetic ring involved in cell division (Figure 24). The observed localisation of CIB1 overlaps with known sites of CIN-mediated cytoskeletal dynamics.

Whereas co-localisation analysis can be used to confirm and strengthen an interaction that was found by other methods, the co-localisation of two proteins in the apparent same cellular compartment does not necessarily mean that these two proteins interact with each other. To confirm the interaction of CIN and CIB1 proteins in cells with other imaging techniques, we performed FRET analyses.

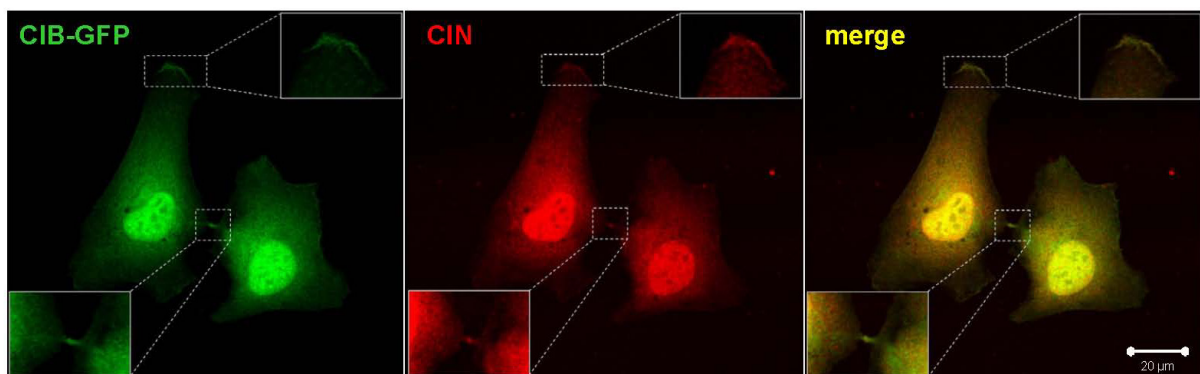


Figure 24: Colocalisation analysis of CIB1-GFP with endogenous CIN protein.

The subcellular localisation of overexpressed CIB1-GFP and endogenous CIN was analysed by confocal microscopy in HeLa cells (n=3, more than 30 cells). Endogenous CIN and CIB1-GFP fusion protein colocalise in the nucleus, in dynamic membrane areas involved in cell motility and in the cytokinetic ring involved in cell division. Dashed boxes indicate the enlarged areas.

5.11.2 CIN – CIB1 interaction analysis by FRET

To measure the CIN – CIB1 interaction by FRET, we first determined optimal transfection conditions such that both fluorophores (CIN-YFP and CIB1-CFP) would be expressed in cells at approximately equal amounts. As shown in Figure 25A, optimal conditions were achieved by transfection of 75 ng CIN-YFP and 375 ng of CIB1-CFP plasmids.

Several FRET techniques can be used to measure protein – protein interactions in living as well as in fixed cells. Acceptor or donor photobleaching and sensitised emission FRET techniques are some of them. To measure the CIN – CIB1 interaction, we tried both acceptor photobleaching and sensitised emission FRET. The approach of acceptor photobleaching in fixed cells had to be abandoned for technical reasons, because under our microscopy settings, we observed unacceptable bleaching of the donor (CIB1-CFP) during acceptor (CIN-YFP) photobleaching (data not shown).

To measure sensitised emission FRET, we overexpressed CIN-YFP and CIB1-CFP in HeLa cells and then collected images from the cells expressing these constructs using the confocal microscope. Several coefficients from obtained images were determined in ImageJ software, using the PixFRET plug-in for further FRET calculations. To determine the Donor Bleed-Through coefficient (BT_{don}), stacks of two images of cells expressing only CIB1-CFP were used: the first one in the FRET setting and the second one in the Donor setting. Acceptor Bleed-Through coefficients (BT_{acc}) were determined from stacks of two images of the cells expressing only CIN-YFP: the first one in the FRET setting, the second one in the Acceptor setting. Thresholds in these cases were determined automatically from the images using the PixFRET plug-in, which also automatically calculates the mean of the spectral bleed-throughs and the parameters corresponding to the linear or exponential fit of the data (Feige et al., 2005). In case of FRET, NFRET and FRET efficiency calculation thresholds were determined manually so that the FRET efficiency in case of negative control was equal null (empty images). With these thresholds settings, the FRET efficiency determined for cells expressing the FRET positive control was about 40%.

In our case, the FRET efficiency of the CIN – CIB1 interaction was calculated in ImageJ software, using the PixFRET plug-in with the following settings:

$$BT_{don} = 0.14119 + 0.05433 * \exp(0.00186 * DONOR_{don})$$

$$BT_{acc} = 0.10558 * ACCEPTOR_{acc} + 0.00034$$

Thresholds for	FRET channel	0.4
	Donor channel	7.5
	Acceptor channel	8.0

DONOR_{don}, fluorescence intensities of CIB1-CFP in Donor settings;

ACCEPTOR_{acc}, fluorescence intensities of CIN-YFP in Acceptor settings.

Using the PixFRET plug-in with these settings in the ImageJ software, we calculated FRET images and FRET efficiency from these images of the CIN – CIB1 interaction. A typical histogram of FRET efficiency distribution is shown in Figure 25B and representative FRET images are shown in Figure 25C. FRET efficiency between CIN and CIB1 calculated by sensitised emission FRET is about 8%.

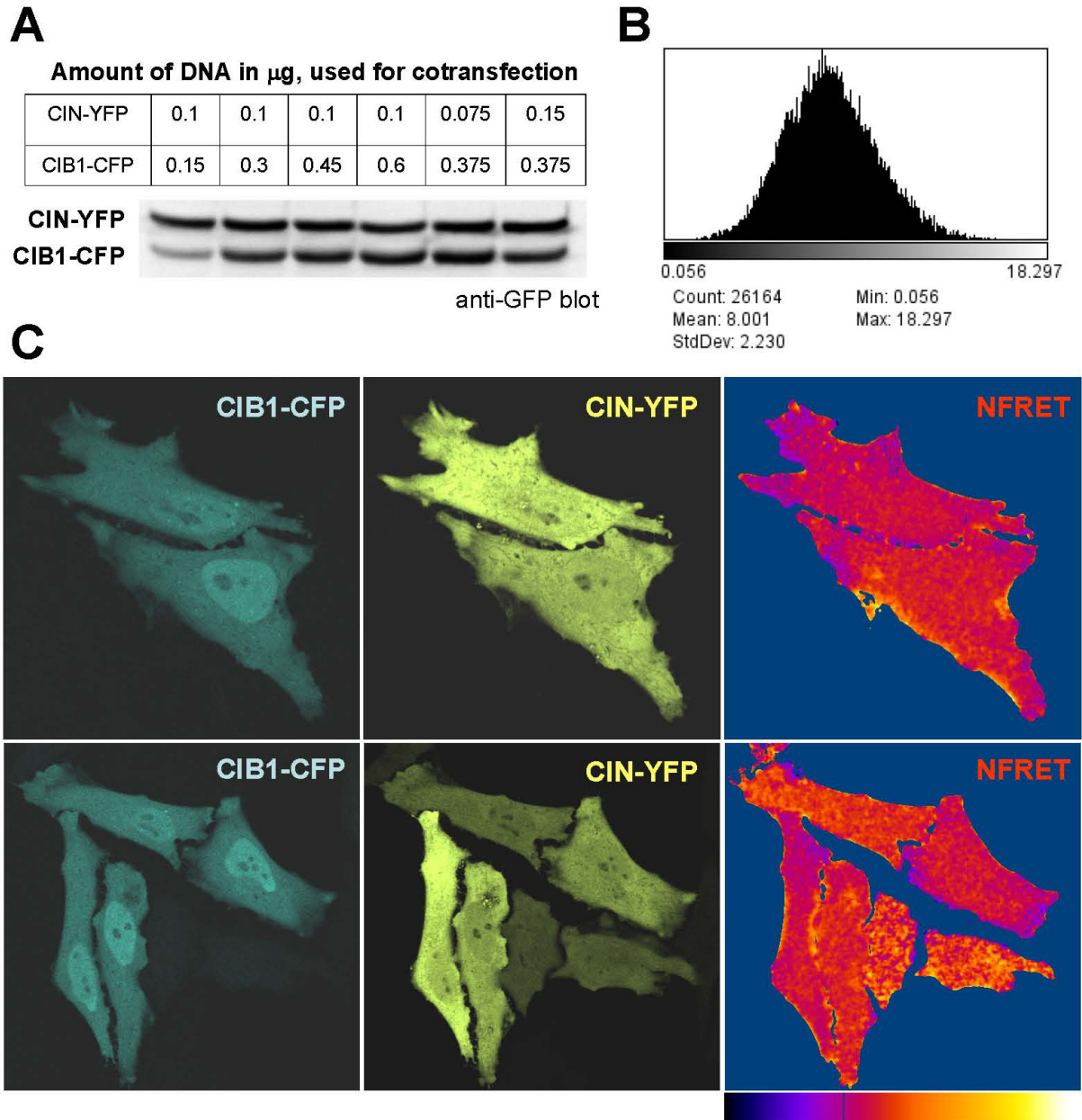


Figure 25: FRET analysis of the CIN – CIB1 interaction.

(A) HeLa cells were transfected with different amounts of CIN-YFP and CIB1-CFP plasmids to determine optimal expression conditions for both constructs. Cells were lysed and analysed per immunoblotting with anti-GFP Ab. FRET efficiency was measured by sensitised emission method in living HeLa cells expressing CIB1-CFP and CIN-YFP fusion proteins at the same concentration. Images were taken on a LSM 510 Meta confocal microscope. FRET analysis was performed with the ImageJ software and the PixFRET plug-in. (B) Representative histogram of FRET efficiency distribution for the CIN – CIB1 interaction in HeLa cells. (C) Representative experiments of FRET images ($n=2$ independent experiments, FRET for 10 images with more than 30 cells was calculated). The FRET efficiency between CIN-YFP and CIB-CFP calculated by the sensitised emission method is about 8%.

5.11.3 Effect of CIB1 on the CIN phosphatase activity

CIB1 is known to bind calcium ions with an affinity of 0.5 and 1.9 μM (Yamniuk et al., 2007). Ca^{2+} has been shown to inhibit the catalytic activity of HAD-type phosphatases (Peeraer et al., 2004). Since we observed an interaction between CIN and CIB1 proteins (which was also extensively investigated and confirmed biochemically in our group, data not shown), we next investigated the possible effects of CIB1 on the CIN-mediated dephosphorylation of the general phosphatase substrate *p*-NPP and the specific CIN substrate PLP under different Ca^{2+} concentrations.

As shown in Figure 26A, 1 μM Ca^{2+} inhibits the activity of CIN towards *p*-NPP a more than 70% (as reported previously; see Gohla et al., 2005). Interestingly, the addition of CIB1 stabilises the activity of CIN against Ca^{2+} -induced inhibition (Figure 26B). In the presence of CIB1 at a concentration of 10 μg in the reaction mix (1 μg CIN, 1 μM Ca^{2+}) the inhibition of CIN phosphatase by Ca^{2+} was less than 50%. In the absence of Ca^{2+} the same concentration of CIB1 also increases the activity of CIN phosphatase towards *p*-NPP a (approximately 25%, data not shown).

Based on these findings and the fact that CIN dephosphorylates *p*-NPP very slowly (Jang et al., 2003), we performed *in vitro* phosphatase assays in the presence or absence of CIB1 over a wide range of Ca^{2+} concentrations using PLP as a specific CIN substrate. To detect free phosphate liberated by dephosphorylation, we used the PiPer Assay as described under Experimental Procedures.

Interestingly, the effect of Ca^{2+} on the specific CIN PLP-phosphatase activity is less pronounced than toward *p*-NPP as a CIN substrate (Figure 26C). The inhibition of CIN PLP phosphatase activity by approximately 70% is seen in the presence of 0.2 mM Ca^{2+} . In this case, the addition of a two-fold molar excess of CIB1 (1.4 μg versus 10 μg of CIB1 protein used in the *p*-NPP reaction) stabilises the activity of CIN against Ca^{2+} -induced inhibition up to almost 80% as compared to the CIN activity in the absence of Ca^{2+} (Figure 26C). Interestingly, a two-fold molar excess of CIB1 over CIN is able to maintain up to 20% of the CIN activity at 1 mM Ca^{2+} concentration, which is likely irrelevant for intracellular processes.

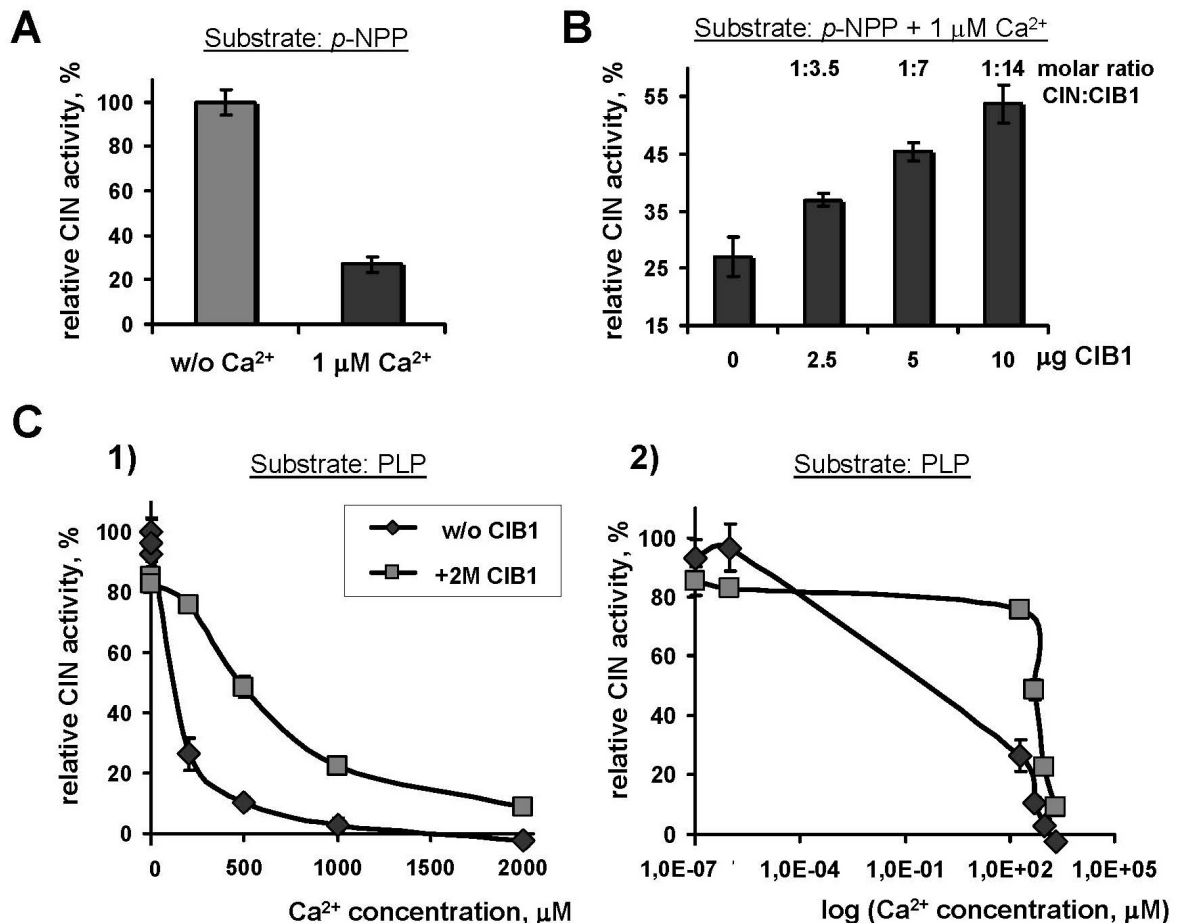


Figure 26: Effect of CIB1 and Ca²⁺ on the CIN phosphatase activity.

(A) Ca²⁺-mediated inhibition of CIN phosphatase activity in *in vitro* *p*-NPP phosphatase assays. 1 μM Ca²⁺ inhibits CIN activity towards *p*-NPP by more than 70%. (B) Addition of CIB1 protein in the reaction mix stabilises the activity of CIN against Ca²⁺-mediated inhibition towards *p*-NPP. (C) Effect of CIB1 protein against Ca²⁺-mediated inhibition towards PLP. All experiments were done at least three times. Indicated are mean values ± SD from the final experiment done in triplicates and the results are shown in 1) linear and 2) logarithmic coordinates.

5.11.4 Effect of CIN phosphatase activity on CIB1 protein expression

We showed the interaction of CIN phosphatase with CIB1 protein by colocalisation and FRET analysis and also found that CIB1 protein has an effect on CIN phosphatase activity. Our next question was if CIN in turn has any effects on CIB1 protein.

We first investigated the localisation of endogenous CIB1 protein in HeLa cells overexpressing CIN phosphatase. Interestingly, we found that overexpression of CIN increases the levels of endogenous CIB1 protein (Figure 27A). To confirm this finding biochemically, we overexpressed both proteins in HeLa cells and found that increasing the

cellular concentration of CIN phosphatase also increases the levels of CIB1-CFP fusion protein (Figure 27B). Interestingly, only the overexpression of active CIN phosphatase has an apparent effect on CIB1 protein expression levels. As shown in Figure 27C, the overexpression of either GFP or CIN-D25N (a phosphatase-inactive point mutant) in GBM6840 cells has no effect on CIB1 expression level, whereas overexpression of active CIN phosphatase in GBM6840 leads to increased levels of CIB1 protein.

Furthermore, the stable depletion of CIN in GBM6840 cells by shRNA also leads to increased expression levels of CIB1 protein (Figure 27D) and to increased PAK4 expression, as described above.

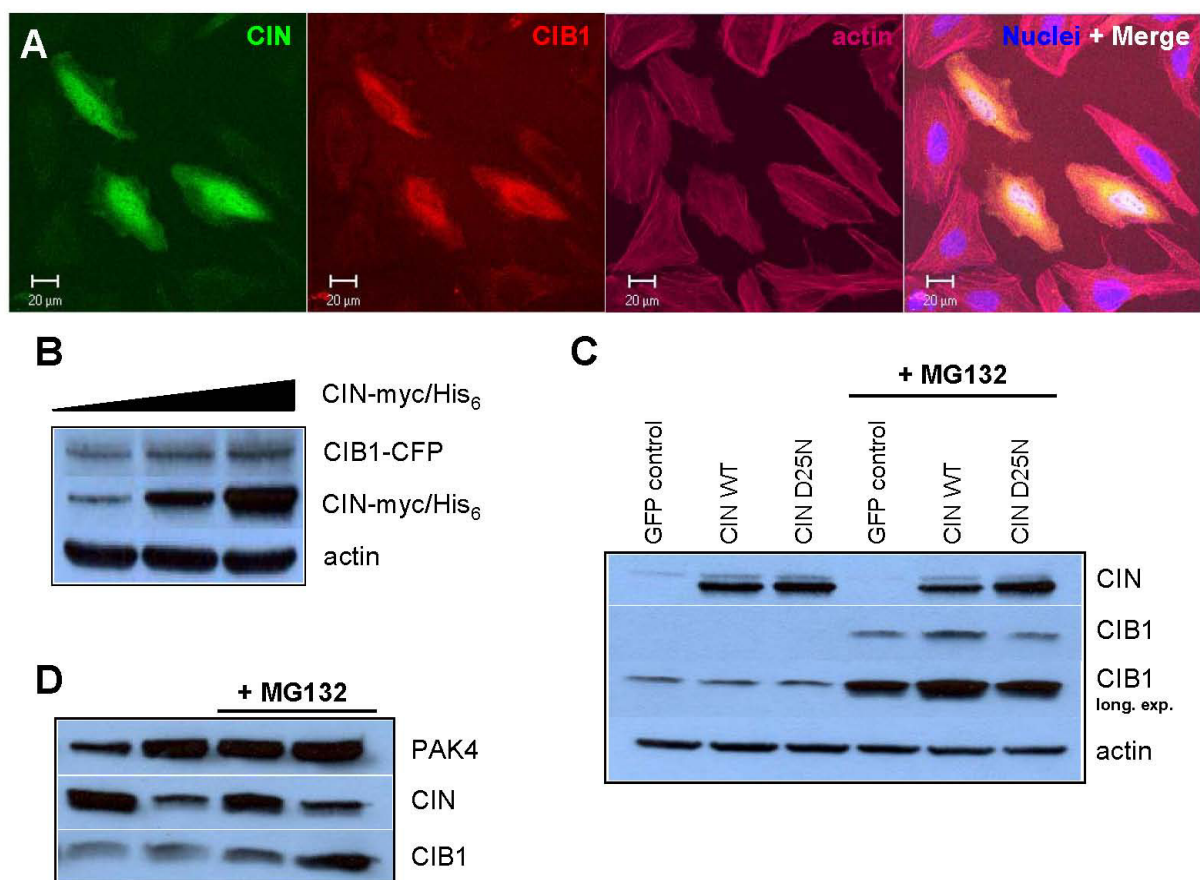


Figure 27: Effect of CIN phosphatase activity on CIB1 expression levels.

(A) HeLa cells were transfected with the CIN-myc/His₆ construct. Next day, cells were fixed and stained with anti-myc (green) and anti-CIB1 (red) antibodies. Phalloidin was used to stain F-actin (magenta) and DAPI was employed to visualise nuclei (blue). Overexpression of CIN leads to increased levels of CIB1 protein. (B) HeLa cells were transfected with 150 ng of CIB1-CFP and 50, 100 or 200 ng of CIN-myc/His₆. The steady-state expression levels of CIB1-CFP and CIN were analysed by immunoblotting. (C) GBM6840 cells were transfected with pEGFP, pcDNA3-CIN or pcDNA3-CIND25N constructs. The day after transfection, cells were incubated with or without 20 mM of MG132 for 4 hours and then lysed in RIPA buffer and analysed by immunoblotting for the indicated antigens. Actin was used as a loading control. Overexpression of active CIN phosphatase leads to increased levels of CIB1 protein. (D) GBM6840 cells, stably expressing CIN or control shRNA constructs, were incubated in the presence or absence of MG132 for 4 h and the lysed and analysed by immunoblotting for the indicated antigens. Downregulation of CIN phosphatase leads to increased expression levels of CIB1 and PAK4 proteins.

The incubation of cells with the proteasome inhibitor MG132 strongly increased the levels of CIB1 protein and also PAK4 in GBM6840 cells (Figure 27C and D). From this we can conclude that CIB1 and PAK4 protein levels are regulated by proteasomal degradation pathways. Role of CIN phosphatase in this pathway is unknown, but the reported interaction of CIN with the Hsp90 protein (Huang et al., 2008) may indicate a possible role of CIN phosphatase in proteasomal functions. The molecular chaperone Hsp90 was shown to play a role in the assembly and maintenance of the 26S proteasome (Imai et al., 2003). At the same time Hsp90 is known to stabilise proteins. For example, Hsp90 regulates the levels of the LIM kinases by promoting their homo-dimerisation and trans-phosphorylation (Bernard, 2007).

Taken together, these results indicate that CIN phosphatase activity may be important for CIB1 protein stability. Dysregulations in CIN phosphatase activity and –expression may induce increased levels of CIB1 and PAK4 proteins in cells.

6 Discussion

Due to its ability to bind to and to fragment polymerised actin in response to diverse extracellular stimuli, cofilin plays essential roles in fundamental actin-based cellular processes, such as cell cycle control, cell division, cell motility and invasion, morphogenesis, endocytosis and phagocytosis (Bamburg, 1999; DesMarais et al., 2005; Wang et al., 2007a). Cofilin activity is negatively regulated by the reversible phosphorylation of a single serine residue, which blocks the binding of cofilin to actin.

Cofilin activity has been directly linked to invasion, intravasation, and metastasis of mammary tumours (Condeelis et al., 2005; Wang et al., 2006). However, it is becoming increasingly clear that the balanced activity of the entire cofilin pathway (that is, the expression and activity of cofilin itself and of cofilin regulatory proteins, see chapters 1.3 and 1.5) determines the cellular responses. Therefore, it is essential to investigate the signalling output of the entire cofilin pathway when the activity of either cofilin or of cofilin regulatory proteins is altered (Wang et al., 2007a).

CIN is a recently identified HAD-type phosphatase, which directly dephosphorylates cofilin with high specificity and regulates cofilin activity in motile and dividing cells (Gohla et al., 2005). The mapping of the human CIN gene to a reported 'hot spot' in glial tumours, where nonidentified genes involved in gliomagenesis are suspected (Schwartzbaum et al., 2006) (see chapter 1.6), together with the strong CIN expression in brain (Gohla et al., 2005; Jang et al., 2003) and the known effects of CIN loss in cells (cell division defects, accumulation of aneuploid cells, deformed nuclei) (Gohla et al., 2005), which are consistent with morphological hallmarks of glioblastoma cells (Reifenberger and Collins, 2004), led us to investigate a possible role of CIN phosphatase in glioblastoma pathogenesis.

6.1 CIN expression and cellular localisation analysis

As analysed by Northern blot and immunoblotting assays, CIN phosphatase is a broadly expressed protein that is found in all investigated human and murine tissues with highest expression levels in brain (Gohla et al., 2005).

Using a newly developed CIN rabbit monoclonal antibody, we first tested the antibody sensitivity and verified its specificity by analysing CIN protein expression in a panel of mouse tissues (Figure 10). We confirmed a broad distribution of CIN protein in all tissues with the highest expression level in brain. Immunohistochemical analysis of adult mouse brain with this antibody showed a distinct distribution of CIN phosphatase in different brain regions. In the dentate gyrus (a part of the hippocampal formation), CIN is expressed at very high levels (Figure 12A and B) as compared to other regions of the mouse brain. Interestingly, a recent

report on PLPP/CIN phosphatase has suggested an important role for CIN in the regulation of long-term potentiation in the rat dentate gyrus (Kim et al., 2009), supporting our immunohistochemical CIN localisation.

The dentate gyrus is one of the few regions in adult human brain that is characterised by high rates of neurogenesis (Cameron and McKay, 2001). Other known regions of neurogenesis in human brain are the olfactory bulb (Graziadei and Monti Graziadei, 1985) and the cerebellum (Ponti et al., 2008). Several findings demonstrate the involvement of brain tumour stem cells in the initiation and progression of brain tumours. Tumours are presumed to arise from a series of mutations that occur in few or even single founder cells (Vescovi et al., 2006). In particular, tumour stem cells have been identified in glioblastomas (Bao et al., 2006; Ignatova et al., 2002). Human glioblastomas contain a small portion of cancer stem cells (tumour-initiating cells), which have a low proliferation rate, but a high tumorigenic potential (Altaner, 2008).

Loss of heterozygosity and deletions (occurring in ~40% of primary and ~80% of secondary glioblastomas) have been reported for a chromosomal region encompassing the CIN locus on chromosome 22q13.1 (Nakamura et al., 2005). Our findings confirm a dramatic reduction of CIN expression both on the transcript level (Figure 14), as well as on the protein level (Figures 13 and 15). We found an apparent tumour stage-specific decrease in CIN protein expression (Figure 15A and B). However, whereas the trend towards a decrease in CIN expression with increasing grades of malignancy was clearly seen in the individual tested samples, the evaluation of the pooled results did not reach statistical significance (Figure 15C).

A morphological characteristic of glioblastomas is the deregulation of the cell cycle (Schwartzbaum et al., 2006) and the presence of multinucleated giant cells in the tumour (Reifenberger and Collins, 2004). CIN was shown to control cofilin phosphorylation during mitosis and the expression of the phosphatase-dead mutant CIN-D25N prolonged the progression through all phases of mitosis, including telophase/cytokinesis (Gohla et al., 2005), which may also lead to lower proliferation rates. The analysis of the subcellular localisation of CIN phosphatase in mitotic GBM6840 and HeLa cells revealed an accumulation of CIN on the mitotic apparatus (Figure 20). Interestingly, F-actin was also shown to localise to the mitotic apparatus, and to play an essential role for mitotic spindle function (Woolner et al., 2008; Yasuda et al., 2005). The localisation of CIN to the predominantly microtubule-based mitotic apparatus during cell division may indicate an additional role of CIN for microtubule dynamics. Therefore, the CIN depletion-dependent increase in the percentage of deformed and lobulated nuclei may be a combined effect of CIN function for actin and cytoskeletal dynamics.

6.2 Cofilin pathway in glioblastomas

We showed that the CIN expression decreases in astrocytoma grade II to astrocytoma grade III as compared to normal cerebrum. In glioblastoma multiforme, CIN expression was hardly detectable (Figures 13 and 15). These findings are in good correlation with known data about loss of chromosome 22q in glial tumours, which was related to glioma progression (Laigle-Donadey et al., 2006), and suggest that CIN expression is progressively lost due to chromosomal deletion. In support of this, the expression of another cofilin-activating phosphatase, Slingshot-1L, was comparable to the control samples. The gene encoding for the human Slingshot ortholog has been mapped to chromosome 12q24.11, which is not known to be affected in astrocytomas. Along with the downregulation of CIN, we observed an upregulation of cofilin-inactivating kinases LIMK1 and LIMK2, and a massive upregulation of the upstream activating kinase PAK4. Such dysregulations of the cofilin pathway have not been described before. Currently published findings show a coordinated overexpression of cofilin and LIMK (Wang et al., 2004), or a coordinated overexpression of LIMK and SSH (Wang et al., 2007b), but not an overexpression of cofilin-inactivating kinases concomitant with a downregulation of a cofilin-activating phosphatase.

In the literature overexpression of PAK and LIM kinase genes in invasive cells has been linked to regulation of the location, timing, and sharpness of cofilin-dependent actin polymerisation transients that are required for chemotaxis (Condeelis et al., 2005). Observed increase in invasive potential of CIN-depleted GBM6840 cells through matrigel towards EGF (Figure 23C) may also indicate an increased migration ability of these cells, but additional experiments are required to confirm this assumption.

6.3 Consequences of CIN depletion in GBM6840

To understand the functional consequences of CIN loss in glioblastomas we depleted CIN in the glioblastoma model cell line GBM6840 using different RNAi methods. In the comparison of different glioma cell lines, the GBM6840 cell line showed a maximum CIN expression, as assessed by RT-PCR and immunoblotting assays. These results correlate with the karyotypic analysis of the GBM6840 cell line, which revealed that chromosome 22, on which the CIN gene is located, is not affected (Di Tomaso et al., 2000).

Investigation of the expression levels of proteins involved in the cofilin pathway in CIN depleted GBM6840 cells (Figure 18C) revealed the same dysregulations which we observed in glioblastomas samples (Figure 15D). These results suggest that the depletion of CIN is not simply a result of the multiple alterations typically found in tumours, but rather has a causal role in the observed upregulation of LIMK2 and PAK4. As expected, we observed a robust increase of the total p-cofilin pool in these cells (Figure 18B and C). We also investigated the

astrocytic tumor samples for changes in p-cofilin levels (data not shown). However, since these gliomas are very rare and since some of the samples were over 10 years old, we were unable to detect p-cofilin.

The increased p-cofilin levels in CIN depleted cells may explain several of the observed morphological and functional effects, which we found in these cells. Phosphorylation/dephosphorylation of cofilin was shown to be a critical step in the process of cell division (Amano et al., 2002) and CIN was shown to control cofilin phosphorylation during mitosis (Gohla et al., 2005). Thus, CIN depletion with the following increase in p-cofilin level is likely to be a functional explanation for the accumulation of lobulated and deformed nuclei in CIN depleted GBM6840 cells (Figure 19). We also observed accumulation of F-actin in CIN depleted GBM6840 cells (Figure 21B) and an increase in the cell area (Figure 21C), which can be also explained by increased cellular p-cofilin level. The cytoskeleton provides the cell and also the nucleus with structure and shape. Therefore, alterations in actin cytoskeletal dynamics often also influence the nuclear architecture, which can be observed as an accumulation of lobulated and deformed nuclei (Figure 19). In addition, the localisation of CIN on the mitotic spindle (Figure 20) may indicate a previously unidentified role for CIN in microtubule dynamics. Changes in mitotic microtubule dynamics can lead to aneuploidy (Abe et al., 1996; Amano et al., 2002; Gunsalus et al., 1995; Yang et al., 2004) and result in nuclear deformities.

We also studied the effect of CIN depletion on their ability of GBM6840 cells to grow in an anchorage-independent manner in soft-agar. We showed that CIN depletion using siRNA oligoribonucleotides increases the anchorage-independent growth of these cells by 40%, whereas the stable depletion of CIN phosphatase expression using shRNA increased the anchorage-independent growth more than two-fold as compared to control shRNA cells (Figure 22). We suppose that this effect is due to an upregulation of PAK4 kinase in GBM6840 cells, which we observed after CIN depletion (Figure 18B and C). PAK4 is the only one member of the whole PAK family that was shown to be tumorigenic and that has been linked to cell transformation and anchorage-independent cell growth (Callow et al., 2002; Qu et al., 2001).

Another interesting observation in CIN-depleted GBM6840 cells is the increased invasion of these cells through matrigel towards EGF as a chemoattractant. We found that CIN depleted GBM6840 cells show increased invasive responses to EGF and have more p-cofilin as compared to control GBM6840 cells (Figure 23A, B). Glioblastomas are characterised by a diffuse tissue-distribution pattern, with extensive dissemination of the tumour cells within the brain (Vescovi et al., 2006), which is due to high locally invasive behavior of GBMs towards different chemoattractant sources (Hoelzinger et al., 2005).

Interestingly, differences in the expression levels and activity of LIMK1 were shown in the literature to have major effects on tumour cell motility and invasion. However, there are several conflicting studies on the effects of LIMK1 expression on tumour cell invasion. It was shown that siRNA-mediated inhibition of LIMK1 expression inhibits the motility of Jurkat T cells (Nishita et al., 2005), and the overexpression of LIMK1 increases invasiveness of prostate epithelial cells and a reduction of LIMK1 expression level in these cells decreases their ability to invade matrigel *in vitro* (Davila et al., 2003). Because of technical problems due to the limited specificity and sensitivity of available LIMK1 antibodies, we were not able to investigate LIMK1 expression levels in CIN depleted GBM6840 cells (data not shown). Nevertheless, we were able to show an upregulation of LIMK1 in samples from patients with glioblastomas (Figure 15D). Increased invasive potential of CIN depleted GBM6840 cells can be explained by dysregulation of the cofilin pathway with upregulation of LIMKs and PAK4 and downregulation of cofilin-specific phosphatase CIN with a subsequent increase in p-cofilin levels.

All our findings are summarised and shown schematically in . Taken together, these results demonstrate that the depletion of CIN in GBM6840 cells increases their tumorigenic and invasive potential.

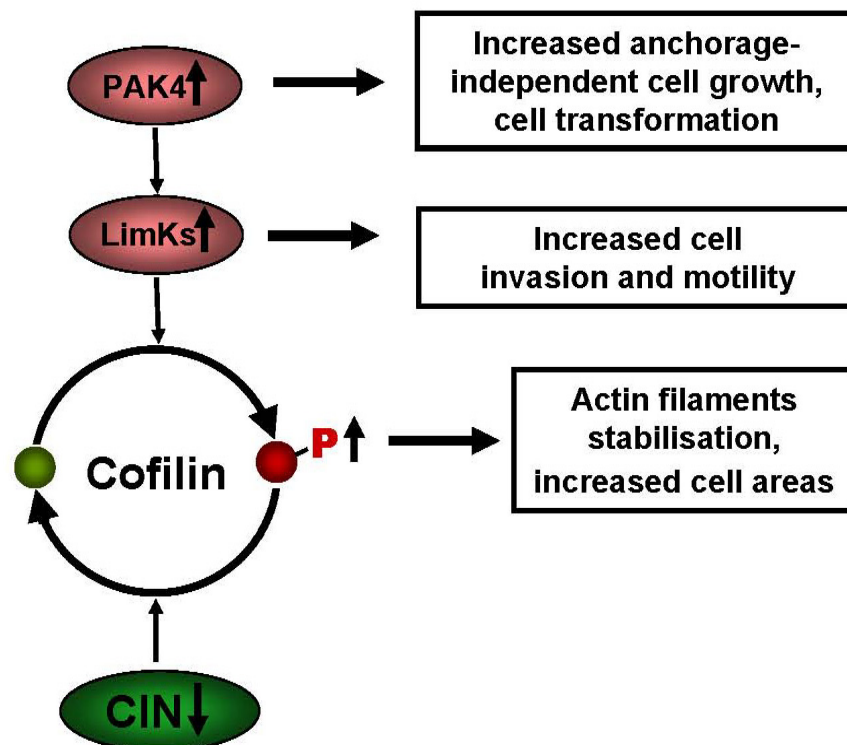


Figure 28: Observed dysregulation of the cofilin pathway with cellular consequences. Obtained model GBM6840 cell line has similar phenotype to glial tumours, with an upregulation of cofilin-inactivating kinases LIMKs and PAK4 and a downregulation of a cofilin reactivating phosphatase CIN. These dysregulations in cofilin pathway have several cellular consequences indicated in square boxes. For more details, see text.

6.4 CIN regulation

The mechanism of how the depletion of CIN phosphatase may lead to increased tumour formation or tumour progression is still unclear. Understanding the mechanisms of the regulation of CIN phosphatase activity and the involvement of CIN in different molecular pathways may help to explain this phenomenon. Recently, the inhibitory regulation of CIN phosphatase activity through Hsp90 binding has been suggested as a molecular mechanism for the coupling of ATP-deprivation stress to homeostatic and pathological changes in the actin cytoskeleton (Huang et al., 2008).

Our group has identified the calcium- and integrin-binding protein 1 (CIB1) as an interacting partner of CIN phosphatase using a yeast two-hybrid screen and various biochemical approaches (Jeanclos, Hoffmann, Fedorchenko, Gohla; unpublished results). Here, we have further analysed this interaction by colocalisation studies and FRET analysis, and have observed a substantial and constitutive co-localisation (Figure 24) and interaction of CIN and CIB1 (Figure 25). Interestingly, we also found that the interaction between CIN and CIB1 moderately increases the phosphatase activity of CIN in the absence of Ca^{2+} and that the presence of CIB1 “protects” CIN against Ca^{2+} -mediated inhibition (Figure 26). The molecular details of this effect will need further investigation. We also observed that in cells, siRNA-mediated depletion either CIN phosphatase or CIB1 protein leads to increased levels of p-cofilin (data not shown). This may indicate on a presence of a functional CIN/CIB1 dimer, which may be responsible for the regulation of cofilin phosphorylation. Interestingly, Calcineurin B, which has 57% homology to CIB1, is also known as the regulatory subunit of Ca^{2+} -dependent protein phosphatase 2B.

Together, our results are consistent with the existence of a functional CIN/CIB1 phosphatase complex, which may be involved in the regulation of the subcellular localisation of CIN to target it to regions of actin dynamics.

In further experiments, we found that the CIN phosphatase activity appears to be important for CIB1 expression levels. Altered CIN phosphatase activity (either by overexpression of active CIN phosphatase or through its RNA interference-mediated depletion) leads to increased expression levels of CIB1 protein. As mentioned above, the depletion of CIN leads to increased levels of PAK4 and LIMKs. One possible explanation for this effect may be the interaction of CIN with the molecular chaperone Hsp90, which is known to regulate protein stability and protein degradation. Moreover, using the proteasome inhibitor MG132 increased CIB1 and PAK4 protein levels (Figure 27C and D), indicating that CIB1 and PAK4 proteins are regulated by proteasomal degradation pathways. Therefore,

CIN may have effects on the activity of Hsp90 proteins and on proteasomal degradation pathways.

Because we observed effects of the CIN phosphatase activity on CIB1 protein expression levels, we can not exclude possible indirect effects of CIN on the increasing numbers of identified CIB1-interacting partners, such as on PAK1 (Leisner et al., 2005), Rac3 (Haataja et al., 2002), Pax3 (Hollenbach et al., 2002), presenilin 2 (Stabler et al., 1999), or on DNA-Pk (Wu and Lieber, 1997). The existence of numerous known CIB1 interacting proteins may also indicate a possible involvement of CIN phosphatase in these different molecular pathways.

7 Summary

Actin cytoskeletal dynamics are organised by a large number of actin binding proteins. Among these, the ubiquitously expressed proteins of the cofilin family are particularly important for stimulus-dependent actin remodelling. Active cofilin is able to bind and depolymerise actin filaments in cells. Thus, a tightly regulated cofilin activity is essential for fundamental actin-based process such as cell cycle control and cell division, as well as cell migration and –invasion. Cofilin dysregulation leads to defects in mitosis and cytokinesis, an accumulation of aneuploid cells and genomic instability. Aneuploidy is a hallmark of most tumours, and an altered cofilin activity has been causally linked to the initiation and progression of malignant tumours. Cofilin activity is controlled by phosphorylation of a single serine residue. Whereas kinases that inactivate cofilin by phosphorylating it on serine 3 are well characterised, much less is understood about specific phosphatases that reactivate cofilin functions. CIN is a recently identified cofilin phosphatase of the haloacid dehalogenase family of hydrolases that is highly expressed in brain. Currently, very little is known about the physiological and pathophysiological functions of CIN.

The CIN gene maps to human chromosome 22q13.1 in a region that is frequently deleted in astrocytic gliomas. Malignant gliomas are the most common primary brain tumours with a mean survival time of less than 12 months for grade IV tumours, also known as glioblastomas. Over the past two decades, a number of recurrent chromosomal, genetic and epigenetic alterations have been associated with the different histological types and malignancy grades of astrocytic tumours. However, the complex mechanisms that underlie tumour initiation and progression are still far from being understood. Interestingly, the frequency of loss of heterozygosity on chromosome 22q13.1 strongly increases with the tumour malignancy grade, suggesting the presence of a hitherto unidentified astrocytoma tumour suppressor gene in this chromosomal region.

In this work,

- We have analysed the expression of cofilin regulatory proteins in tumour samples from patients with astrocytic gliomas of different malignancy grades and, using quantitative real-time PCR and a newly developed CIN rabbit monoclonal antibody, we were able to show that CIN expression was strongly reduced in the majority of grade III and grade IV astrocytomas. In contrast, the expression of the functional CIN antagonist LIMK and its upstream regulator PAK4 was increased in most of the investigated samples.

-
- To investigate the role of CIN in astrocytic tumours on a cellular level, we have depleted CIN in the astrocytoma cell line GBM6840, using different RNA interference approaches (by transient transfection of specific siRNA or by establishing stable GBM6840 cell line, expressing CIN specific shRNA).
 - We have shown that the reduction of CIN phosphatase levels in GBM6840 cells has several molecular and cellular consequences:
 - decreased CIN level lead to an upregulation of LIMKs and PAK4, thus showing the same phenotype that we observed in tumour samples from patients with glioblastoma;
 - depletion of CIN phosphatase leads to a stabilisation of actin structures in GBM6840 cell line and increases the cell sizes;
 - CIN depleted GBM6840 cells show increased colony formation in soft agar, compared to control cells, suggesting a role for CIN in tumour initiation;
 - the depletion of CIN in GBM6840 cells increases the percentage of aneuploid cells and triggers nuclear deformities, which are clinically relevant markers of glioblastomas;
 - CIN depleted GBM6840 cells show increased EGF signalling and increased invasive potential in *in vitro* invasion assays.
 - The interaction of CIN with CIB1, a newly identified binding partner, was confirmed by co-localisation and FRET analysis.
 - The effects of CIB1 on CIN phosphatase activity towards different substrates, and the effect of CIN phosphatase on CIB1 protein stability were studied.

Together, our results show for the first time a dysregulation of cofilin-dependent actin dynamics in astrocytic gliomas and suggest a function for CIN as an astrocytoma tumour suppressor gene.

8 Zusammenfassung

Die Dynamik des Aktin-Zytoskeletts wird durch eine große Anzahl Aktin-bindender Proteine reguliert. Hierbei sind die ubiquitär exprimierten Proteine der Cofilin Familie von besonderer Bedeutung für die Agonist-induzierte Aktin-Remodellierung. Aktives Cofilin ist in der Lage, an Aktinfilamente zu binden und diese zu fragmentieren und zu depolymerisieren. Daher ist die eng kontrollierte Cofilin-Aktivität essentiell für praktisch alle Aktin-basierten zellulären Prozesse, wie zum Beispiel die Zellzyklus-Kontrolle, die Zellteilung, die Zellmigration und die Zellinvasion. Eine Dysregulation der Cofilin-Aktivität löst Defekte in der Mitose und Zytokinese mit einer Akkumulation aneuploider Zellen und daraus resultierender genomischer Instabilität aus. Aneuploidie ist ein typisches Merkmal von Tumoren, und eine veränderte Cofilin-Aktivität ist kausal mit der Initiation und Progression maligner Tumoren verknüpft worden. Die zelluläre Cofilin-Aktivität wird durch eine inhibitorische Phosphorylierung an einem einzigen Serin-Rest (Serin-3) eng kontrolliert. Während Kinasen, die Cofilin durch Phosphorylierung an Serin-3 inhibieren, gut charakterisiert sind, ist sehr viel weniger über spezifische Cofilin-reaktivierende Phosphatasen bekannt. Chronophin (CIN) ist eine kürzlich identifizierte Cofilin-spezifische Phosphatase aus der Haloazid-Dehalogenase Superfamilie von Hydrolasen mit höchster Expression in Gehirngewebe. Derzeit ist über die physiologischen und möglichen pathologischen Funktionen von CIN fast nichts bekannt.

CIN lokalisiert auf dem humanen Chromosom 22q13.1 in einer Region, die häufig in astrozytären Gliomen deletiert ist. Maligne Gliome stellen die häufigsten primären Gehirntumore dar, und sind im Fall des hochmalignen Glioblastoma multiforme durch eine durchschnittliche Überlebenszeit von weniger als 12 Monaten gekennzeichnet. In den letzten zwei Jahrzehnten sind eine Reihe von wiederkehrenden chromosomalen, genetischen und epigenetischen Veränderungen mit den verschiedenen histologischen Typen und Malignitätsgraden astrozytärer Tumore assoziiert worden. Allerdings sind die komplexen Mechanismen, die der Tumorentstehung und –Progression unterliegen, immer noch sehr unzureichend verstanden. Interessanterweise nimmt die Häufigkeit des Verlustes der Heterozygotie auf Chromosom 22q13.1 mit dem Tumormalignitätsgrad deutlich zu. Diese Befunde legen die Existenz eines bisher nicht identifizierten astrozytären Tumorsuppressor-Gens in dieser chromosomalen Region nahe.

In dieser Arbeit

- haben wir die Expression Cofilin-regulatorischer Proteine in Tumorproben von Patienten mit astrozytären Gliomen unterschiedlicher Malignitätsgrade mittels eines neu entwickelten CIN-spezifischen monoklonalen Antikörpers aus Kaninchen untersucht. Wir konnten zeigen, dass die CIN Expression in der Mehrzahl der Grad III and Grad IV-Astrozytome stark reduziert war. Im Gegensatz dazu war die Expression

des CIN-antagonistischen Kinase LIMK, und der LIMK-aktivierenden Kinase PAK4 in den meisten Tumorproben deutlich erhöht.

- Um die Rolle von CIN auf der zellulären Ebene untersuchen zu können, haben wir die CIN-Expression in der Glioblastom-Zelllinie GBM6840, mittels RNA-Interferenz-Verfahren depletiert (hier ist die transiente Transfektion spezifischer siRNAs zum Einsatz gekommen, und es ist eine stabil CIN-depletierte GBM6840 Zelllinie etabliert worden, welche CIN-gerichtete shRNAs exprimiert).
- Wir haben gezeigt, dass die Reduktion der CIN Phosphatase-Spiegel in GBM6840 eine Reihe molekularer und zellulärer Konsequenzen hat:
 - verminderte CIN Spiegel führen zu einer Hochregulation von LIMKs und PAK4, und lösen somit denselben Phänotyp aus, den wir in Tumorproben von Glioblastom-Patienten beobachtet haben;
 - die Depletion der CIN Phosphatase führt zu einer Stabilisierung von Aktin-Strukturen in GBM6840 Zellen und vergrößert die Zellfläche;
 - im Vergleich zu Kontrollzellen zeigen CIN-depletierte GBM6840 Zellen eine erhöhte Koloniebildungsfähigkeit in *soft agar*, was auf eine mögliche Rolle von CIN für die Tumorentstehung hindeutet;
 - die Depletion von CIN in GBM6840 Zellen erhöht den Prozentsatz aneuploider Zellen und lost Kerndeformierungen aus, welche als klinisch relevante Marker von Glioblastomen angesehen werden;
 - CIN-depletierte GBM6840 Zellen zeigen ein verstärktes Ansprechen auf EGF und erhöhtes invasives Potential in *in vitro* Invasionsexperimenten.
- The Interaktion von CIN mit CIB1, einem in unserer Arbeitsgruppe neu identifizierten CIN-Bindungspartner, wurde in Ko-Lokalisationsstudien und mittels FRET-Analyse bestätigt.
- Die Effekte von CIB1 auf die CIN Phosphatase-Aktivität gegenüber verschiedenen Substraten, sowie der Effekt der CIN Phosphatase-Aktivität auf die CIB1-Proteinstabilität wurde untersucht.

Zusammengenommen zeigen unsere Ergebnisse erstmals eine Dysregulation der Cofilin-vermittelten Aktin-Dynamik in astrozytären Tumoren, und legen eine Funktion für CIN als ein astrozytäres Tumorsuppressorgen nahe.

9 References

- Abe, H., Obinata, T., Minamide, L.S., and Bamburg, J.R. (1996). *Xenopus laevis* actin-depolymerizing factor/cofilin: a phosphorylation-regulated protein essential for development. *J Cell Biol* 132, 871-885.
- Abo, A., Qu, J., Cammarano, M.S., Dan, C., Fritsch, A., Baud, V., Belisle, B., and Minden, A. (1998). PAK4, a novel effector for Cdc42Hs, is implicated in the reorganization of the actin cytoskeleton and in the formation of filopodia. *EMBO J* 17, 6527-6540.
- Acevedo, K., Moussi, N., Li, R., Soo, P., and Bernard, O. (2006). LIM kinase 2 is widely expressed in all tissues. *J Histochem Cytochem* 54, 487-501.
- Agnew, B.J., Minamide, L.S., and Bamburg, J.R. (1995). Reactivation of phosphorylated actin depolymerizing factor and identification of the regulatory site. *J Biol Chem* 270, 17582-17587.
- Ahmed, T., Shea, K., Masters, J.R., Jones, G.E., and Wells, C.M. (2008). A PAK4-LIMK1 pathway drives prostate cancer cell migration downstream of HGF. *Cell Signal* 20, 1320-1328.
- Altaner, C. (2008). Glioblastoma and stem cells. *Neoplasma* 55, 369-374.
- Amano, T., Kaji, N., Ohashi, K., and Mizuno, K. (2002). Mitosis-specific activation of LIM motif-containing protein kinase and roles of cofilin phosphorylation and dephosphorylation in mitosis. *J Biol Chem* 277, 22093-22102.
- Ambach, A., Saunus, J., Konstandin, M., Wesselborg, S., Meuer, S.C., and Samstag, Y. (2000). The serine phosphatases PP1 and PP2A associate with and activate the actin-binding protein cofilin in human T lymphocytes. *Eur J Immunol* 30, 3422-3431.
- Arber, S., Barbayannis, F.A., Hanser, H., Schneider, C., Stanyon, C.A., Bernard, O., and Caroni, P. (1998). Regulation of actin dynamics through phosphorylation of cofilin by LIM-kinase. *Nature* 393, 805-809.
- Bamburg, J.R. (1999). Proteins of the ADF/cofilin family: essential regulators of actin dynamics. *Annu Rev Cell Dev Biol* 15, 185-230.
- Bamburg, J.R., McGough, A., and Ono, S. (1999). Putting a new twist on actin: ADF/cofilins modulate actin dynamics. *Trends Cell Biol* 9, 364-370.
- Bamburg, J.R., and Wiggan, O.P. (2002). ADF/cofilin and actin dynamics in disease. *Trends Cell Biol* 12, 598-605.
- Bao, S., Wu, Q., McLendon, R.E., Hao, Y., Shi, Q., Hjelmeland, A.B., Dewhirst, M.W., Bigner, D.D., and Rich, J.N. (2006). Glioma stem cells promote radioresistance by preferential activation of the DNA damage response. *Nature* 444, 756-760.
- Bernard, O. (2007). Lim kinases, regulators of actin dynamics. *Int J Biochem Cell Biol* 39, 1071-1076.
- Cai, L., Marshall, T.W., Uetrecht, A.C., Schafer, D.A., and Bear, J.E. (2007). Coronin 1B coordinates Arp2/3 complex and cofilin activities at the leading edge. *Cell* 128, 915-929.

- Callow, M.G., Clairvoyant, F., Zhu, S., Schryver, B., Whyte, D.B., Bischoff, J.R., Jallal, B., and Smeal, T. (2002). Requirement for PAK4 in the anchorage-independent growth of human cancer cell lines. *J Biol Chem* 277, 550-558.
- Cameron, H.A., and McKay, R.D. (2001). Adult neurogenesis produces a large pool of new granule cells in the dentate gyrus. *J Comp Neurol* 435, 406-417.
- Chhabra, E.S., and Higgs, H.N. (2007). The many faces of actin: matching assembly factors with cellular structures. *Nat Cell Biol* 9, 1110-1121.
- Chomczynski, P., and Sacchi, N. (1987). Single-step method of RNA isolation by acid guanidinium thiocyanate-phenol-chloroform extraction. *Anal Biochem* 162, 156-159.
- Combeau, C., and Carlier, M.F. (1992). Covalent modification of G-actin by pyridoxal 5'-phosphate: polymerization properties and interaction with DNase I and myosin subfragment 1. *Biochemistry* 31, 300-309.
- Condeelis, J., Singer, R.H., and Segall, J.E. (2005). The great escape: when cancer cells hijack the genes for chemotaxis and motility. *Annu Rev Cell Dev Biol* 21, 695-718.
- Condeelis, J.S., Wyckoff, J.B., Bailly, M., Pestell, R., Lawrence, D., Backer, J., and Segall, J.E. (2001). Lamellipodia in invasion. *Semin Cancer Biol* 11, 119-128.
- Davila, M., Frost, A.R., Grizzle, W.E., and Chakrabarti, R. (2003). LIM kinase 1 is essential for the invasive growth of prostate epithelial cells: implications in prostate cancer. *J Biol Chem* 278, 36868-36875.
- Davila, M., Jhala, D., Ghosh, D., Grizzle, W.E., and Chakrabarti, R. (2007). Expression of LIM kinase 1 is associated with reversible G1/S phase arrest, chromosomal instability and prostate cancer. *Mol Cancer* 6, 40.
- DesMarais, V., Ghosh, M., Eddy, R., and Condeelis, J. (2005). Cofilin takes the lead. *J Cell Sci* 118, 19-26.
- Di Tomaso, E., Pang, J.C., Lam, H.K., Tian, X.X., Suen, K.W., Hui, A.B., and Hjelm, N.M. (2000). Establishment and characterization of a human cell line from paediatric cerebellar glioblastoma multiforme. *Neuropathol Appl Neurobiol* 26, 22-30.
- Ding, S.J., Li, Y., Shao, X.X., Zhou, H., Zeng, R., Tang, Z.Y., and Xia, Q.C. (2004). Proteome analysis of hepatocellular carcinoma cell strains, MHCC97-H and MHCC97-L, with different metastasis potentials. *Proteomics* 4, 982-994.
- dos Remedios, C.G., Chhabra, D., Kekic, M., Dedova, I.V., Tsubakihara, M., Berry, D.A., and Nosworthy, N.J. (2003). Actin binding proteins: regulation of cytoskeletal microfilaments. *Physiol Rev* 83, 433-473.
- Edwards, D.C., Sanders, L.C., Bokoch, G.M., and Gill, G.N. (1999). Activation of LIM-kinase by Pak1 couples Rac/Cdc42 GTPase signalling to actin cytoskeletal dynamics. *Nat Cell Biol* 1, 253-259.
- Etienne-Manneville, S., and Hall, A. (2002). Rho GTPases in cell biology. *Nature* 420, 629-635.
- Feige, J.N., Sage, D., Wahli, W., Desvergne, B., and Gelman, L. (2005). PixFRET, an ImageJ plug-in for FRET calculation that can accommodate variations in spectral bleed-throughs. *Microsc Res Tech* 68, 51-58.

- Fonda, M.L. (1992). Purification and characterization of vitamin B6-phosphate phosphatase from human erythrocytes. *J Biol Chem* 267, 15978-15983.
- Freedman, V.H., and Shin, S.I. (1974). Cellular tumorigenicity in nude mice: correlation with cell growth in semi-solid medium. *Cell* 3, 355-359.
- Gao, G.J., and Fonda, M.L. (1994). Kinetic analysis and chemical modification of vitamin B6 phosphatase from human erythrocytes. *J Biol Chem* 269, 7163-7168.
- Ghosh, M., Song, X., Mouneimne, G., Sidani, M., Lawrence, D.S., and Condeelis, J.S. (2004). Cofilin promotes actin polymerization and defines the direction of cell motility. *Science* 304, 743-746.
- Gohla, A., Birkenfeld, J., and Bokoch, G.M. (2005). Chronophin, a novel HAD-type serine protein phosphatase, regulates cofilin-dependent actin dynamics. *Nat Cell Biol* 7, 21-29.
- Gohla, A., and Bokoch, G.M. (2002). 14-3-3 regulates actin dynamics by stabilizing phosphorylated cofilin. *Curr Biol* 12, 1704-1710.
- Graziadei, P.P., and Monti Graziadei, G.A. (1985). Neurogenesis and plasticity of the olfactory sensory neurons. *Ann N Y Acad Sci* 457, 127-142.
- Guerini, D., Krinks, M.H., Sikela, J.M., Hahn, W.E., and Klee, C.B. (1989). Isolation and sequence of a cDNA clone for human calcineurin B, the Ca²⁺-binding subunit of the Ca²⁺/calmodulin-stimulated protein phosphatase. *DNA* 8, 675-682.
- Gunnarsen, J.M., Spirkoska, V., Smith, P.E., Danks, R.A., and Tan, S.S. (2000). Growth and migration markers of rat C6 glioma cells identified by serial analysis of gene expression. *Glia* 32, 146-154.
- Gunsalus, K.C., Bonaccorsi, S., Williams, E., Verni, F., Gatti, M., and Goldberg, M.L. (1995). Mutations in twinstar, a Drosophila gene encoding a cofilin/ADF homologue, result in defects in centrosome migration and cytokinesis. *J Cell Biol* 131, 1243-1259.
- Gurniak, C.B., Perlas, E., and Witke, W. (2005). The actin depolymerizing factor n-cofilin is essential for neural tube morphogenesis and neural crest cell migration. *Dev Biol* 278, 231-241.
- Haataja, L., Kaartinen, V., Groffen, J., and Heisterkamp, N. (2002). The small GTPase Rac3 interacts with the integrin-binding protein CIB and promotes integrin alpha(IIb)beta(3)-mediated adhesion and spreading. *J Biol Chem* 277, 8321-8328.
- Hanahan, D. (1983). Studies on transformation of Escherichia coli with plasmids. *J Mol Biol* 166, 557-580.
- Hoelzinger, D.B., Mariani, L., Weis, J., Woyke, T., Berens, T.J., McDonough, W.S., Sloan, A., Coons, S.W., and Berens, M.E. (2005). Gene expression profile of glioblastoma multiforme invasive phenotype points to new therapeutic targets. *Neoplasia* 7, 7-16.
- Hollenbach, A.D., McPherson, C.J., Lagutina, I., and Grosveld, G. (2002). The EF-hand calcium-binding protein calmyrin inhibits the transcriptional and DNA-binding activity of Pax3. *Biochim Biophys Acta* 1574, 321-328.
- Huang, T.Y., Minamide, L.S., Bamburg, J.R., and Bokoch, G.M. (2008). Chronophin mediates an ATP-sensing mechanism for cofilin dephosphorylation and neuronal cofilin-actin rod formation. *Dev Cell* 15, 691-703.

- Ignatova, T.N., Kukekov, V.G., Laywell, E.D., Suslov, O.N., Vrionis, F.D., and Steindler, D.A. (2002). Human cortical glial tumors contain neural stem-like cells expressing astroglial and neuronal markers in vitro. *Glia* 39, 193-206.
- Imai, J., Maruya, M., Yashiroda, H., Yahara, I., and Tanaka, K. (2003). The molecular chaperone Hsp90 plays a role in the assembly and maintenance of the 26S proteasome. *EMBO J* 22, 3557-3567.
- Ino, Y., Silver, J.S., Blazejewski, L., Nishikawa, R., Matsutani, M., von Deimling, A., and Louis, D.N. (1999). Common regions of deletion on chromosome 22q12.3-q13.1 and 22q13.2 in human astrocytomas appear related to malignancy grade. *J Neuropathol Exp Neurol* 58, 881-885.
- Jaffer, Z.M., and Chernoff, J. (2002). p21-activated kinases: three more join the Pak. *Int J Biochem Cell Biol* 34, 713-717.
- Jang, Y.M., Kim, D.W., Kang, T.C., Won, M.H., Baek, N.I., Moon, B.J., Choi, S.Y., and Kwon, O.S. (2003). Human pyridoxal phosphatase. Molecular cloning, functional expression, and tissue distribution. *J Biol Chem* 278, 50040-50046.
- Jiang, L., He, L., and Fountoulakis, M. (2004). Comparison of protein precipitation methods for sample preparation prior to proteomic analysis. *J Chromatogr A* 1023, 317-320.
- Kaji, N., Ohashi, K., Shuin, M., Niwa, R., Uemura, T., and Mizuno, K. (2003). Cell cycle-associated changes in Slingshot phosphatase activity and roles in cytokinesis in animal cells. *J Biol Chem* 278, 33450-33455.
- Keshamouni, V.G., Michailidis, G., Grasso, C.S., Anthwal, S., Strahler, J.R., Walker, A., Arenberg, D.A., Reddy, R.C., Akulapalli, S., Thannickal, V.J., *et al.* (2006). Differential protein expression profiling by iTRAQ-2DLC-MS/MS of lung cancer cells undergoing epithelial-mesenchymal transition reveals a migratory/invasive phenotype. *J Proteome Res* 5, 1143-1154.
- Kim, J.E., Kim, D.W., Kwak, S.E., Ryu, H.J., Yeo, S.I., Kwon, O.S., Choi, S.Y., and Kang, T.C. (2009). Pyridoxal-5'-phosphate phosphatase/chronophin inhibits long-term potentiation induction in the rat dentate gyrus. *Hippocampus*.
- Kiuchi, T., Ohashi, K., Kurita, S., and Mizuno, K. (2007). Cofilin promotes stimulus-induced lamellipodium formation by generating an abundant supply of actin monomers. *J Cell Biol* 177, 465-476.
- Kligys, K., Claiborne, J.N., DeBiase, P.J., Hopkinson, S.B., Wu, Y., Mizuno, K., and Jones, J.C. (2007). The slingshot family of phosphatases mediates Rac1 regulation of cofilin phosphorylation, laminin-332 organization, and motility behavior of keratinocytes. *J Biol Chem* 282, 32520-32528.
- Knobbe, C.B., Merlo, A., and Reifenberger, G. (2002). Pten signaling in gliomas. *Neuro Oncol* 4, 196-211.
- Kolokoltsov, A.A., Weaver, S.C., and Davey, R.A. (2005). Efficient functional pseudotyping of oncoretroviral and lentiviral vectors by Venezuelan equine encephalitis virus envelope proteins. *J Virol* 79, 756-763.
- Kozak, M. (1986). Point mutations define a sequence flanking the AUG initiator codon that modulates translation by eukaryotic ribosomes. *Cell* 44, 283-292.

- Kozak, M. (1987). An analysis of 5'-noncoding sequences from 699 vertebrate messenger RNAs. *Nucleic Acids Res* 15, 8125-8148.
- Kumar, R., Gururaj, A.E., and Barnes, C.J. (2006). p21-activated kinases in cancer. *Nat Rev Cancer* 6, 459-471.
- Kumar, R., and Vadlamudi, R.K. (2002). Emerging functions of p21-activated kinases in human cancer cells. *J Cell Physiol* 193, 133-144.
- Laemmli, U.K. (1970). Cleavage of structural proteins during the assembly of the head of bacteriophage T4. *Nature* 227, 680-685.
- Laigle-Donadey, F., Criniere, E., Benouaich, A., Lesueur, E., Mokhtari, K., Hoang-Xuan, K., and Sanson, M. (2006). Loss of 22q chromosome is related to glioma progression and loss of 10q. *J Neurooncol* 76, 265-268.
- Le Clainche, C., and Carlier, M.F. (2008). Regulation of actin assembly associated with protrusion and adhesion in cell migration. *Physiol Rev* 88, 489-513.
- Leisner, T.M., Liu, M., Jaffer, Z.M., Chernoff, J., and Parise, L.V. (2005). Essential role of CIB1 in regulating PAK1 activation and cell migration. *J Cell Biol* 170, 465-476.
- Leisner, T.M., Yuan, W., DeNofrio, J.C., Liu, J., and Parise, L.V. (2007). Tickling the tails: cytoplasmic domain proteins that regulate integrin α 5 β 3 activation. *Curr Opin Hematol* 14, 255-261.
- Li, R., and Gundersen, G.G. (2008). Beyond polymer polarity: how the cytoskeleton builds a polarized cell. *Nat Rev Mol Cell Biol* 9, 860-873.
- Li, X., Oghi, K.A., Zhang, J., Krones, A., Bush, K.T., Glass, C.K., Nigam, S.K., Aggarwal, A.K., Maas, R., Rose, D.W., *et al.* (2003). Eya protein phosphatase activity regulates Six1-Dach-Eya transcriptional effects in mammalian organogenesis. *Nature* 426, 247-254.
- Liu, Y., Xiao, H., Tian, Y., Nekrasova, T., Hao, X., Lee, H.J., Suh, N., Yang, C.S., and Minden, A. (2008). The pak4 protein kinase plays a key role in cell survival and tumorigenesis in athymic mice. *Mol Cancer Res* 6, 1215-1224.
- Maekawa, M., Ishizaki, T., Boku, S., Watanabe, N., Fujita, A., Iwamatsu, A., Obinata, T., Ohashi, K., Mizuno, K., and Narumiya, S. (1999). Signaling from Rho to the actin cytoskeleton through protein kinases ROCK and LIM-kinase. *Science* 285, 895-898.
- Mahlamaki, E.H., Kauraniemi, P., Monni, O., Wolf, M., Hautaniemi, S., and Kallioniemi, A. (2004). High-resolution genomic and expression profiling reveals 105 putative amplification target genes in pancreatic cancer. *Neoplasia* 6, 432-439.
- Martoglio, A.M., Tom, B.D., Starkey, M., Corps, A.N., Charnock-Jones, D.S., and Smith, S.K. (2000). Changes in tumorigenesis- and angiogenesis-related gene transcript abundance profiles in ovarian cancer detected by tailored high density cDNA arrays. *Mol Med* 6, 750-765.
- Meberg, P.J., Ono, S., Minamide, L.S., Takahashi, M., and Bamburg, J.R. (1998). Actin depolymerizing factor and cofilin phosphorylation dynamics: response to signals that regulate neurite extension. *Cell Motil Cytoskeleton* 39, 172-190.
- Meyer, G., Kim, B., van Golen, C., and Feldman, E.L. (2005). Cofilin activity during insulin-like growth factor I-stimulated neuroblastoma cell motility. *Cell Mol Life Sci* 62, 461-470.

- Mielke, C., Tumbler, M., Schubeler, D., von Hoegen, I., and Hauser, H. (2000). Stabilized, long-term expression of heterodimeric proteins from tricistronic mRNA. *Gene* 254, 1-8.
- Moffat, J., Grueneberg, D.A., Yang, X., Kim, S.Y., Kloepfer, A.M., Hinkle, G., Piqani, B., Eisenhaure, T.M., Luo, B., Grenier, J.K., *et al.* (2006). A lentiviral RNAi library for human and mouse genes applied to an arrayed viral high-content screen. *Cell* 124, 1283-1298.
- Nagaoka, R., Abe, H., Kusano, K., and Obinata, T. (1995). Concentration of cofilin, a small actin-binding protein, at the cleavage furrow during cytokinesis. *Cell Motil Cytoskeleton* 30, 1-7.
- Nagata-Ohashi, K., Ohta, Y., Goto, K., Chiba, S., Mori, R., Nishita, M., Ohashi, K., Kousaka, K., Iwamatsu, A., Niwa, R., *et al.* (2004). A pathway of neuregulin-induced activation of cofilin-phosphatase Slingshot and cofilin in lamellipodia. *J Cell Biol* 165, 465-471.
- Naik, U.P., Patel, P.M., and Parise, L.V. (1997). Identification of a novel calcium-binding protein that interacts with the integrin α 5 β 1 cytoplasmic domain. *J Biol Chem* 272, 4651-4654.
- Nakamura, M., Ishida, E., Shimada, K., Kishi, M., Nakase, H., Sakaki, T., and Konishi, N. (2005). Frequent LOH on 22q12.3 and TIMP-3 inactivation occur in the progression to secondary glioblastomas. *Lab Invest* 85, 165-175.
- Nakamura, M., Shimada, K., Ishida, E., Higuchi, T., Nakase, H., Sakaki, T., and Konishi, N. (2007). Molecular pathogenesis of pediatric astrocytic tumors. *Neuro Oncol* 9, 113-123.
- Nebl, G., Meuer, S.C., and Samstag, Y. (1996). Dephosphorylation of serine 3 regulates nuclear translocation of cofilin. *J Biol Chem* 271, 26276-26280.
- Nishita, M., Tomizawa, C., Yamamoto, M., Horita, Y., Ohashi, K., and Mizuno, K. (2005). Spatial and temporal regulation of cofilin activity by LIM kinase and Slingshot is critical for directional cell migration. *J Cell Biol* 171, 349-359.
- Niwa, R., Nagata-Ohashi, K., Takeichi, M., Mizuno, K., and Uemura, T. (2002). Control of actin reorganization by Slingshot, a family of phosphatases that dephosphorylate ADF/cofilin. *Cell* 108, 233-246.
- Ohta, Y., Kousaka, K., Nagata-Ohashi, K., Ohashi, K., Muramoto, A., Shima, Y., Niwa, R., Uemura, T., and Mizuno, K. (2003). Differential activities, subcellular distribution and tissue expression patterns of three members of Slingshot family phosphatases that dephosphorylate cofilin. *Genes Cells* 8, 811-824.
- Ott, E.B., Te Velthuis, A.J., and Bagowski, C.P. (2007). Comparative analysis of splice form-specific expression of LIM Kinases during zebrafish development. *Gene Expr Patterns* 7, 620-629.
- Pawlak, G., and Helfman, D.M. (2002). MEK mediates v-Src-induced disruption of the actin cytoskeleton via inactivation of the Rho-ROCK-LIM kinase pathway. *J Biol Chem* 277, 26927-26933.
- Peeraer, Y., Rabijns, A., Collet, J.F., Van Schaftingen, E., and De Ranter, C. (2004). How calcium inhibits the magnesium-dependent enzyme human phosphoserine phosphatase. *Eur J Biochem* 271, 3421-3427.
- Pellegrin, S., and Mellor, H. (2007). Actin stress fibres. *J Cell Sci* 120, 3491-3499.

- Pihan, G.A., and Doxsey, S.J. (1999). The mitotic machinery as a source of genetic instability in cancer. *Semin Cancer Biol* 9, 289-302.
- Ponti, G., Peretto, P., and Bonfanti, L. (2008). Genesis of neuronal and glial progenitors in the cerebellar cortex of peripuberal and adult rabbits. *PLoS ONE* 3, e2366.
- Qu, J., Cammarano, M.S., Shi, Q., Ha, K.C., de Lanerolle, P., and Minden, A. (2001). Activated PAK4 regulates cell adhesion and anchorage-independent growth. *Mol Cell Biol* 21, 3523-3533.
- Reifenberger, G., and Collins, V.P. (2004). Pathology and molecular genetics of astrocytic gliomas. *J Mol Med* 82, 656-670.
- Ressad, F., Didry, D., Xia, G.X., Hong, Y., Chua, N.H., Pantaloni, D., and Carlier, M.F. (1998). Kinetic analysis of the interaction of actin-depolymerizing factor (ADF)/cofilin with G- and F-actins. Comparison of plant and human ADFs and effect of phosphorylation. *J Biol Chem* 273, 20894-20902.
- Revenu, C., Athman, R., Robine, S., and Louvard, D. (2004). The co-workers of actin filaments: from cell structures to signals. *Nat Rev Mol Cell Biol* 5, 635-646.
- Ridder, I.S., and Dijkstra, B.W. (1999). Identification of the Mg²⁺-binding site in the P-type ATPase and phosphatase members of the HAD (haloacid dehalogenase) superfamily by structural similarity to the response regulator protein CheY. *Biochem J* 339 (Pt 2), 223-226.
- Ridley, A.J. (2001). Rho family proteins: coordinating cell responses. *Trends Cell Biol* 11, 471-477.
- Ross, J.S. (1996). DNA ploidy and cell cycle analysis in cancer diagnosis and prognosis. *Oncology (Williston Park)* 10, 867-882, 887; discussion 887-890.
- Sahai, E., Olson, M.F., and Marshall, C.J. (2001). Cross-talk between Ras and Rho signalling pathways in transformation favours proliferation and increased motility. *EMBO J* 20, 755-766.
- Schmid, J.A., Scholze, P., Kudlacek, O., Freissmuth, M., Singer, E.A., and Sitte, H.H. (2001). Oligomerization of the human serotonin transporter and of the rat GABA transporter 1 visualized by fluorescence resonance energy transfer microscopy in living cells. *J Biol Chem* 276, 3805-3810.
- Schneider, L., Essmann, F., Kletke, A., Rio, P., Hanenberg, H., Wetzel, W., Schulze-Osthoff, K., Nurnberg, B., and Piekorz, R.P. (2007). The transforming acidic coiled coil 3 protein is essential for spindle-dependent chromosome alignment and mitotic survival. *J Biol Chem* 282, 29273-29283.
- Schwartzbaum, J.A., Fisher, J.L., Aldape, K.D., and Wrensch, M. (2006). Epidemiology and molecular pathology of glioma. *Nat Clin Pract Neurol* 2, 494-503; quiz 491 p following 516.
- Scott, R.W., and Olson, M.F. (2007). LIM kinases: function, regulation and association with human disease. *J Mol Med* 85, 555-568.
- Selengut, J.D. (2001). MDP-1 is a new and distinct member of the haloacid dehalogenase family of aspartate-dependent phosphohydrolases. *Biochemistry* 40, 12704-12711.

- Sinha, P., Hutter, G., Kottgen, E., Dietel, M., Schadendorf, D., and Lage, H. (1999). Increased expression of epidermal fatty acid binding protein, cofilin, and 14-3-3-sigma (stratifin) detected by two-dimensional gel electrophoresis, mass spectrometry and microsequencing of drug-resistant human adenocarcinoma of the pancreas. *Electrophoresis* 20, 2952-2960.
- Smith-Beckerman, D.M., Fung, K.W., Williams, K.E., Auersperg, N., Godwin, A.K., and Burlingame, A.L. (2005). Proteome changes in ovarian epithelial cells derived from women with BRCA1 mutations and family histories of cancer. *Mol Cell Proteomics* 4, 156-168.
- Smith, P.K., Krohn, R.I., Hermanson, G.T., Mallia, A.K., Gartner, F.H., Provenzano, M.D., Fujimoto, E.K., Goeke, N.M., Olson, B.J., and Klenk, D.C. (1985). Measurement of protein using bicinchoninic acid. *Anal Biochem* 150, 76-85.
- Soosairajah, J., Maiti, S., Wiggan, O., Sarmiere, P., Moussi, N., Sarcevic, B., Sampath, R., Bamburg, J.R., and Bernard, O. (2005). Interplay between components of a novel LIM kinase-slingshot phosphatase complex regulates cofilin. *EMBO J* 24, 473-486.
- Stabler, S.M., Ostrowski, L.L., Janicki, S.M., and Monteiro, M.J. (1999). A myristoylated calcium-binding protein that preferentially interacts with the Alzheimer's disease presenilin 2 protein. *J Cell Biol* 145, 1277-1292.
- Stewart, S.A., Dykxhoorn, D.M., Palliser, D., Mizuno, H., Yu, E.Y., An, D.S., Sabatini, D.M., Chen, I.S., Hahn, W.C., Sharp, P.A., *et al.* (2003). Lentivirus-delivered stable gene silencing by RNAi in primary cells. *RNA* 9, 493-501.
- Strelkov, S.V., Herrmann, H., and Aebi, U. (2003). Molecular architecture of intermediate filaments. *Bioessays* 25, 243-251.
- Sunesen, M., Huchet-Dymanus, M., Christensen, M.O., and Changeux, J.P. (2003). Phosphorylation-elicited quaternary changes of GA binding protein in transcriptional activation. *Mol Cell Biol* 23, 8008-8018.
- Toshima, J., Toshima, J.Y., Amano, T., Yang, N., Narumiya, S., and Mizuno, K. (2001a). Cofilin phosphorylation by protein kinase testicular protein kinase 1 and its role in integrin-mediated actin reorganization and focal adhesion formation. *Mol Biol Cell* 12, 1131-1145.
- Toshima, J., Toshima, J.Y., Takeuchi, K., Mori, R., and Mizuno, K. (2001b). Cofilin phosphorylation and actin reorganization activities of testicular protein kinase 2 and its predominant expression in testicular Sertoli cells. *J Biol Chem* 276, 31449-31458.
- Towbin, H., Staehelin, T., and Gordon, J. (1979). Electrophoretic transfer of proteins from polyacrylamide gels to nitrocellulose sheets: procedure and some applications. *Proc Natl Acad Sci U S A* 76, 4350-4354.
- Turhani, D., Krapfenbauer, K., Thurnher, D., Langen, H., and Fountoulakis, M. (2006). Identification of differentially expressed, tumor-associated proteins in oral squamous cell carcinoma by proteomic analysis. *Electrophoresis* 27, 1417-1423.
- Tuschl, T., and Borkhardt, A. (2002). Small interfering RNAs: a revolutionary tool for the analysis of gene function and gene therapy. *Mol Interv* 2, 158-167.
- Unwin, R.D., Craven, R.A., Harnden, P., Hanrahan, S., Totty, N., Knowles, M., Eardley, I., Selby, P.J., and Banks, R.E. (2003). Proteomic changes in renal cancer and co-ordinate demonstration of both the glycolytic and mitochondrial aspects of the Warburg effect. *Proteomics* 3, 1620-1632.

- Vadlamudi, R.K., and Kumar, R. (2003). P21-activated kinases in human cancer. *Cancer Metastasis Rev* 22, 385-393.
- Vescovi, A.L., Galli, R., and Reynolds, B.A. (2006). Brain tumour stem cells. *Nat Rev Cancer* 6, 425-436.
- Vogel, S.S., Thaler, C., and Koushik, S.V. (2006). Fanciful FRET. *Sci STKE* 2006, re2.
- Walczak, C.E., and Heald, R. (2008). Mechanisms of mitotic spindle assembly and function. *Int Rev Cytol* 265, 111-158.
- Wang, W., Eddy, R., and Condeelis, J. (2007a). The cofilin pathway in breast cancer invasion and metastasis. *Nat Rev Cancer* 7, 429-440.
- Wang, W., Goswami, S., Lapidus, K., Wells, A.L., Wyckoff, J.B., Sahai, E., Singer, R.H., Segall, J.E., and Condeelis, J.S. (2004). Identification and testing of a gene expression signature of invasive carcinoma cells within primary mammary tumors. *Cancer Res* 64, 8585-8594.
- Wang, W., Mouneimne, G., Sidani, M., Wyckoff, J., Chen, X., Makris, A., Goswami, S., Bresnick, A.R., and Condeelis, J.S. (2006). The activity status of cofilin is directly related to invasion, intravasation, and metastasis of mammary tumors. *J Cell Biol* 173, 395-404.
- Wang, W., Wyckoff, J.B., Goswami, S., Wang, Y., Sidani, M., Segall, J.E., and Condeelis, J.S. (2007b). Coordinated regulation of pathways for enhanced cell motility and chemotaxis is conserved in rat and mouse mammary tumors. *Cancer Res* 67, 3505-3511.
- Wang, Y., Shibasaki, F., and Mizuno, K. (2005). Calcium signal-induced cofilin dephosphorylation is mediated by Slingshot via calcineurin. *J Biol Chem* 280, 12683-12689.
- Weaver, B.A., and Cleveland, D.W. (2007). Aneuploidy: instigator and inhibitor of tumorigenesis. *Cancer Res* 67, 10103-10105.
- Wiggin, O., Bernstein, B.W., and Bamburg, J.R. (2005). A phosphatase for cofilin to be HAD. *Nat Cell Biol* 7, 8-9.
- Woolner, S., O'Brien, L.L., Wiese, C., and Bement, W.M. (2008). Myosin-10 and actin filaments are essential for mitotic spindle function. *J Cell Biol* 182, 77-88.
- Wu, X., and Lieber, M.R. (1997). Interaction between DNA-dependent protein kinase and a novel protein, KIP. *Mutat Res* 385, 13-20.
- Yamniuk, A.P., Silver, D.M., Anderson, K.L., Martin, S.R., and Vogel, H.J. (2007). Domain stability and metal-induced folding of calcium- and integrin-binding protein 1. *Biochemistry* 46, 7088-7098.
- Yang, F., Li, X., Sharma, M., Zarnegar, M., Lim, B., and Sun, Z. (2001). Androgen receptor specifically interacts with a novel p21-activated kinase, PAK6. *J Biol Chem* 276, 15345-15353.
- Yang, N., Higuchi, O., Ohashi, K., Nagata, K., Wada, A., Kangawa, K., Nishida, E., and Mizuno, K. (1998). Cofilin phosphorylation by LIM-kinase 1 and its role in Rac-mediated actin reorganization. *Nature* 393, 809-812.
- Yang, X., Yu, K., Hao, Y., Li, D.M., Stewart, R., Insogna, K.L., and Xu, T. (2004). LATS1 tumour suppressor affects cytokinesis by inhibiting LIMK1. *Nat Cell Biol* 6, 609-617.

-
- Yasuda, H., Kanda, K., Koiwa, H., Suenaga, K., Kidou, S., and Ejiri, S. (2005). Localization of actin filaments on mitotic apparatus in tobacco BY-2 cells. *Planta* 222, 118-129.
- Yonezawa, N., Homma, Y., Yahara, I., Sakai, H., and Nishida, E. (1991). A short sequence responsible for both phosphoinositide binding and actin binding activities of cofilin. *J Biol Chem* 266, 17218-17221.
- Yoshioka, K., Foletta, V., Bernard, O., and Itoh, K. (2003). A role for LIM kinase in cancer invasion. *Proc Natl Acad Sci U S A* 100, 7247-7252.
- Zebda, N., Bernard, O., Bailly, M., Welte, S., Lawrence, D.S., and Condeelis, J.S. (2000). Phosphorylation of ADF/cofilin abolishes EGF-induced actin nucleation at the leading edge and subsequent lamellipod extension. *J Cell Biol* 151, 1119-1128.
- Zhan, Q., Bamburg, J.R., and Badwey, J.A. (2003). Products of phosphoinositide specific phospholipase C can trigger dephosphorylation of cofilin in chemoattractant stimulated neutrophils. *Cell Motil Cytoskeleton* 54, 1-15.
- Zhu, H., Fang, K., and Fang, G. (2009). Mechanism, function and regulation of microtubule-dependent microtubule amplification in mitosis. *Mol Cells* 27, 1-3.

10 Curriculum Vitae

Name: Oleg Fedorchenko
Sex: male
Date of birth: 20.09.1980
Place of birth: Kimovsk (Russian Federation)
Citizenship: Russian Federation
Marital status: single

Professional address: Institute of Biochemistry and Molecular Biology II,
Heinrich-Heine-University Düsseldorf
Universitätsstr. 1
40225 Düsseldorf
Germany
Tel.: +49 (0) 211 811 18 36
E-mail: oleg.fedorchenko@uni-duesseldorf.de

Personal address: Schönblick 7
51515 Kürten
Germany
Tel.: +49 (0) 178 625 76 13

Education and employment:

Sept. 1987 Jun. 1997 General education secondary-school, Safonovo, Russia

Sept. 1997 Dez. 1997 Bookkeeping courses in Smolensk, Russia

Jan. 1998 Apr. 1998 Bookkeeper at the Military Department in Safonovo, Russia

Mai 1998 Jun. 2003 Lomonosov Moscow State University, Chemistry Faculty,
Department of Enzymology. Diploma in Chemistry with
honors

Jan. 2000 Feb. 2004 Scientific work at the Lomonosov Moscow State University,
Chemistry Faculty, Department of Enzymology.

Nov. 2003 Dez 2003 Practical work at the Martin-Luther-University, Halle-
Wittenberg, Institut of Biochemistry, Department of
Enzymology

März 2004 Juni 2005 Scientific work at the Institut of Biochemistry I, University
Hospital Köln

Ab Juli to date PhD student at the Institute of Biochemistry and Molecular
2005 Biology II, Heinrich-Heine-University, Düsseldorf

List of publications and abstracts:

A. Drozdov, S. I. Troyanov, **O. Fedorchenko**, G. Battiston, C. Pettinari, F. Marchetti, A. Cingolani, New volatile heterocyclic metal diketonates for MOCVD, J. Phys. IV France 9, Pr8-929-934, 1999.

Fedorchenko O.V., Zorov I.N, Establishment of the new method for measuring the enzyme activities towards non-stark polysacharides, „Lomonosov – 2001“, Moscow, 2001

Fedorchenko O.V., Zorov I.N, Establishment of the new method for measuring the enzyme activities towards non-stark polysacharides, National young-scientists conference „From basic science to new technologies“, Moscow – Tver, 2001

Fedorchenko O., Hoffmann A., Jeanclos E., Odersky A., Nürnberg B., Gohla A., The calcium and integrin binding protein CIB1 is a novel regulator of Chronophin, International Summer School on Molecular Imaging, EMBL Heidelberg, Germany, September 2006

Fedorchenko O., Odersky A., Knobbe C., Reifenberger G., Nürnberg B., Gohla A., Short talk: ‘Role of the HAD-phosphatase Chronophin in glioblastoma pathogenesis’, Europhosphatases 2007, Aveiro, Portugal, July 2007

Hoffmann A. and **Fedorchenko O.**, Jeanclos E., Odersky A., Nürnberg B., Gohla A., The calcium- and integrin- binding protein 1 (CIB1) is a novel regulator of Chronophin, Europhosphatases 2007, Aveiro, Portugal, July 2007

Hoffmann A., **Fedorchenko O.**, Jeanclos E., Odersky A., Duraphe P., Nürnberg B., Gohla A., Role of the calcium- and integrin-binding protein CIB1 as an essential activator of Chronophin, 49th Annual Meeting of Deutsche Gesellschaft für experimentelle und klinische Pharmakologie und Toxikologie, Mainz, Germany, March 2008

Fedorchenko O., Odersky A., Klink B., Hoffmann A., Knobbe C., Reifenberger G., Nürnberg B., Gohla A., Talk: ‘Role of cofilin phosphatase chronophin in glioblastoma pathogenesis’, 49th Annual Meeting of Deutsche Gesellschaft für experimentelle und klinische Pharmakologie und Toxikologie, Mainz, Germany, March 2008

Prizes:

1st Place in the IWAKI and Nature Methods European and Cell Culture Image Award, May 2006

11 Acknowledgements

First of all I would like to thank my supervisor Prof. Dr. Antje Gohla for offering me the great opportunity to conduct this PhD thesis in her scientific group and of course for her excellent guidance and support through the whole work. I am very grateful for interesting and valuable discussions and advice at all stages of this thesis. Her prominent knowledge in different research areas and her insightful ideas made this project so interesting and exciting and helped me to finish this study.

The work was performed at the Institute for Biochemistry and Molecular Biology II, and I would like to thank Prof. Dr. Dr. Bernd Nürnberg for his support and for the excellent working conditions.

I would like to thank Prof. Dr. Lutz Schmitt, Chair of the Institute of Biochemistry, for his interest in this work and his kind willingness to represent this work at the Mathematical and Natural Science Faculty of the Heinrich-Heine University.

I also would like to thank our collaborating partners from the Institut of Neuropathology, Prof. Dr. Guido Reifenberger, Dr. Christiane Knobbe and Dr. Barbara Klink for providing us with rare brain cancer samples and also for the nice collaborative work and valuable discussions.

I also would like to thank:

- Ms. Andrea Odersky, BTA, for her outstanding assistance during the whole project
- my colleague Axel Hoffmann, Dipl.-Biol., for coordinated work in our common project, for providing me with plasmids for mouse CIN and CIB1 constructs, and with recombinant CIN and CIB1 proteins
- Dr. Elisabeth Jeanclos for her help and teaching me some methods and also nice discussions of our projects
- PD Dr. Christian Mielke from the Institute of Clinical Chemistry (Hospital of the Heinrich-Heine-University) for providing me with constructs for positive and negative FRET experiments and his helpful discussions and advice about performing FRET and other experiments on the confocal laser scanning microscope
- all my colleagues from the Institute of Biochemistry and Molecular Biology II for the nice working environment and for their help and collegiality
- all my old friends from Russia, living now all around the World, and my new friends from Germany for their support
- and last but not least my mother for her love and care, for helping and supporting me throughout all my life. I hope you like this work!

Die hier vorgelegte Dissertation habe ich eigenständig und ohne unerlaubte Hilfe angefertigt. Die Dissertation wurde in der vorgelegten oder in ähnlicher Form noch bei keiner anderen Institution eingereicht. Ich habe bisher keine erfolglosen Promotionsversuche unternommen.

Düsseldorf, den 15.05.2009

(Oleg Fedorchenko)